Combining multiple observations to improve our understanding of forest-snow interactions and inform forest management

Cassie Anne Lumbrazo

A dissertation

submitted in partial fulfillment of the

requirements for the degree of

Doctor of Philosophy

University of Washington

2023

Reading Committee:

Jessica D. Lundquist, Chair

Susan Dickerson-Lange

Emily Howe

Program Authorized to Offer Degree:

Civil and Environmental Engineering

University of Washington

Abstract

Combining multiple observations to improve our understanding of forest-snow interactions and inform forest management

Cassie Anne Lumbrazo

Chair of the Supervisory Committee:
Jessica D. Lundquist
Civil and Environmental Engineering

Many regions of the world rely on snowmelt from seasonal snowpacks for water resources. In the Northern Hemisphere, half of the seasonal snow zone overlaps with forests which interact with both snowfall and snow on the ground to influence total snow storage and water avaibility. This dissertation expands observations of forest-snow interactions to inform global modeling of canopy-snow interception in Chapter 2 and inform forest management in Washington State in Chapters 3 and 4.

In previous work, we identified the need for global meteorological variable thresholds that determine canopy-snow unloading to reduce the need for site specific parameter calibration of unloading models. Thus, in Chapter 2 we create a dataset of canopy-snow unloading observations from timelapse photography at three different sites and combine them with meteorological data to determine what variable thresholds determine snow unloading across climates. Our results identify four primary unloading regimes that vary the thresholds for wind

and temperature dependent unloading by climate and shortwave radiation. Furthermore, our unique dataset can be used for future model development and evaluation.

In Chapter 3, we used aerial snow-on lidar from NCALM over 63 km^2 of the Eastern Cascades of Washington State, USA, to quantify the effects of forest cover and topography on snow depth in this climate transition zone. We found that topographic position and canopy cover matter for snow depth in the Eastern Cascades, where the most snow at all elevations is found in topographically shaded gaps. We also found that forest cover is particularly important in predicting snow depth in warmer, low elevation terrain.

In Chapter 4, we collect, process, and analyze drone lidar data before and after forest treatments on Cle Elum Ridge over a 3 km^2 area in this low elevation zone of the Eastern Cascades to determine how forest treatments for fire resiliency impact hydrologic resiliency. We found that forest treatments on north-facing aspects increase snow storage in this climate transition zone compared to treatments with greater solar exposure which do not significantly affect snow depth. Thus, forest thinning and especially canopy-gap creation, on north-facing slopes provides a viable path forward for managing forests for both fire and hydrologic resilience in this climate zone.

Acknowledgements

Academia is a land of endless invisible efforts. Each effort, a shared moment that changes lives.

My PhD committee, Jessica Lundquist, Susan Dickerson-Lange, Emily Howe, Brian Harvey, and Brittney Johnson, have all contributed their fair share of endless invisible efforts to help me arrive at the end of this journey. While they each deserve their own novel which shines light on what we cannot see, I hope I can provide a small glimpse into the unknown.

My advisor, Jessica Lundquist, is a master in the art of mentorship in academia—a challenging trade indeed. Jessica intuitively fell into step during the moments when I needed a strong push of motivation and balanced that with moments when she knew I only needed an open ear. We've all heard stories of negative advisor-advisee relationships, and until I started my post-graduate career in academia, I did not understand how important this mentorship relationship is in the happiness, and ultimately the success, of PhD students. Every week I would enter Jessica's office with a scattered mind and endless graphics I could not make sense of, and each week I would leave her office thinking clearly and feeling confident about my next steps. Jessica makes a tremendous effort to learn each of her students individually and takes care to crafts projects that highlight their strengths. I admire Jessica's ability to make abstract ideas a reality. There are so many people in our lives who talk without action, Jessica however, does not have a moment to waste. When Jessica invited me, quite casually, to join her on her sabbatical to Switzerland a few years ago (which I should remind everyone is a professor's only opportunity to get some space from their graduate students), my voyager soul immediately responded, "of course I would join you if I could!". The next day there was Swiss VISA information in my email inbox. Like I said, not a moment wasted. I can never thank Jessica enough for inviting me to join her, for that experience inevitably changed the course of my life entirely.

Susan Dickerson-Lange, being the first woman to receive her PhD from our research group, did not waste a moment supporting me, the second women to receive their PhD from our research group. Susan, with her own exceptionally busy personal and professional life, always had a moment for me. Susan invisibly supported me in grant writing for successful and unsuccessful datasets and fellowships. She once told me that any piece of writing she works on or graphic she creates is never without a specific purpose for a proposal or paper. Since, I've moved forward in my research with intention, always creating something with a purpose.

Emily Howe is a powerhouse in the field, and I looked forward to our early morning field days with earnest. When the forest road was covered in snow, I watched grown men fumble with putting on chains. Emily had already crawled under the truck and attached the last chain, while the men were still calculating how they could manage without getting their coats dirty. Emily exudes honesty and strength, that I not only admire, but aspire to hold in my daily life.

Thank you to my committee members, Brian Harvey and Brittney Johnson. Brian taught my absolute favorite course I've taken at the University of Washington. I learned more on a few field days during that forest ecosystems course than I've learned inside of any classroom. Brittney, thank you for the invisible efforts it took to join my committee and contribute to this science.

I'm fortunate to have a long list of mentors that does not end at my committee members. Clare Webster, thank you for your continuous support in research, and in life. You have a beautifully clear way of thinking about the world that I aspire to reach in my daily life. Your mentorship and friendship are truly the reason I got through the most challenging year of my PhD. Giulia Mazzotti, thank you for your continued interest in my research and life. You approach research with a passion that inspires me every time we talk or anytime I read a comment from you.

My PhD experience has been many things, but one of them is not lonely.

My cohort of graduate students and I truly got here together. Thank you to the members of the "Fishbowl" and "Treehouse" who created a culture of transparency and support that is unmatched. A special thank you to Michelle Hu, Friedrich Knuth, Shashank Bhushan, and Steven Pestana for creating the team that got me through the first and the last year of graduate school. I look forward to our future collaborations. I'm proud of you all.

A special thank you to the Mountain Hydrology Research Group members, past and present. To the crew from the first part of my PhD, Ryan Currier, Justin Pflug, Dylan Reynolds, Vic Ly, Steven Pestana, and Joe Ammatelli who showed me the ropes of graduate school. And, to the crew who saw me out with a bang, Hannah Besso, Ross Mower, Danny Hogan, Eli Schwatt, Clinton Alden, Emma Boudreau, John Cramblitt, and Matthew Bonner. Thank you all for providing the correct (or incorrect—Eli) amount of humor and feedback into my life. We have all grown up together through this process and I look forward to seeing where you all end up next.

Thank you to my Seattle roommates for helping me survive the city life. To the Keystone Place inhabitants, thank you for being my first West Coast family and to the Kirkwood Café inhabitants, thank you for being my last. Through all 11 of you (yes, 11), I've learned life lessons, inside and outside the kitchen, that I will keep with me. Thank you to my Norwegian roommates for the daily spiritual lessons, and to my Davos roommates who always welcomed me with open arms, and open hearts. You supported me in some of the hardest times of my life—thank you.

Thank you for my tiny, but mighty army of women that have surrounded me for the past 10+ years. Thank you to my forever roommate, Kayla Jurchak, my spiritual partner in crime, Sonja Gagen, my friend with a parallel life, Nicole Zaino, my work wife, Hannah Besso, my fellow voyager, Ellie Hands, my sister by choice, Ella Carver, and my twin flame in a million ways and one, Grace Fast. I cherish you all, and I will keep this beautiful army of women close for the rest of my life.

Thank you to my family. Thank you to my big sister, Corrin Lumbrazo, for never leaving my side. The strength of our relationship gives me hope for the future. And thank you to my Mother, Laura Lumbrazo, for your continuous support in my forever-interesting life decisions. And finally, thank you to my life partner, Louis Quéno. You have shown me balance in life. Thank you for your unwavering love and continuous support. Je t'aime mon amour, you are everything beautiful about the world.

Table of Contents

Contents

List of Figures

List of Tables

Chapter 1. Introduction.

Many regions of the world rely on snowmelt from seasonal mountain snowpacks for water resources (Immerzeel et al., 2020). In the Northern Hemisphere, forests overlap with 50% of the seasonal snow zone (Kim et al., 2017). In these forested regions, the forest plays a role in the total snow accumulation and duration, which has implications for streamflow amounts and timing (Dickerson-Lange et al., 2021). The forest canopy interacts with snow through intercepting the snowfall before it reaches the ground, and also providing shade to or melting the snowpack on the ground (Lundquist et al., 2021). We summarize these physical processes in the term "forest-snow interactions".

In this dissertation, we use observations of snow depth from timelapse photography and lidar to better understand these forest-snow interactions. The two overarching goals of this dissertation are to better understand forest-snow interactions, (1) on a global scale to inform snow modeling, and (2) in the Eastern Cascades of Washington State, USA, to inform forest management for fire and water resilience. Thus, this dissertation is subsequently divided into three main chapters, Chapter 2 falling under goal (1), and Chapters 3 and 4 under goal (2).

In previous work, we found that canopy-snow unloading models were not transferable across climates (Lumbrazo et al., 2022). This research motivated Chapter 2 of this dissertation, where we aim to determine meteorological variable thresholds for canopy-snow unloading using observations across multiple climates. In Chapters 3 and 4, we take what we learned about forest-snow processes and use the first snow-on lidar datasets in the Eastern Cascades to evaluate how forests interact with the snowpack in this region. Specifically, in Chapter 3 we establish the baseline relationships between forest cover, topography, and snow depth across a range of elevations and hypothesize how forest management in this region will impact the snowpack, and therefore, water resources. Finally, in Chapter 4, we focus on a smaller region of the domain where experimental forest treatments for fire resiliency were performed. Here, we are able to test the hypothesis established in Chapter 3 and provide evidence-based suggestions on how to manage forests for fire and water resources to forest managers in Washington State.

Chapter 2, titled "*Determining meteorological variable thresholds for canopy-snow unloading across multiple climates"* will be submitted for peer-review in early 2024 with the corresponding canopy-snow unloading dataset and supplemental materials. This research expands observations of canopy-snow unloading and provides insights into how the community can move forward in modeling canopy-snow across multiple climates. This work was funded by the Steve and Sylvia Burges Presidential Fellowship and the Valle Scandinavian Scholarship Program both through the University of Washington Department of Civil and Environmental Engineering. This research was performed in collaboration with researchers at the WSL Institute for Snow and Avalanche Research SLF, Switzerland and in the Department of Geosciences at University of Oslo, Norway.

Chapter 3, titled "*Combined effects of forest cover and topography on snow depth in the Eastern Cascades, Washington, USA*" was submitted to the Washington State Department of Natural Resources (WADNR) as a final report in August 2023. This chapter provides technical details and reproduceable methods for WADNR to calculate topographic and forest metrics that

influence snow depth for any region with snow-on lidar data to aid in planning for forest management across Washington State. This chapter was primarily funded by the Washington State Department of Natural Resources (WADNR) and performed in collaboration with the National Center for Airborne Laster Mapping (NCALM).

Chapter 4, titled "*Forest treatments for fire resilience result in more snow storage on north-facing aspects in the Eastern Cascades, Washington, USA"* will be submitted to for peer-review in 2024 with the corresponding lidar dataset and supplemental materials. In this chapter we are able to directly test hypotheses established over many years that forest thinning and gap-creation on north-facing slopes would increase total snow storage in this climate transition zone. As the title of the chapter would suggest, those hypotheses proved true. Since we expect some adaptations will be made to this chapter in preparation for peer-review, we encourage forest managers to contact us regarding management decisions based on this research to receive the most recent versions of this work. This chapter was funded by the WADNR and the Nature Conservancy (TNC) and performed in collaboration with the NHERI Natural Hazards Reconnaissance (RAPID) Team at the University of Washington.

Chapter 2. Determining meteorological variable thresholds for canopy-snow unloading across multiple climates

Cassie Lumbrazo[1], Clare Webster[2], Giulia Mazzotti[3,4], Johanna Malle[4], Vincent Haagmans[4], Tobias Jonas[4], Jessica Lundquist[1]

[1] Department of Civil and Environmental Engineering, University of Washington, Seattle, WA, USA.

[2] Department of Geosciences, University of Oslo, Oslo, Norway

[3] Centre d'Etudes de la Neige, Météo-France, Grenoble, France

[4] WSL Swiss Federal Institute for Snow and Avalanche Research, Davos, Switzerland

Notes. This chapter will be submitted for peer-review.

Key Points.

- The threshold for wind dependent unloading is lower in the arctic, compared to mid-latitude climates.
- The threshold for temperature dependent unloading is higher in mid-latitudes, compared to the arctic, due to increased snow cohesion between -3 and 0ºC.
- This canopy-snow unloading dataset from this study spans multiple climates and it can be used for future model development and evaluation.

Abstract.

Canopy-snow interception and unloading is a complex physical process that is difficult to model and evaluate due to lack of observations. In this work, we provide a dataset of snow unloading across three different climates created with timelapse photography. We combined the unloading observations with meteorological data to determine what meteorological variable thresholds determine snow unloading globally. Our results identify four primary unloading regimes, that vary the thresholds for wind and temperature dependent unloading by climate and shortwave radiation. During times of little shortwave radiation, wind speed is the strongest predictor of snow unloading at a threshold of 3.5 m s^{-1} compared to times of moderate shortwave radiation, where air temperature is the strongest predictor of snow unloading at 0.5ºC. When shortwave radiation is above 230 Wm^{-2}, air temperature is the strongest predictor of snow unloading where during cold temperatures, snow starts unloading at wind speeds of 5.5 ms^{-1} and during high temperatures, snow is more likely to stay in the canopy between -2.5 and 1.5ºC, then fully unload once air temperatures exceed 1.5ºC. While often represented in snow interception models, we recommend that all unloading models represent the decrease in snow unloading due to increased adhesion and cohesion of snow in the canopy when temperatures range from -3ºC to 0ºC. We found that the four unloading regimes do not unload snow with the same efficiency, where wind dependent unloading that occurs during very low shortwave radiation mainly results in partial unloading events, compared to temperature dependent unloading in mid-latitudes which often result in full unloading events. Finally, this canopy-snow unloading dataset from this study spans multiple climates and it can be used for future model development and evaluation.

2.1. Introduction.

Forests cover approximately 31% of the global land surface (FAO, 2010) and overlap with 50% of the Northern Hemisphere snow zone (Kim et al., 2017). In these forested regions, the canopy can intercept 30-80% of snowfall from a single storm depending on the climate (Hedstrom & Pomeroy, 1998; Lundquist et al., 2013; Martin et al., 2013). Once snow is intercepted by the forest, it can leave the canopy through a number of physical processes such as meltwater drip, solid snow unloading, and sublimation back to the atmosphere (Lundquist et al., 2021). These physical processes are difficult to measure and observe, which makes it challenging to develop and evaluate exisiting model formulations of the processes. Canopy-snow interception and unloading model formulations that are widely used today were developed from isolated field experiments (Lundquist et al., 2021). Thus, the observational history of canopy-snow unloading is either limited to observations over small spatial scales (Nakai et al., 1994), small temporal scales (Storck et al., 2002), or both.

Forest-snow interception and unloading has a large influence on the land surface energy balance (Essery, 1998). The naturally low albedo of dark coniferous forests can increase 20% when snow covered (Webster & Jonas, 2018). Canopy-snow also increases the energy feedback to the atmosphere (Thackeray et al., 2014). These changes to the land surface albedo can happen quickly and are an important, yet poorly understood, feedback mechanism in global climate models (Lundquist et al., 2021). Previous studies have demonstrated that properly representing forest-snow processes such as canopy-snow interception and unloading can improve the modeled albedo over forested regions (Niu & Yang, 2004).

To observe snow unloading from the canopy, one must be in a single location for a long time or in multiple locations over shorter periods of time. Timelapse photography provides the opportunity survey multiple locations over extended time spans. Timelapse photos taken before, during, and after a storm provide high temporal resolution information on when snow is intercepted and unloaded from the trees in the photographs. The timelapse photos can provide additional information about the physical conditions when snow is unloading, such as if the canopy-snow is sunlit or if the trees are moving between two timelapse images. However, this method only quantifies when snow is intercepted and unloaded from the canopy; it does not provide any information about the amount of snow in the canopy or the physical process which caused snow to unload from the canopy (i.e., melt, solid snow unload, or sublimation).

Often the physical processes of snow unloading are not explicitly modeled; instead canopy-snow unloading models estimate unloading either with as an exponential-decay function of time (Hedstrom & Pomeroy, 1998) or use meteorological conditions to estimate when snow will unload from the canopy (Andreadis et al., 2009; Roesch et al., 2001). Most models that use meteorological conditions to estimate canopy-snow unloading simply threshold by air temperature, where unloading begins at or near 0°C. The few models that also consider wind-dependent unloading (Roesch et al., 2001), consider both temperature- and wind-dependent unloading functions as two separate formulations. While it is known that incoming shortwave radiation heats canopy elements well above 0°C while air temperatures remain below 0°C (Webster et al., 2016), the impact of this physical process on canopy-snow unloading is neither physically or statistically represented in any existing canopy-snow unloading models.

Lumbrazo et al. (2022) reviewed three commonly used canopy-snow unloading parameterizations and found that the formulations were generally adequate when parameter

values for the rate of unloading were tuned to local canopy-snow unloading observations for that site. Thus, we need a model formulation which uses readily available meterological conditions for parameter tuning, and not niche unloading observations. Due to the complexity of interactions between air temperature, wind speed, and shortwave radiation that drive snow unloading, all parameterizations (especially highly simplified models) lacked transferability across sites. The snow interception dataset from Lumbrazo et al. (2022) only classified timesteps with presence or absence of snow in the canopy. However, to isolate the physical process of canopy-snow unloading, a dataset which deciphers if snow in the canopy is staying or unloading is needed.

In this work, we evaluate the meteorological conditions that occur when snow is actively unloading over larger temporal and spatial scales than has been previously studied. This allows us to identify how the relationship between unloading and meteorological variables varies across climates. Air temperature, wind speed, and shortwave radiation are hydrologic model inputs that are already used as estimates for when snow will unload from the canopy. If we understand how they interact in different climates when unloading occurs, then we can improve exisiting formulations of canopy-snow unloading models to be transferable across climates without local calibration. Thus, our goal is to determine,

- What thresholds for air temperature, incoming shortwave radiation, and wind speed determine snow unloading globally?
- How effective is snow unloading above these determined thresholds?

2.2. Methods.

2.2.1. Study sites.

We observed snow unloading from three sites across multiple climates with variable forest structures and meteorological conditions (Figure 2.1).

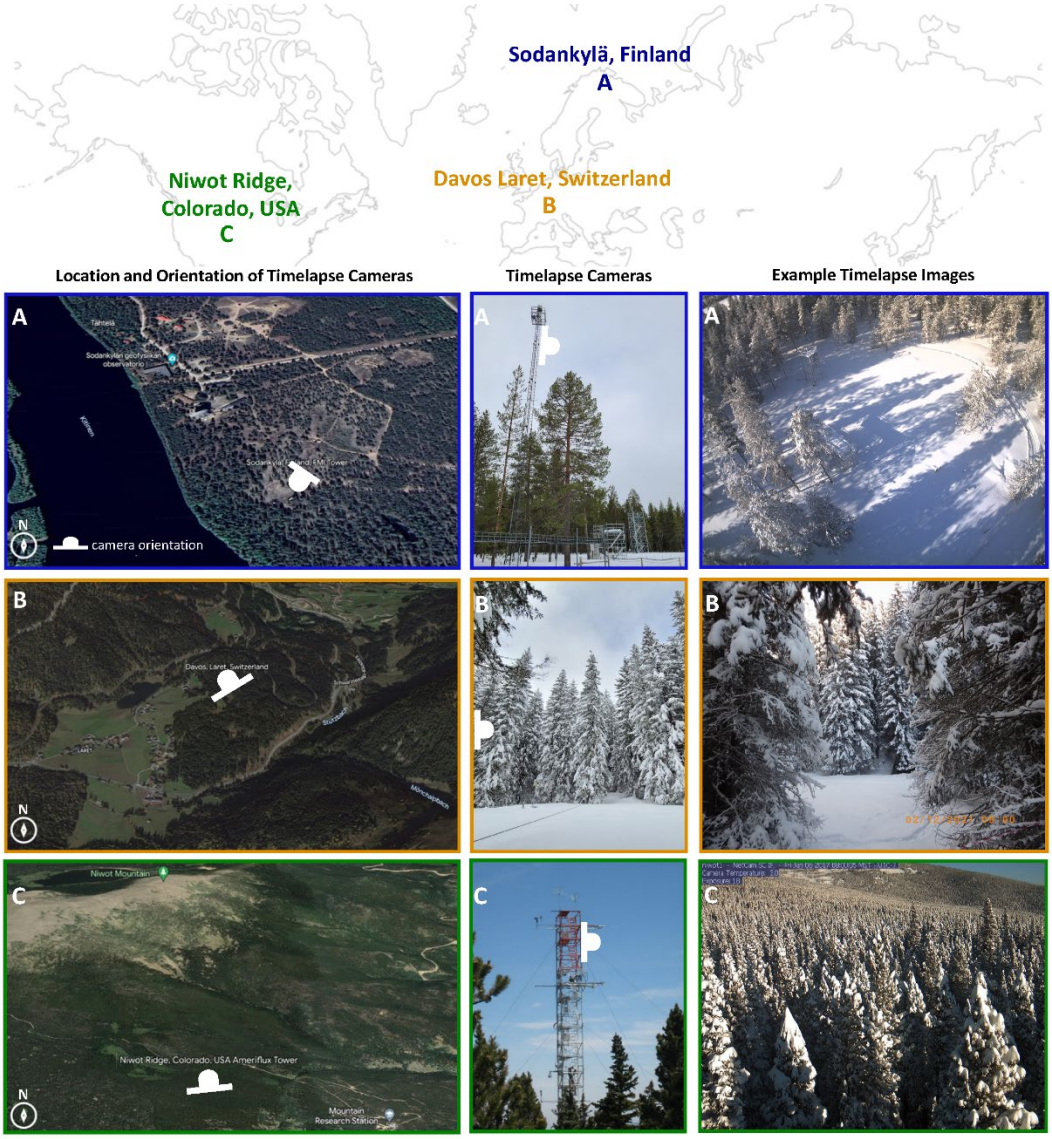

Figure 2.1. *Location and orientation of the timelapse cameras with example images for each site A) Sodankylä, Finland in blue B) Davos Laret, Switzerland in orange and C) Niwot Ridge, Colorado, USA in green.*

2.2.1.1. Sodankylä, Finland

The Sodankylä study site (67°21′47″N, 26°38′03″E, 179 m, Figure 2.1A) is located in Northern Finland 90 km north of the Arctic Circle on the Finnish Meteorological Institute's Arctic Research Center (FMI ARC) grounds and has been the location of many snow surveys and field

campaigns (e.g., Essery et al., 2016; Lemmetyinen et al., 2016; Leppänen et al., 2016; Mazzotti et al., 2020). The sparse forest is mostly Scots pine (*Pinus sylvestris*) standing 15 m in height which represents a typical managed forest in Northern Finland. In this subarctic climate with flat topography, we observed the relationship between air temperature and wind speed on canopy-snow unloading with only little influence from incoming shortwave radiation in the winter months.

We used timelapse images from an established camera on a 22 m tower in the Intensive Observation Area (IOA) which took a photo every 15 minutes archived by FMI ARC (https://litdb.fmi.fi/ioa0010_data.php). The camera was oriented south-west at a height above the trees enough to view some trees from top-down, and others in the distance from the side. During even the darkest winter months, the combination of the ambient light and camera exposure settings ensured we had at least four hours of observations every day. We used meteorological data for water year (WY; 1 October — 30 September) 2019 from the FMI ARC 50 m EC tower (https://en.ilmatieteenlaitos.fi/ghg-sodankyla-forest) with measurements taken at 22 m.

2.2.1.2. Davos Laret, Switzerland

The Davos Laret study site (46°50′42″N, 09°52′19″E, 1530 m, Figure 2.1B) is located in the Eastern Swiss Alps and has been the location of numerous forest-snow campaigns (e.g., Malle et al., 2019; Mazzotti et al., 2020, 2021; Moeser et al., 2014; Webster et al., 2016; Webster & Jonas, 2018). The forest is predominantly Norway spruce (*Picea abies*) between 10 and 30 m in height (Moeser et al., 2014). The field site is in a topographically sheltered location with low wind speeds, and thus provided the opportunity to observe the relationship between air temperature and shortwave on canopy-snow unloading with limited influences from wind speed.

We set up timelapse cameras to collect observations of canopy-snow unloading at Davos Laret from mid-February through May 2021. While this was a shorter observational time period compared to the other sites, we had the opportunity to establish multiple timelapse cameras to cover different canopy orientations. The camera used in this study, shown in Figure 2.1B, was attached to a tree orientated north/north-west which viewed trees on the sunlit side of a gap. We collected meteorological data for Davos Laret from the WSL Institute for Snow and Avalanche Research SLF weather station (Mazzotti et al., 2020) located in an open area near the timelapse cameras.

2.2.1.3. Niwot Ridge, Colorado, USA

The Niwot Ridge study site (40°01′58″N, -105°32′47″E, 3050 m, Figure 2.1C) is located on the leeward side of the Continental Divide in Colorado, USA which has been the location of other forest-snow observations (e.g., Lumbrazo et al., 2022; Raleigh et al., 2022). The dense coniferous forest is made up of Ponderosa Pine (*Pinus ponderosa*) and Subalpine Fir (*Abies lasiocarpa*) standing 7-8 m tall. The notoriously windy and cold field site receives many clear sky days throughout the winter, and thus provided the opportunity to observe how all three meteorological variables (i.e., air temperature, incoming shortwave radiation, and wind speed) interact throughout the season to unload snow from the canopy.

We used timelapse images from an established camera on the 20 m Niwot Ridge Ameriflux Tower (Ameriflux Site US-NR1) which takes a photo every 30 minutes archived by the PhenoCam Network (Milliman, 2018). The tower stands in a small clearing just above the trees, oriented north viewing some of the tops and mostly the sides of trees in a dense forest. We used meteorological data from measurements taken on the same tower as the timelapse camera images for WY 2017.

2.2.2. Timelapse camera observations.

To determine when canopy-snow was unloading, we first determined timesteps when there was snow in the canopy. Using the methods described in Lumbrazo et al. (2022), timelapse images were evaluated by citizen scientists for the presence or absence of snow in the canopy. We expanded on these methods by adding additional classifications to the timesteps when citizen scientists identified snow in the canopy. We visually inspected the timelapse images for additional information, such as snow unloading, active snowfall, sunlight on the canopy, tree sway, and blowing snow. In this work, we mainly focus on the observations of snow unloading.

For the timesteps when citizen scientists identified snow in the canopy, we visually inspected the timelapse images for canopy-snow unloading. We classified the timestep, t_1, as snow unloading from the canopy when the amount of snow in the canopy in the current image, t_1, was less than the amount of snow in the canopy in the previous image, t_0. We classified the timestep, t_1, as snow staying in the canopy when the amount of snow in the canopy in the previous image, t_0, and the current image, t_1, were the same.

This classification method defined canopy-snow unloading as any mass loss of snow in the canopy that was visible to the naked eye. Thus, this classification included canopy-snow melting and dripping from the canopy, snow unloading from the canopy to the snowpack below, and snow sublimating from the canopy back to the atmosphere. We did not attempt to use visual inspection of timelapse images to decipher between these physical processes; rather, we used this information to quantify the timing of mass loss from the canopy, then looked to meteorological data to provide more information on what physical processes might have occurred to cause unloading.

To ensure that the meteorological data and timelapse photography were capturing the same time period, the meteorological data were averaged over the time between the two images. This ensures we captured meteorological conditions that occurred during the classification of snow unloading.

We added an additional classification to each unloading event to determine if the unloading resulted in a partial or a full unloading of snow from the canopy. We defined a partial unloading event as snow remaining in the canopy after unloading occurs over some continuous amount of time, and a full unloading event as all the snow being removed from the canopy as a result of the unloading over some continuous amount of time. We use this classification of partial vs. full unloading to evaluate how effective meterological variable conditions are at completely removing snow from the canopy.

2.2.3. Random forest classifier to predict snow unloading.

Since prior work showed that commonly used parameters in existing unloading models are not transferable across sites (Lumbrazo et al. year), our goal here is to statistically determine thresholds for air temperature, incoming shortwave radiation, and wind speed that determine snow unloading across multiple climates. Decision tree models are a non-parametric machine learning method for determining statistically significant splits in datasets that have complex variable interactions. Since single decision trees are known to have high variance and are prone to overfitting, we ran an ensemble of decision trees using the random forest classifier algorithm implemented by the scikit-learn Python package (Pedregosa et al., 2011). The random forest classifier uses averaging to improve the predictive accuracy of the decision trees and control over-fitting the model to the dataset, rather than majority voting (Hu & Shean, 2022).

We combined the data from all three sites into a single dataset, with snow unloading as the target variable and air temperature, solar radiation, and wind speed as the input features to the random forest model (Figure 2.2). The dataset contained 1288 observations of snow staying and 446 observations of snow unloading from the canopy. During preliminary testing, we observed little improvement in accuracy after 300 iterations, and thus the final model parameters were 500 decision trees (*n_estimators*), with a maximum tree depth (*max_depth*) of three decision nodes. We evaluated the importance of each input feature with the scikit-learn feature importance metric (*feature_importances*), and evaluated the performance of each decision tree with the scikit-learn accuracy score metric (*accuracy_score*) (Pedregosa et al., 2011). We visualize the decision tree with the highest accuracy score to intuitively find the thresholds that determine snow unloading. This method provides the intuitive visualization power of a single decision tree, while reducing the variance associated with a single decision tree by running 500 iterations to find the tree with the highest accuracy. Finally, we compare the random forest model prediction of snow unloading with our observations of snow unloading to evaluate what physical processes our unloading dataset is not capturing.

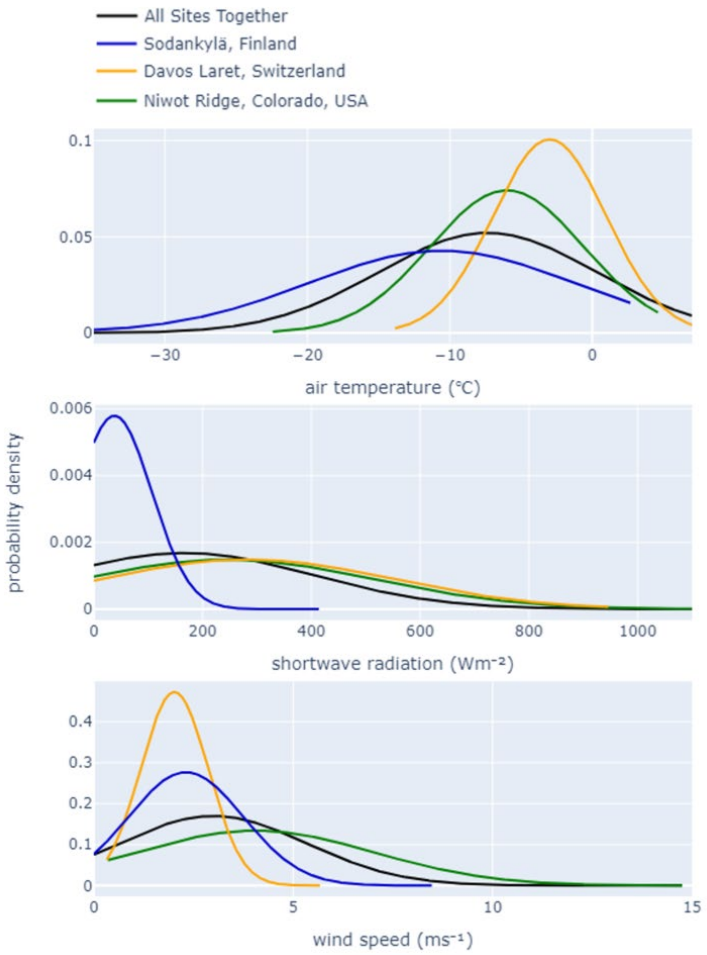

Figure 2.2. *Probability density functions (PDF)s for air temperature, ºC, incoming shortwave radiation, Wm^{-2}, and wind speed, ms^{-1}, for Sodankylä, Finland in blue, Davos Laret, Switzerland in yellow, Niwot Ridge, Colorado, USA in green, and all the sites together in black.*

The probability density functions (PDF)s for the combined meteorological data show that our observations of air temperature range from -38 to 7ºC, shortwave radiation ranges from 0 to 1100 Wm^{-2}, and wind speeds range from 0 to 15 ms^{-1} (Figure 2.2). These distributions represent the range of meteorological conditions that occurred when snow was present in the canopy (e.g., there are no observations of snow in the canopy above 7ºC). While there are no other global canopy-snow observational datasets to compare this to, we believe that these distributions provide meteorological conditions that enable a global look at canopy-snow unloading.

2.3. Results.

2.3.1. Canopy-snow unloading observations.

We categorize observations of snow in the canopy in two groups, as timesteps with snow staying in the canopy and timesteps when snow is unloading (Figure 2.3).

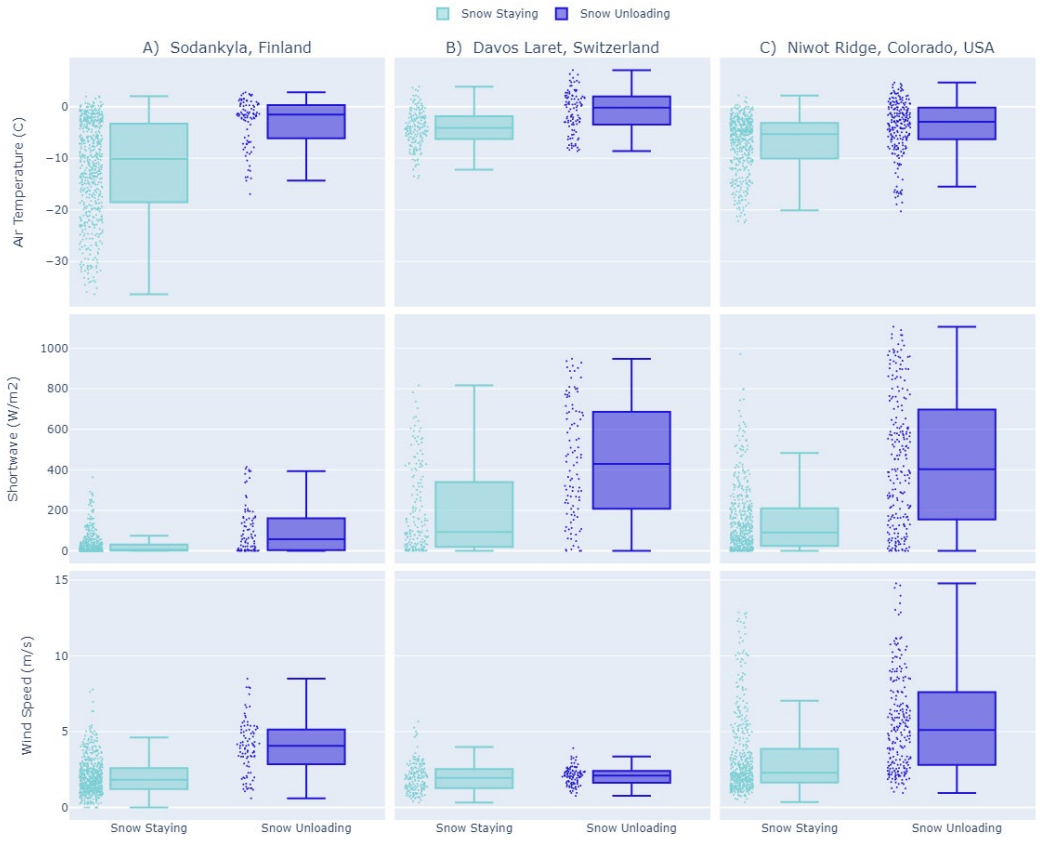

Figure 2.3. *Box plots of snow staying in the canopy, in blue, and snow unloading, in purple, for air temperature, ºC, incoming shortwave radiation, Wm^{-2}, and wind speed, ms^{-1}, for each site.*

This dataset shows that the median air temperature is significantly higher when snow is unloading for all sites (Figure 2.3). While snow rarely stays in the canopy above 0ºC, there are often observations of snow unloading below 0ºC. There are a significant number of unloading events between 0 and -10ºC at all sites, and still a handful of unloading events occurring below -10ºC at Sodankylä and Niwot Ridge. For Davos Laret and Niwot Ridge, where we observe the impact of shortwave radiation on unloading, the median shortwave radiation is above 400 Wm^{-2} when snow is unloading and below 200 Wm^{-2} during observations of snow staying in the canopy. For Sodankylä and Niwot Ridge, where we can observe the impact of wind speed on snow unloading, the median wind speed is above 3 and 5 ms^{-1} respectively, when snow is unloading.

However, visualizing observations of snow staying and snow unloading as a function of a single meterological variable does not resolve dependencies between meterological variables. Thus, we use the random forest algorithm to determine these variable thresholds which inherently account for the complex interactions between meteorological variables.

2.3.2. Random forest classifier.

2.3.2.1. Canopy-snow unloading regimes from a decision tree.

As outlined above, we combined data from all three sites into a single dataset with air temperature, incoming shortwave radiation, and wind speed as the input features to the random forest model to determine the target variable, snow unloading from the canopy (Section 2.2.3). The importance of each feature for the full random forest model ensemble (Figure 2.4) ranks shortwave radiation first, followed by air temperature and then wind speed.

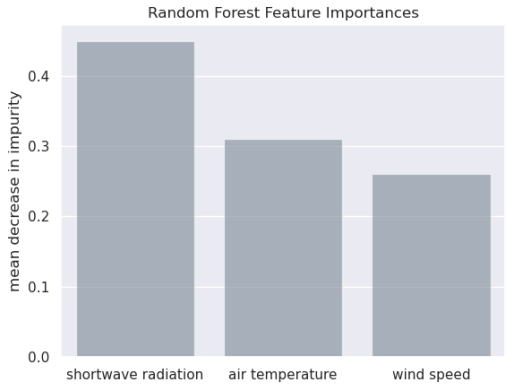

Figure 2.4. *The random forest model feature importance in classifying snow unloading from a forest of 500 decision trees.*

To better understand the random forest model decisions that determine the importance of each feature, we visualize the highest performing decision tree from the random forest model with the distribution of snow staying and snow unloading observations at each decision node (Figure 2.5).

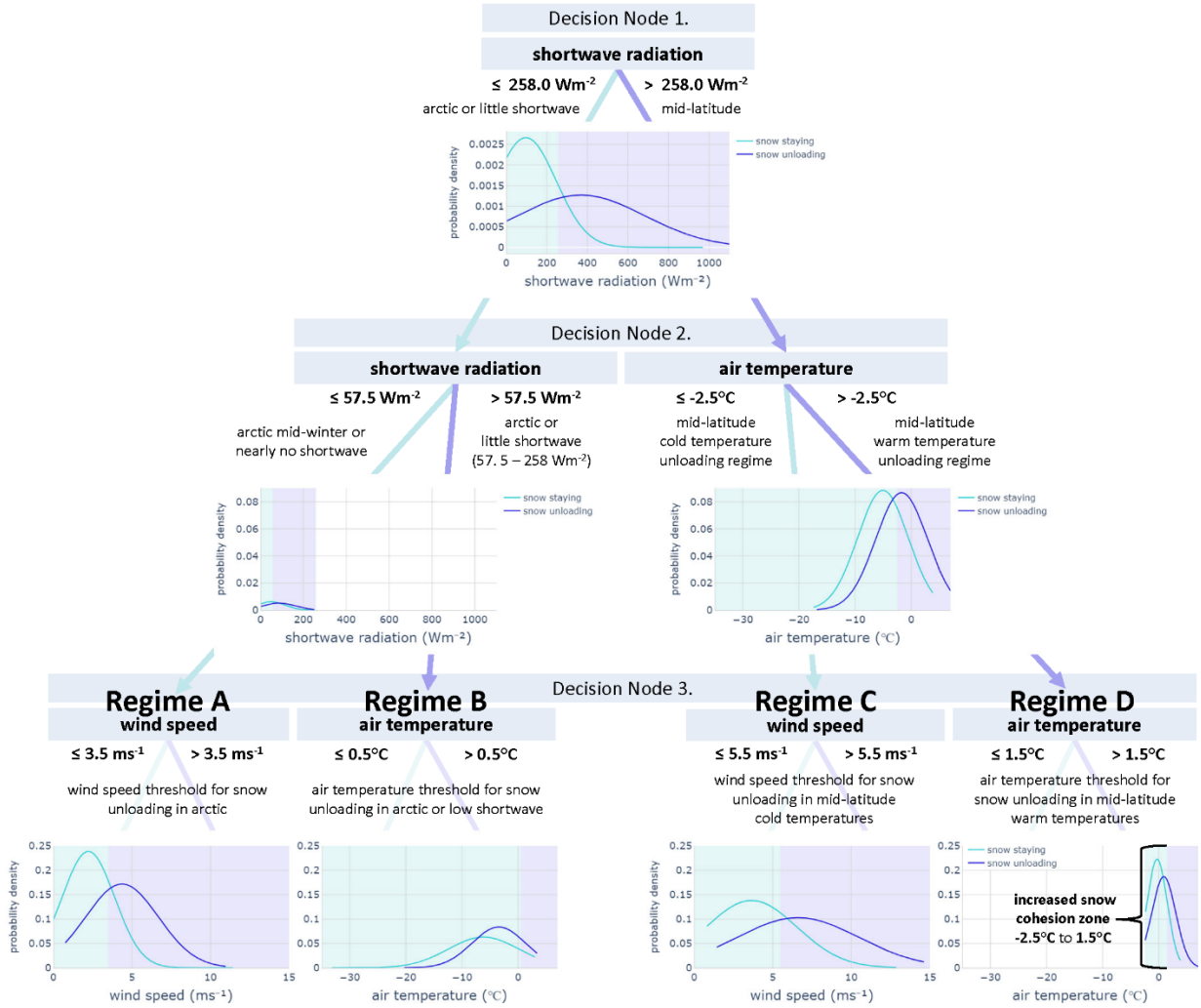

Figure 2.5. *Decision tree predicting snow unloading from the random forest model. The probability density functions (PDFs) of snow staying in the canopy, in blue, and snow unloading, in purple are plotted for each subset of the data determined by the decision notes for air temperature, ºC, shortwave radiation, Wm^{-2}, and wind speed, ms^{-1}. The four resulting unloading regimes are indicated by A, B, C, and D.*

Each decision node statistically determines a threshold value for binary splits in the data (e.g., 0 for snow unloading in purple, 1 for snow staying in blue), one input feature at a time (Dickerson-Lange et al., 2021). We can track the decision nodes through the tree where the first decision represents the largest split in the data, where the data in each subsequent node is a subset of data from the previous node (Molnar, 2023). The result is a decision tree with three decision nodes, which creates four subsets of the data, each with snow staying and snow unloading classifications (labeled Regime A, B, C, and D Figure 2.5), determined by three meteorological variable thresholds (Figure 2.5). We interpret these groups as four unique unloading regimes defined by the prevalence of different physical processes (Table 2.1).

Table 2.1. *Summary of meteorological variable conditions and final thresholds for snow unloading and snow staying in each unloading regime.*

Regime	**shortwave radiation** Wm^{-2}	**air temperature** ºC	**wind speed** ms^{-1}
Regime A	≤ 57.5	-	snow staying ≤ 3.5 snow unloading > 3.5
Regime B	57.5 — 258	snow staying ≤ 0.5 snow unloading > 0.5	-
Regime C	> 258	≤ -2.5	snow staying ≤ 5.5 snow unloading > 5.5
Regime D	> 258	> -2.5 snow staying -2.5 —1.5 snow unloading >1.5	-

The first decision node thresholds shortwave radiation at 258.0 Wm^{-2}, which can be interpreted as a proxy for determining different snow unloading regimes by insolation regimes (see Sodankylä shortwave distribution in Figure 2.2). We interpret the left side of the first decision node split of shortwave radiation values less than 258.0 Wm^{-2} as arctic climates or conditions with little shortwave radiation. While the right side of the first decision node split represents mid-latitude climates where shortwave radiation values are frequently greater than 258.0 Wm^{-2}.

For arctic climates or timesteps with very little shortwave radiation, the second decision node splits at shortwave radiation again, with a threshold of 57.5 Wm^{-2}. This subsets the arctic climate unloading regime into two unloading regimes. First, during mid-winter in the arctic, when there is little to no shortwave radiation (less than 57.5 Wm^{-2}), wind speed is the most important feature in determining snow unloading (Figure 2.5; Table 2.1 Regime A). In the third decision node for this subset of data (Figure 2.5; Table 2.1 Regime A), the wind speed threshold for unloading is 3.5 ms^{-1}, where wind speeds less than that threshold result in snow staying in the canopy, and wind speeds greater than that threshold results in snow unloading. Second, during times of little shortwave radiation in the arctic (i.e., between 57.5 and 258.0 Wm^{-2}), air temperature is the most important feature in determining snow unloading (Figure 2.5; Table 2.1 Regime B). In the third decision node for this subset of data (Figure 2.5; Table 2.1 Regime B), the air temperature threshold for snow unloading is 0.5ºC, where temperatures less than that threshold result in snow staying in the canopy, and temperatures greater than that threshold results in snow unloading.

For mid-latitude climates, the second decision node splits at air temperature with a threshold of -2.5ºC. This subsets the mid-latitude climate unloading regime into two unloading regimes. First, during conditions when air temperatures are below -2.5ºC, wind speed is the most important feature in determining snow unloading (Figure 2.5; Table 2.1 Regime C). In the third decision node for this subset of data (Figure 2.5; Table 2.1 Regime C), the wind speed threshold for unloading is 5.5 ms^{-1}. Second, during conditions when air temperature is above -2.5ºC, another air temperature threshold is set at 1.5ºC to determine snow unloading (Figure 2.5; Table 2.1 Regime D). This creates two groups in decision node 3 regime A, where air temperatures

between -2.5 and 1.5ºC result in snow staying in the canopy, and temperatures above 1.5ºC result in snow unloading from the canopy.

2.3.2.2. Predicting canopy-snow unloading.

We trained a random forest classification model to predict if snow will stay in the canopy or unload based on meterological conditions. While the model was trained on various subsets of the data to prevent overfitting, we can visualize the predictive capacity of the model on the full snow unloading dataset (Figure 2.6). We visualize where the global thresholds (Figure 2.5) fall on the distributions of meteorological variables for both observations and the random forest model prediction of snow staying and snow unloading from the canopy (Figure 2.6).

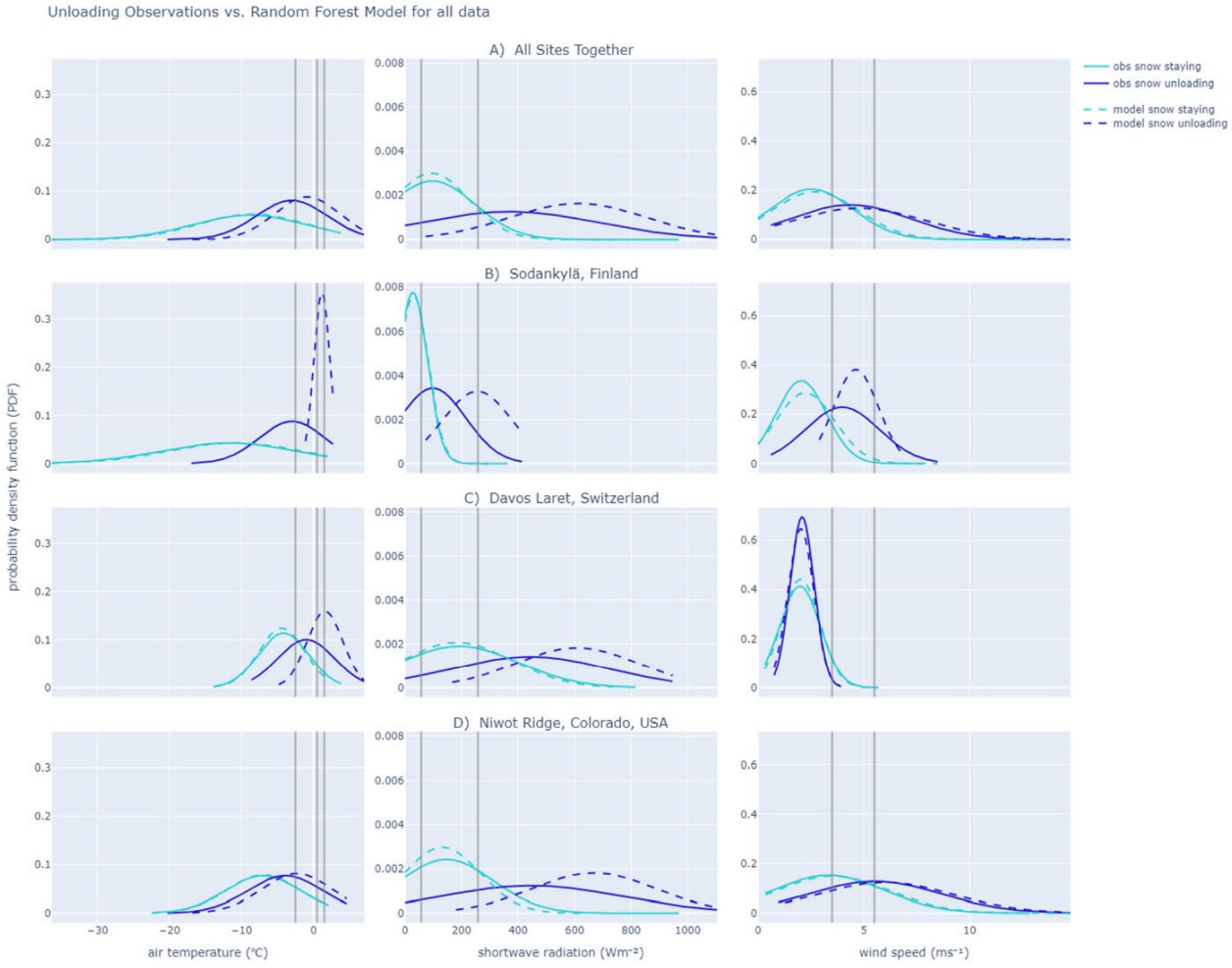

Figure 2.6. *Probability density functions (PDFs) of snow staying in the canopy, in blue, and snow unloading, in purple, for air temperature, ºC, shortwave radiation, Wm^{-2}, and wind speed, $m\ s^{-1}$, for A) all the sites together, B) Sodankylä, Finland, C) Davos Laret, Switzerland, and D) Niwot Ridge, Colorado, USA. Solid lines represent PDFs from observations, and dashed lines represent PDFs from the random forest model prediction. The threshold values determined by the decision tree in Figure 2.5 are indicated as vertical grey lines.*

The random forest model predictions of snow staying closely match the observations of snow staying across all meterological variables and sites (Figure 2.6). Compared to the random forest model predictions of snow unloading which closely match observations of snow unloading during periods of low wind speed and shortwave radiation, but overestimates snow unloading during times of high shortwave radiation (Figure 2.6). Since snow unloading is a relatively fast process, there are more observations of snow staying in the canopy in our dataset (i.e., 1288 timesteps) compared to snow unloading (i.e., 446). In addition, a third of the shortwave radiation values in our dataset are in mid-winter arctic conditions and therefore contain a high number of observations in low shortwave radiation conditions. As a result of these factors, the random forest model had more observations of snow staying to learn what meteorological conditions often occur when snow stays in the canopy, compared to unloading. Another reason the random forest model is better at predicting snow staying compared to snow unloading is because the meterological conditions that occur while snow is staying in the canopy are often more consistent compared to the high variability of meteorological conditions that can occur over short periods of snow unloading (i.e., sudden increases in wind speed to unload snow from the canopy).

The wind speeds at Davos Laret never surpass the threshold for snow unloading identified for mid-latitude climates, which is why we rarely observed snow unloading from wind alone at this location (Figure 2.6C). Shortwave radiation at Sodankylä is often below the first shortwave threshold of 258.0 Wm^{-2}, which explains why did not observe shortwave radiation driven unloading at this location (Figure 2.6B).

2.3.3. Effectiveness of the unloading regimes.

The physical processes that remove snow from the canopy are not equal in how efficient they are in removing snow from the canopy. If an unloading event only partially removes snow from the canopy, compared to fully removing snow from the canopy, this impacts the canopy-snow albedo feedback of that unloading event (Webster & Jonas, 2018). While we cannot determine the amount of snow in the canopy with our dataset, we can determine if the unloading event results in a partial or a full unloading of snow from the canopy. We define a partial unloading event as snow remaining in the canopy after unloading occurs over some continuous amount of time, and a full unloading event as all the snow being removed from the canopy as a result of the unloading over some continuous amount of time. We use this additional classification on the snow unloading observations to determine how effective each unloading regime is at unloading snow from the canopy (Figure 2.7).

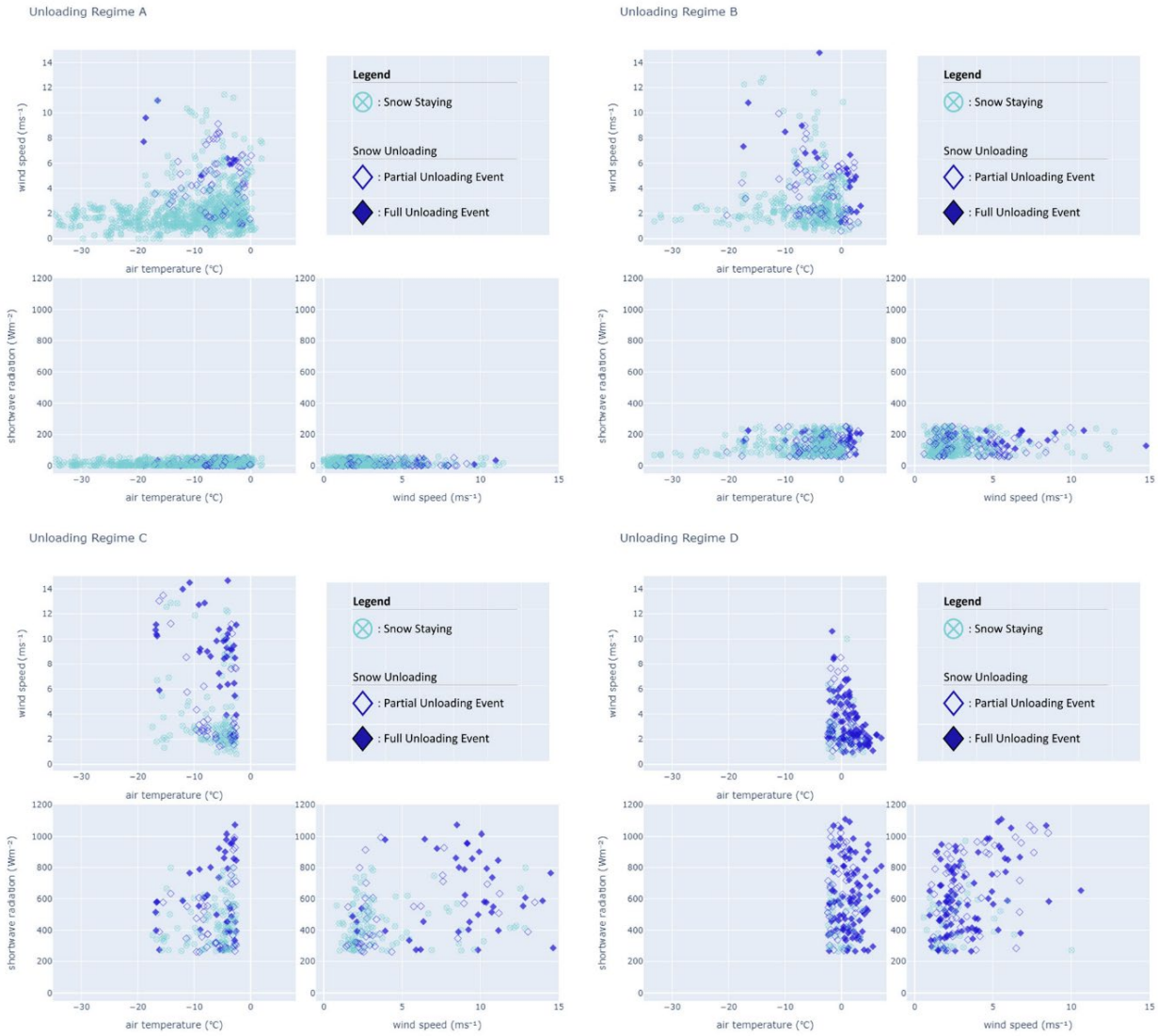

Figure 2.7. *Scatter matrix of snow staying in the canopy, in light blue, and snow unloading, in dark blue, for air temperature, ºC, shortwave radiation, Wm^{-2}, and wind speed, m s^{-1} for each unloading regime A, B, C, and D (Figure 2.5; Table 2.1). Each snow unloading event is classified as either a partial unloading event, empty diamond, where the canopy remained partially snow covered or a full unloading event, full diamond, where the continuous unloading event resulted in all of the snow leaving the canopy.*

When snow is unloading during unloading regime A, the result is almost all partial unloading events making this regime the least effective at removing snow from the canopy (Figure 2.7A). Unloading regime B is similar but with more total unloading events (Figure 2.7B). The only full unloading events that happen in unloading regime A and B happen when air temperature is near freezing or when a combination of very cold temperatures and high wind speeds occur simultaneously (Figure 2.7AB). We see a clear shift in unloading efficiency when looking at unloading regimes C and D, compared to A and B (Figure 2.7). Unloading regime C results in a mix of partial and full unloading events, mostly associated with high wind speeds, or increased

shortwave radiation (Figure 2.7C). Finally, unloading regime D is the most efficient at removing snow from the canopy with nearly all full unloading events, specifically above 1.5ºC. Previous observations of snow unloading report snow rapidly unloading when air temperature is above 0ºC (Nakai et al., 1994), which has gone on to inform unloading parameterizations such as Roesch et al. (2001). While our findings from unloading regime D are in alignment with these observations, air temperature rising above 0ºC is not the only method for snow unloading from the canopy, and thus, it cannot be the only method for unloading considered in model formulations.

2.4. Discussion.

2.4.1. What physical processes do the unloading regimes represent?

Our results show that in arctic climates, represented by very low shortwave radiation conditions, wind speeds as low as 3.5 ms^{-1} can cause snow unloading (Table 2.1 Regime A). In these conditions, the snow in the canopy often has a low moisture content, making it prone to blowing off at lower wind speeds because the snow crystals have not formed strong bonds to each other. While previous studies have observed less snow interception when wind speeds exceed 2.0 ms^{-1} (Miller, 1962), we are not aware of any wind dependent snow unloading observations near this low threshold. In comparison, our results show that in mid-latitude climates (represented by higher shortwave radiation), wind speeds of 5.5 ms^{-1} are needed to unload snow from the canopy (Table 2.1 Regime C). Previous observations closely align with this threshold value for wind unloading, where snow unloading in previous studies was observed at wind speeds greater than 5 ms^{-1} (Betts & Ball, 1997).

Our results suggest that once temperatures exceed -2.5ºC in mid-latitude climates, temperature controls the unloading regime, and wind speed does not have as strong of an impact on snow in the canopy. Instead, during these conditions, the only way to remove snow from the canopy is for it to melt out once the air temperature exceeds 1.5ºC. However, when the air temperature is between -2.5ºC and 1.5ºC, our results show an increase in observations of snow staying in the canopy. This temperature range closely aligns with previous snow interception observations which observed an increase in cohesion and adhesion of snow crystals between -3ºC and 0ºC (Kobayashi, 1987). The phenomenon of snow cohesion and adhesion changing with temperature is well studied, and previous observations have shown that the increase in snow cohesion in this temperature range leads to an increase in snow interception in the canopy (Bunnell et al., 1985). Another possible explanation for an increase in snow staying in the canopy at this temperature range is that snow gets glued onto the canopy through ice layers, and it takes more warming to remove that stuck-on snow from the canopy.

Regardless of the physical processes causing snow to stay in the canopy in this temperature range, the concept should be included in unloading models. While some snow interception (i.e., loading) models have adapted this into the empirical equations, the same idea has not been included in any unloading models. Lundquist et al. (2021) recommends that all interception models should represent the increase in loading due to increased adhesion and cohesion of snow in the canopy when temperatures range from -3ºC to 0ºC. Based on our results, we recommend that the same idea be included in the snow unloading models, where unloading decreases in this

temperature range and other factors such as wind dependent unloading, have less of an impact until temperatures increase enough to fully melt snow from the canopy.

2.4.2. How do our thresholds compare to values used in exisiting canopy-snow unloading models?

We found that the threshold for wind dependent unloading in the arctic is 3.5 ms^{-1}, compared to 5.5 ms^{-1} in mid-latitudes. While the threshold for air temperature dependent unloading in the arctic is simply near freezing, at 0.5ºC, the thresholds are more complicated for unloading in mid-latitudes. If a single threshold is considered for temperature, then a threshold of -2.5ºC provides the most variance between snow staying and snow unloading from the canopy. However, our results show that an additional temperature threshold should be considered for warm air temperatures above -2.5ºC where snow is more likely to stay in the canopy between -2.5 and 1.5ºC, then fully unload once air temperatures exceed 1.5ºC.

In previous work, we evaluated three commonly used unloading parameterizations and found that each model required site specific calibration (Lumbrazo et al., 2022). When only default parameter values were used, we found that the wind and temperature dependent unloading model, Roesch et al. (2001), performed better than Andreadis et al. (2009) and Hedstrom & Pomeroy (1998). The Roesch et al. (2001) model is comprised of two functions that operate independently of each other, where wind dependent unloading occurs once wind speeds exceed a wind speed threshold, with a default value of 5 ms^{-1} and the temperature dependent unloading occurs once temperatures exceed a temperature threshold, with a default value of -3ºC. These default values closely match the values from the unloading regimes C and D (Figure 2.5) in this study, which represent unloading regimes in mid-latitude climates. The Roesch et al. (2001) model was informed by a number of observations, such as Nakai et al. (1994), who observed snow rapidly unloading when air temperatures exceeded 0ºC in Sapporo, Japan, and Betts & Ball (1997) whom never observed high albedos in BOREAS canopies when wind speeds exceeded 5 ms^{-1} (Lundquist et al., 2021). This unloading parameterization is in commonly used hydrologic models, such as VISA, CLM, Noah MP (Lundquist et al., 2021), and SUMMA v3.0 (Lumbrazo et al., 2022), where the default parameter values are often hardcoded.

The results from this study provide insights into how the thresholds for wind and temperature dependent unloading can be improved to capture unloading regimes across many climates by thresholding regimes by shortwave radiation. For example, the thresholds for temperature and wind dependent unloading in models can be adapted to vary depending on incoming shortwave radiation (Decision Node 1; Figure 2.5). If shortwave radiation is below 258.0 Wm^{-2}, then the thresholds can follow those outlined in unloading regimes A and B (Figure 2.5AB), and if shortwave radiation is above 258.0 Wm^{-2}, then the thresholds can follow values from unloading regimes C and D (Figure 2.5CD). Additional empirical changes could be made to account for the different unloading regimes, such as the wind dependent unloading function being inactive while air temperatures are in the increased snow cohesion and adhesion temperature zone, since snow will not easily blow out of the canopy and would need to melt out to be removed.

2.4.3. What physical processes are not captured in our unloading regimes results?

Our canopy-snow unloading dataset provides insights into the meteorological conditions that occur during snow unloading in multiple climates that have not been compared directly before. While this dataset includes snow unloading an arctic climate and mid-latitude climates, it does not include observations from a maritime climate. Thus, the meteorological conditions that occur in maritime climates that impact canopy-snow unloading, such as rime ice formation in the canopy, are not represented in these results. Observations from timelapse cameras provide the opportunity to look at snow unloading over larger spatial and temporal scales than previously observed. However, there are limitations to using timelapse photography. For example, these methods are sensitive to the location and orientation of the timelapse camera, and thus, we do not fully capture localized shortwave radiation impacts. Additionally, we are simply observing the timing of snow unloading and not the amount of snow unloading from the canopy. Canopy-snow unloading is a complex physical process, and other features such as differences in tree species and canopy structure can impact snow interception and unloading between climates.

2.5. Conclusions.

Canopy-snow interception and subsequent unloading is a complex physical process that is difficult to model and evaluate due to lack of observations. Timelapse photography can provide information about conditions at a site, including observations of the timing of snow unloading from the canopy. This study provides a dataset of snow unloading across three different climates that can be used to evaluate exisiting model formulations or develop new models. We combined the observations and meteorological data from the three sites into a single dataset to determine what meteorological variable thresholds determine snow unloading globally. We ran a random forest model on this dataset to predict snow unloading from air temperature, shortwave radiation, and wind speed.

Our results identify four primary unloading regimes, that vary the thresholds for wind and temperature dependent unloading by climate and shortwave radiation. We found that during times of little shortwave radiation, such as the mid-winter arctic, wind speed is the strongest predictor of snow unloading at a threshold of 3.5 m s^{-1} and during times when shortwave radiation ranges from 57 Wm^{-2} to 230 Wm^{-2}, air temperature is the strongest predictor of snow unloading at 0.5ºC. When shortwave radiation is above 230 Wm^{-2}, such as mid-winter conditions in mid-latitude climates, we found air temperature is the strongest predictor of snow unloading. During the cold temperature unloading regime, snow starts unloading at wind speeds of 5.5 ms^{-1}. During the warm temperature unloading regime, snow is more likely to stay in the canopy between -2.5 and 1.5ºC, then fully unload once air temperatures exceed 1.5ºC.

Our threshold values for mid-latitude unloading closely align with Roesch et al. (2001) default threshold values for temperature and wind dependent unloading. However, these results highlight how those thresholds vary with climate (i.e., shortwave radiation). Additionally, our results determined a secondary temperature threshold for unloading in mid-latitude climates which aligns with the well-known fact that snow cohesion and adhesion increases with increasing temperatures between -3ºC to 0ºC. Lundquist et al. (2021) recommends that all interception models should represent the increase in loading due to increased adhesion and cohesion of snow in the canopy when temperatures range from -3ºC to 0ºC. Based on our results, we recommend

that the same idea be included in the snow unloading models, where unloading decreases in this temperature range and other factors such as wind dependent unloading, have less of an impact until temperatures increase enough to fully melt snow from the canopy in mid-latitude climates.

While we identified four primary unloading regimes, we highlight that they do not unload snow with the same efficiency. We found that wind dependent unloading that occurs during very low shortwave radiation mainly results in partial unloading events, compared to temperature dependent unloading in mid-latitudes which often result in full unloading events. While we cannot quantify the amount of snow in the canopy, previous studies have demonstrated that there are large spatial and temporal variations in the canopy-snow albedo when the canopy snow cover transitions from snow covered to snow free (Webster & Jonas, 2018). Thus, the differences in how effective each unloading regime is at unloading snow from the canopy can have impacts on the albedo feedback to the atmosphere and should be a topic of future research.

2.6. Additional Information.

2.6.1. Data Avaibility.

The unique canopy-snow unloading dataset created in this research will be published with the manuscript. Please do not hesitate to reach out to the authors for the dataset ahead of publication. We believe this dataset provides important insights into global canopy-snow unloading patterns and can be used to develop and validate model parameterizations.

2.6.2. Funding and Acknowledgements.

This research was funded by the Valle Scholarship & Scandinavian Exchange Program. A special thank you to Clare Webster for hosting me in Oslo, Norway and to the entire forest-snow research group at WSL Institute for Snow and Avalanche Research SLF for letting me join on your arctic field campaign in Finland, which inspired this research.

Chapter 3. Combined effects of forest cover and topography on snow depth in the Eastern Cascades, Washington, USA

Cassie Lumbrazo[1], Susan Dickerson-Lange[2], Emily Howe[3], Jessica Lundquist[1]

[1]Civil and Environmental Engineering, University of Washington, Seattle, Washington, USA

[2]Natural Systems Design, Seattle, Washington, USA

[3]The Nature Conservancy of Washington, Seattle, Washington, USA

Notes. This chapter was submitted to the Washington State Department of Natural Resources as a final report in August 2023. The only differences are in the section, figure, and table numbering.

Executive Summary.

A major challenge that the Washington Department of Natural Resources (WA DNR) faces in implementing its 20 Year Forest Health Strategic Plan is to address climate impacts related to wildfire and water scarcity, while also maintaining habitat for fish and other wildlife species that depend on forest-mediated hydrologic regimes.

Salmonid populations are threatened by climate change, as reduced and earlier snowmelt leads to lower flows and less cold water for habitat. In the Pacific Northwest, reducing forest canopy cover through management is a viable climate adaptation strategy to offset this change, as forest change can alter snowmelt and streamflow timing as much as climate change. However, the magnitude and direction of this effect varies drastically with winter temperatures and local topography. A decreasing snowpack also contributes to larger and more intense wildfires. While thinning is being widely implemented to reduce wildfire hazards, less attention has been given to the impact of these actions on hydrologic resilience and snow storage.

This project investigates how the spatial distribution of forest canopy thinning prescriptions for fire resilience influences hydrologic resilience in Washington State's Eastern Cascade Mountains. The project builds on four years of collaboration with Dr. Jessica Lundquist, Dr. Susan-Dickerson Lange, Dr. Emily Howe, and Cassie Lumbrazo (PhD Candidate). The study sites encompass the NCALM Hydrologic Effects of Forest Restoration snow-on lidar dataset (Lumbrazo, 2021). The area overlaps with previous forest-snow ground monitoring efforts (Dickerson-Lange et al., 2023), in a climate transition zone, from warmer and wetter on the western slopes to colder on the eastern slopes of the Cascades.

Multiple features often interact with forest cover at the landscape scale to influence snow depth. Thus, we calculate topographic metrics based on elevation, slope, and aspect to consider in conjunction with forest cover in predicting snow depth. We ran a Random Forest model on the lidar data in distinct elevation zones to determine which metrics are the strongest predictors of snow depth in each elevation zone.

We found that both topographic position and canopy cover matter for snow depth in the Eastern Cascades, where the most snow at all elevations is found in topographically shaded gaps. Distance to canopy edge is the strongest predictor of snow depth in warmer, low elevation terrain (< 1000 m), with large gaps, greater than half the average tree height, on shaded slopes having significantly deeper snow. Topographic shading, determined by slope angle and slope aspect, is important at all elevations but becomes more important with increasing elevation. In middle to high elevations (> 1000 m), forest gaps in topographically shaded locations also accumulate the most snow. However, the size of the gap does not matter at these higher elevations.

We provide the project overview and background information (Section 1, named 3.1), the methods for processing the pre-treatment lidar data (Section 2, named 3.2), the results from the Random Forest analysis (Section 3, named 3.3), and a description of fieldwork performed in the post-treatment forest (Section 4, named 4.3). We provide links to all the software, code, and data required to reproduce this analysis (Section 5, named 5.3 and Appendix). In particular, we provide detailed guides on how to calculate all of the topographic and forest metrics used here

for any region with snow-off lidar data, to aid in planning of forest treatments across the Washington Eastern Cascades.

3.1. Section 1. Introduction.

3.1.1. Project Overview

Salmonid populations are threatened by climate change, as reduced and earlier snowmelt leads to lower flows and less cold water for habitat (Isaak et al., 2012) In the Pacific Northwest, reducing forest canopy cover through management is a viable climate adaptation strategy to offset this change. Forest change can alter snowmelt and streamflow timing as much as climate change, but the magnitude and even direction of the effect varies drastically with climate and topographic position. Hydrologic modeling studies have shown the Eastern Cascades to be especially sensitive to forest treatments (opening gaps or cutting strips) enhancing late-season streamflow (Currier et al., 2022; Sun et al., 2020), but we currently lack the observations necessary to evaluate these model results, which is necessary assess to what extent they can be trusted for management.

Seasonal snowpack, which drives hydrological flows and thermal regimes critical for aquatic species (Cline et al., 2020), has declined over the last century because of climate change (Mote et al., 2005, 2018), and these losses are projected to continue (Musselman et al., 2017, 2018). Washington's Cascades snowpack is projected to decrease by 50% over the next 70 years (Duan et al., 2017; Li et al., 2017), in tandem with earlier melt-timing and decreased snowmelt-driven peak flow. Flow timing and velocity are critical to transport juvenile fish through tributary rivers of the Columbia River. In the Yakima basin, as few as 20% of the out-migrating juvenile Chinook survive the reach between Prosser Dam and the Columbia River due to thermal stress and predation. Fish migrating through colder, faster reaches of the rivers generally have survival rates of 90%. Thus, earlier outmigrants have higher survival rates, whereas fish out-migrating from headwater systems past early May has mortality rates near 100% (Kock et al., 2016). Thus, if forest management can increase snowpack duration by a few days to weeks, there may be potential to impact the survivorship of endangered salmonids in these climate-threatened snowpack-dominated river systems. Species sensitive to snowpack melt timing and magnitude include ESA-listed Yakima Basin bull trout (threatened), Yakima Basin steelhead (threatened), Upper Columbia Spring Chinook (endangered), Upper Columbia Fall Chinook (threatened), and Pacific lamprey (WA State Species of Concern).

A decreasing snowpack also contributes to larger and more intense wildfires (Abatzoglou & Williams, 2016). Resource managers implementing strategic fuel treatments, such as forest thinning at landscape scales, can help decrease wildfire intensity and severity, improving forest resilience to fire, insects, and drought (Halofsky et al., 2020). While thinning and prescribed burns are being widely implemented to reduce wildfire hazards, less attention has been given to the impact of these actions on hydrologic resilience and snow storage.

The sensitivity of snow accumulation and melt processes to climate change varies spatially, thus predictions for the net effects of change in forest cover on snow storage are site specific (Gleason et al., 2013; Harpold et al., 2020; Lundquist et al., 2021; Sanmiguel-Vallelado et al., 2022). Dickerson-Lange et al. (2021) and Lundquist et al. (2013) demonstrated that the overall effect of

forests on snow storage and duration varies significantly across the landscape, ranging from snow persisting several weeks longer in forest gaps, where more snow accumulates due to lack of canopy-snow interception, to two weeks longer under forest canopy, where ablation rates may be diminished due to shading and wind protection. This implies that forest management actions should not be adopted uniformly without careful attention to supporting empirical evidence and location-specific modeling. Currently, the eastern Cascades represents a data gap in this arena, making it difficult to predict the large-scale landscape effect of wildfire treatments on stream flow timing and magnitude. Forest hydrology models commonly used in Washington State, such as DHSVM, will benefit from empirical data and statistical relationships derived from observations.

Accurately modeling the landscape-scale effect of forest canopy-snowpack interactions is particularly important for the river systems on the eastern flanks of the Cascades because:

1. These rivers are snowpack-dominated systems, with the Yakima River depending on snow for 70% of its instream flow; and

2. ESA-listed salmonids are critically dependent on the flow timing, magnitude, and temperatures associated with snowpack-dominated watersheds to regulate their in-stream growth, juvenile outmigration timing, adult return migration ability, and spawning success.

3.1.2. Project Background.

The upper Yakima watershed is a critical area for endangered salmonids. The Nature Conservancy (TNC) purchased this land because of its high importance for snow, water, and fish, and the Yakama Nation and many other groups have invested in substantial aquatic restoration in this area. The research presented here builds on four years of collaboration between Dr. Jessica Lundquist's lab (University of Washington), Dr. Susan Dickerson-Lange (at Natural Systems design), and Dr. Emily Howe at The Nature Conservancy (TNC). The study area is centered on Cle Elum Ridge (CER), WA, an east-west running ridge with an elevation of 1000m at the headwaters of the Yakima River, where TNC owns and manages 48,000 acres of high elevation forest in collaboration with the Tapash Forest Collaborative.

Located just east of the Cascade crest, this basin is climate-vulnerable due to its heavy dependence on snowpack and its relatively low elevation headwaters (Donley et al., 2012). The region represents a data gap in forest-snow observations (Dickerson-Lange et al., 2021), and in our understanding of how changes in forest canopies can impact snowpack, streamflow, and water temperature.

To fill this data gap, TNC, Dr. Dickerson-Lange, and Tapash partners collaboratively set up a field data collection program to observe the combined influence of forest canopy density and slope aspect on the magnitude and duration of snow in this region. To establish large-scale patterns in forest-snow interactions, the team collected 3-yrs of open/closed canopy snow observations at 6 SNOTEL sites stratified across the Cascade Crest (Dickerson-Lange et al., 2023). These were complemented by 2-yrs of forest-snow observations at CER to establish secondary effects of slope and aspect, and across a gradient of canopy characteristics (open, closed, thinned) and topographic positions during water year (WY) 2020. On 1 April 2021, graduate student Cassie Lumbrazo obtained snow-on lidar data over the area, observing snow

depth spatial patterns at meter spatial resolution across the area. Through a collaborative process, the Tapash executive team also identified a need for patch-level prescriptions to make forest-snow observations more relevant to forest managers. In response, the team co-produced an experimental design with TNC foresters, and have implemented 6-levels of thinning prescriptions, representing a gradient of heavy to light thinning (Basal Area Factor: 20, 50, 60, 70, 80, 120) on north and south slope aspects of CER. Thinning levels reflect practicable forestry prescriptions for fire resilient dry forests. The experimental unit design minimizes differences in elevation and heat load index (McCune & Keon, 2022).

A major challenge that WA DNR and our partners face in implementing the 20 Year Forest Health Strategic Plan is the need to address climate impacts related to wildfire and water scarcity, while also maintaining habitat for fish and other wildlife species that depend on forest-mediated hydrologic regimes. This project investigates how the spatial distribution of forest canopy thinning prescriptions for fire resilience influences hydrologic resilience (i.e., streamflow favorable for fish) in Washington State's Eastern Cascade Mountains. The project builds on four years of collaboration with Dr. Jessica Lundquist, Dr. Susan-Dickerson Lange, Dr. Emily Howe, and Cassie Lumbrazo (PhD-candidate).

The project is centered on Cle Elum Ridge, where:

- TNC has collected 3 years of snowpack-tree canopy observations.
- Cassie Lumbrazo has collected snow-on Lidar data through a graduate student grant from NSF's National Center for Airborne Laser Mapping (NCALM).
- TNC has recently installed a series of experimental forest stand units representing different levels of thinning intensity of two slope aspects.

3.1.3. Final Report Overview.

Below is the scope of work for this research.

Activity 1: Baseline High-resolution Forest-snow Analysis

The overarching research question is how the spatial implementation of forest prescriptions intended to promote fire resiliency influences snow duration and streamflow, with the goal of providing GIS-based maps indicating where on the landscape prescriptions promote the hydrologic resiliency necessary to promote fish survival. To answer this question, we must understand the spatially explicit pre-prescription forest-snow-hydrology relationships before we can assess observations post-prescription.

1. Using the first snow-on Lidar for the Washington Cascades, collected in April 2021, we leverage existing snow depth and duration observations to analyze and develop predictive relationships between snowpack depth, topography, weather, and forest canopy characteristics. The study area includes the extent of the snow-on Lidar flight, which includes Cle Elum Ridge, Sassie Ridge, and Fish Lake- all located in the headwaters of the Yakima Basin in the Eastern Cascades.

2. We then use the lidar, in conjunction with surface observations, to develop geographic predictors of forest-snow interactions and the likely response resulting from thinning or burning prescriptions. These predictive maps and relationships will be available to all practicing forest management in the Cascades, and will provide the baseline hypotheses for designing and testing forest treatments in the east-slope Cascades snow zone.
3. A follow-up project funded by TNC will immediately evaluate these results over areas where forest thinning is taking place in 2022. We will engage in fieldwork at the treatment sites to understand the forest prescriptions and how they fit into the geospatial analysis.

We address Activity 1.1. in Sections 3.2 and 3.3.1. In Section 3.2, we provide methods for processing the pre-treatment snow-on NCALM lidar dataset, and in Section 3.3.1 we discuss the processed lidar datasets. We address Activity 3.1.2. in Section 3.3.2, where we discuss the statistical results of a Random Forest machine learning model. Finally, we address Activity 3.1.3 in Section 3.4. In Section 3.4 we describe the fieldwork performed to evaluate the post-treatment forest-snow relationships on Cle Elum Ridge, including snow-monitoring stations and stream sensors.

3.2. Section 2. Methods and Study Sites

3.2.1. Introduction

In Section 3.2, we provide methods for processing the snow-on lidar dataset in Section 3.2.2 and the statistical methods we use to analyze the high-resolution dataset in Section 3.2.3. These methods can be applied to any lidar dataset with snow-on and snow-off data over the same region. The exact steps to reproduce these methods in ArcGIS Pro can be found in Appendix 1 and are performed step-by-step in a recorded **YouTube video.**

3.2.2. Lidar Data Processing Methods.

3.2.2.1. Standard Lidar Metrics.

Lidar data point clouds are typically processed into two main raster datasets: a digital terrain model (DTM) and a digital surface model (DSM). The DTM represents the bare Earth, excluding all the above ground features, while the DSM represents the bare Earth while including all the above ground features. In forested regions, the DTM represents the bare Earth without forest cover, and the DSM represents the forest surface structure (Figure 3.1). The elevation value of the DTM is often referred to as a digital elevation model (DEM).

We use snow-off lidar data from the WADNR lidar portal and snow-on lidar data from NCALM for our study sites (Lumbrazo, 2021). Snow-off lidar flights refer to a lidar flight flown without snow on the ground, and snow-on lidar flights refer to a lidar flight flown when snow is on the ground. Snow-off lidar covers the bare earth (snow-off DTM) and the surface features (snow-off DSM), while snow-on lidar covers the snow surface (snow-on DTM) and surface features (snow-

on DSM). In areas where there is no canopy present, the snow-on DSM represents the snow-surface elevation (not the ground surface).

We calculate snow depth by differencing the snow-on DTM and the snow-off DTM (Figure 3.1). Errors often arise when differencing two different lidar datasets (Shean et al., 2016). The datasets are often from different sources, who process the raw lidar point clouds differently and produce gridded raster datasets in different spatial resolutions, with different geoids and projections. If the two datasets are even slightly off in their horizontal geolocation (even a few centimeters), then the difference between being on top of a steep cliff and at the bottom of it could result in a 10+ meter vertical error. It is important that we account for these errors because snow depth varies horizontally and vertically on a landscape. Thus, we remove snow depth values that are greater than 3 standard deviations from the mean to account for these errors (Hu & Shean, 2022).

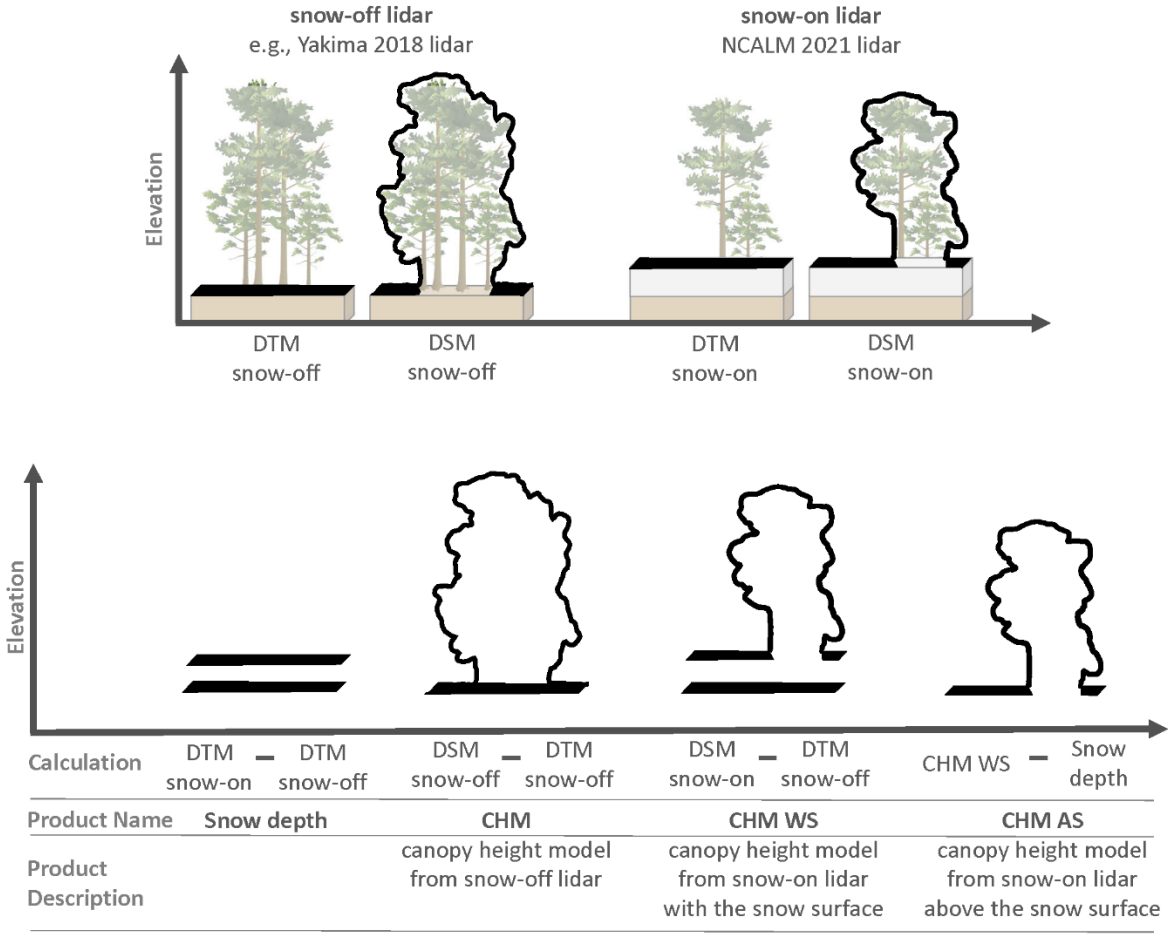

Figure 3.1. *Conceptual diagram of the difference between a digital terrain model (DTM) and digital surface model (DSM) for snow-off and snow-on lidar datasets. The model surface for each is in black, which captures either the bare-earth in brown, the snow surface in white, or a combination of the bare-earth or snow surface, and canopy surface structure in green. We show the calculations performed on those datasets during anaylsis.*

Typically, a canopy height model (CHM) is derived by differencing the DSM from the DTM from snow-off lidar flights (Figure 3.1). Since our snow-on lidar flight is more recent in time, it captures the exact forest structure at the time of snow depth, and since we are interested in the relationship between forest structure and snow, it is important for our analysis to use the most recent forest structure to compare with snow depth. However, if someone reproducing this analysis has a more recent snow-off lidar dataset that represents the true canopy structure at the time of the snow-on lidar flight, then we recommend using the snow-off DSM and snow-off DTM to calculate the snow-off CHM instead.

Since the snow-off lidar data for our site does not represent the forest structure at the of time the snow-on lidar flight, we proceed by calculating a canopy height model with the snow surface (CHM WS) by differencing the snow-on DSM and the snow-off DTM, to produce a canopy height model which includes the snow surface (Figure 3.1). The CHM WS represents the true height of the canopy at the time the snow-on lidar data was collected, but the height of pixels in open regions represents the snow surface height (not the ground surface height).

In further analysis, we need to discern forest pixels from open pixels with a canopy height threshold (typically set at 2 meters, see below). However, if we threshold the CHM WS at 2 meters, then we could risk classifying deep snow in open regions (that is > 2 meters) as forest pixels. Thus, we calculate a final CHM product by subtracting snow depth from the CHM WS to produce a canopy height model above the snow surface (CHM AS) to use in future analysis. The result is the most recent canopy structure information (that does not represent the true height) where pixels in the open simply have a height of 0 m (Figure 3.2).

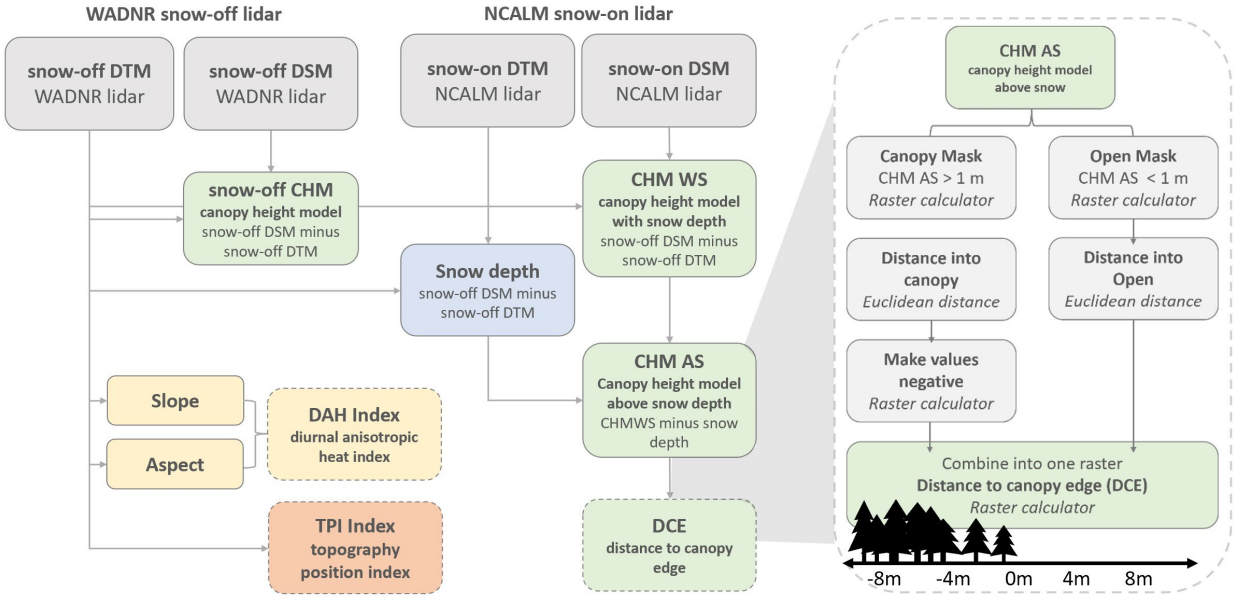

Figure 3.2 *Conceptual diagram for processing the pre-treatment snow-on lidar data.*

This method of using CHM AS (rather than the CHM from the snow-off lidar data) can introduce error in regions with very deep snow where the snow completely buries the canopy. For our sites, the deepest snow is in regions without canopy cover, and in forested regions, the snow depth is

rarely above 3 meters. Recent literature on forest-snow interactions discerns between under-canopy and outside-canopy with a 2-meter threshold above the bare Earth surface from a CHM (Currier & Lundquist, 2018; Tennant et al., 2017). To provide a similar calculation, we proceed with a 1-meter threshold above the snow surface from a CHM AS in our main canopy metric (see Section 3.2.2.2). This metric does not consider the full height of the canopy, which reduces errors associated with using a CHM AS. Additionally, some of the snow-off lidar data for our sites is 7 years old in a forest that is actively being managed. Thus, the benefit of using the most recent canopy structure to determine the forest-snow relationships far outweighs any errors that are introduced.

Furthermore, we can compare the snow-off CHM and the snow-on CHM to see the difference in forest structure between the two flights. In situations where there is a short time-lag between snow-off and snow-on data flights or limited changes in canopy structure occurred (e.g., no wildfires, forest structure changes such as logging, etc.), then one can proceed with the snow-off CHM for the remainder of the analysis. We proceed with the snow-on CHM AS to minimize errors from changes in forest structure between the snow-off and snow-on lidar data collections.

3.2.2.2. Calculated Lidar Metrics.

We are interested in the relationship between forest cover and snow depth for our sites, but often multiple variables interact with forest cover at the landscape scale to influence snow depth. Thus, we calculate other important factors such as elevation, slope, aspect, and topography to consider with forest cover in predicting snow depth. Elevation, slope, and aspect are readily computed by any GIS program, and additional specialty metrics are defined below. The step-by-step instructions to reproduce this analysis in ArcGIS Pro can be found in Appendix 1 and are performed step-by-step in a recorded YouTube video.

We calculate the diurnal anisotropic heating index (DAH) to capture the landscape scale ablation effects estimated from slope aspect and slope angle (Cristea et al., 2017). We calculate DAH as,

$$DAH = \cos(\alpha_{max} - \alpha) * \arctan(\beta),$$

where α_{max} = 202.5° (SSW) is the slope aspect that receives the most heat, and α is the slope angle. DAH ranges from negative one to one and is zero in flat terrain. The highest DAH values are on steep southwest-facing slopes, and lowest are on steep north-facing slopes (Figure 3.2; Cristea et al., 2017). We hypothesize that snow will be deeper where DAH is negative because it is shaded from the sun and that snow depth will be shallower where DAH is positive because of heating from the sun. However, we expect this effect to depend on elevation, where DAH has a stronger relationship to snow depth in elevation bands that are warm enough for mid-winter melt.

We calculate the topographic position index (TPI) to capture the concave and convex features in the land surface that are strong predictors for snow depth spatial variability (Figure 3.2; Cristea et al., 2017; Weiss, 2001). We calculate TPI as,

$$TPI = z_0 - z_{mean}, \qquad where\ z_{mean} = \left(\frac{1}{n_R}\right)\sum_{i \in R} z_i,$$

where z_0 is the elevation of a given grid cell, and z_{mean} is the mean elevation surrounding the given grid cell made up of R cells (Cristea et al., 2017). TPI is a measure of relative position of a DEM grid cell to the mean elevation of surrounding grid cells (Revuelto et al., 2014; Weiss, 2001). A negative TPI value indicates that a given grid cell is lower than the surrounding mean elevations, and a positive TPI value indicates a given grid cell is higher. We hypothesize that snow is deeper in locations with a negative TPI and shallower in locations with a positive TPI because snow blows from ridges into depressions to smooth the landscape (Filhol & Sturm, 2019).

We calculate the distance to canopy edge (DCE) to capture the forest cover impact on snow accumulation and ablation. We calculate DCE from the CHM AS, following the steps described in Appendix 1. We follow similar methods to those described in Mazzotti et al. (2019), where every grid cell is assigned a value for the distance is it to a canopy element (Figure 3.2). The DCE is a distance, in meters, from the canopy, where the edge of the canopy is defined as zero. Grid cells in the open are increasingly positive away from the canopy edge, and grid cells under the canopy are increasingly negative. The larger the positive number, the larger the gap, and the larger the negative number, the denser the surrounding forest.

3.2.3. Lidar Data Statistical Methods.

3.2.3.1. Spatial Autocorrelation.

The large sample size from high-resolution gridded raster datasets inhibits standard statistical methods from being used on the full resolution dataset. Spatial datasets such as snow depth often present strong spatial autocorrelation, which can bias the results of statistical techniques that presume independent samples. Spatial autocorrelation occurs when values closer in space are more similar than values further in space (Currier et al., 2019). Thus, we proceed with the following methods to reduce the sample size of the datasets to the point where the samples can be assumed independent.

First, we calculate Moran's Index (I) for the full-resolution snow depth data to determine if the dataset is spatially autocorrelated. Moran's I is a measure of spatial autocorrelation from negative one to positive one, where values between 0.25 and 0.5 indicate weak spatial autocorrelation and 0.7 to 0.9 indicate strong spatial autocorrelation (Currier et al., 2019).We calculate Moran's I with the ArcGIS Pro spatial autocorrelation tool, named Global Moran's I tool. Snow depth at all three of our sites presented strong spatial autocorrelation, with a Moran's I greater than 0.8 on the high-resolution, non-subsampled snow depth datasets.

We create a variogram of the snow depth datasets to determine the spatial extent of the autocorrelation at each site. A variogram is a spatial statistic function used to describe the degree of spatial dependence of a dataset. We produce a variogram of the snow depth raster datasets to determine the spatial extent of the snow depth autocorrelation (Figure 3.3a). We use the package xDEM (xDEM Contributors., 2021) to produce the variograms in python and subsample all the datasets at each site based on the result of the variogram (Figure 3.3b).

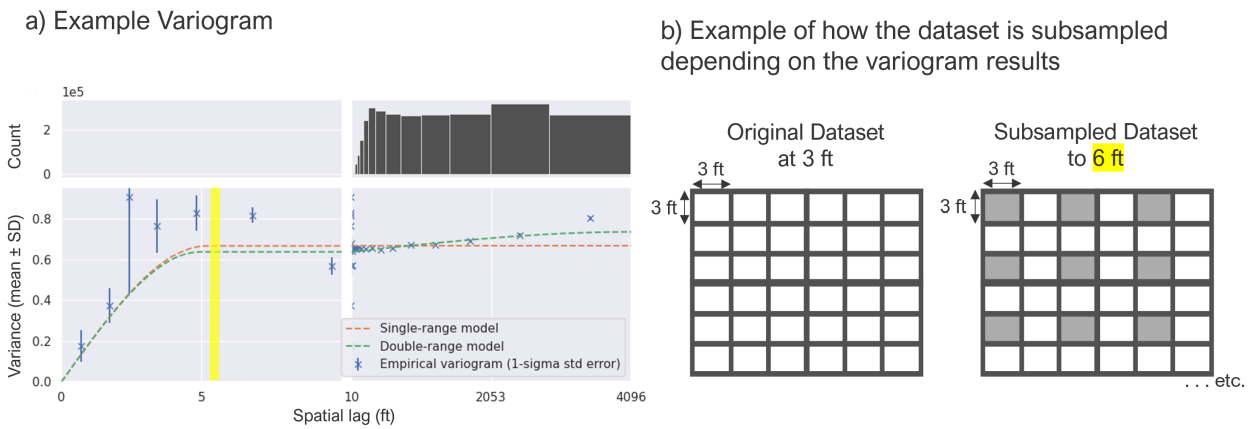

Figure 3.3. *a) An example variogram for one of the sites that represents the spatial lag of the raster dataset and b) represents how that dataset would be subsampled based on the variogram result.*

Finally, we recalculate Moran's I on the subsampled snow depth datasets to determine if they still present strong spatial autocorrelation. We repeat the steps of producing a variogram, subsampling based on the variogram, and calculating Moran's I until the value is below 0.5 for the datasets. The result is a sub-sampled dataset that does not present strong spatial autocorrelation and has a reduced sample size (Figure 3.3b). We use the subsampled dataset to proceed with further statistical methods and analysis.

3.2.3.2. Random Forest.

The goal of Activity 1.2 of this work is to use the snow-on lidar data to develop geographic predictors of forest-snow interactions in this region. In situations where the relationships between the input features (such as DEM, DAH, TPI, DCE) and the target outcome (snow depth) are not linear, linear regression or logistic repression models simply do not work (Molnar, 2023). However, decision tree models provide one method for working with complex feature interactions. Decision trees predict the value of the target variable by learning simple decision rules inferred from the data (Pedregosa et al., 2011). Decision trees are a simple to understand, non-parametric machine learning method since the results can be visualized intuitively. However, they are prone to overfitting; often overly complex trees are created that do not generalize the data well. They are known to have low bias but high variance which means a single decision tree can be unstable.

Thus, we mitigate this problem by running an ensemble of decision trees, called a Random Forest model. We combine all the data from all three sites into a single dataset with snow depth as the target variable for the model and DEM, DAH, TPI, and DCE as the input features. We run a Random Forest ensemble with 1000 iterations (which fits 1000 unique decision trees on various subsets of the dataset). We set the maximum depth of the decision trees in the model to three nodes and set the minimum number of samples required for the decision node to split (and subset the data again) to 2000 samples. Our goal is to capture the large-scale patterns of snow

depth across the landscape, thus requiring a minimum number of samples prevents the model from capturing isolated features with a small sample size (i.e., features such as large piles of snow next to a road from snow plowing). The maximum depth of any given decision tree may not be reached if the decision node cannot split into further subsets of the data with at least 2000 samples in each subset.

The Random Forest model uses averaging to improve the predictive accuracy of the decision tree and control over-fitting to the dataset (Pedregosa et al., 2011). Random Forest models have low bias and low variance since they run an ensemble of decision trees to reduce the high variability from a single tree. We determine the feature importance for each input feature from the entire ensemble of decision trees, but since the goal of Random Forest is to reduce the high variability of a single decision tree, there is not a single "best" decision tree result (Molnar, 2023).

We want to utilize the simply visualized results of a decision tree, while using the power of a Random Forest model to reduce the variance of a single decision tree. Thus, we visualize the "best" decision tree from the Random Forest model by evaluating the performance of the decision trees with the sklearn accuracy score metric (Pedregosa et al., 2011). We select the decision tree with the highest accuracy score as the final decision tree to visualize in the Random Forest results. This method provides the intuitive visualization power of a single decision tree, while reducing the variance associated with a single decision tree by running 1000 iterations to find a tree with the highest accuracy.

3.2.4. Study Sites.

The three study sites in this work are established by the NCALM *Hydrologic Effects of Forest Restoration, WA 2021* snow-on lidar dataset collected as part of a successful NCALM Seed graduate student grant written by Cassie Lumbrazo (Lumbrazo, 2021). We strategically identified sites in the proposal to overlap with three of the Eastern Cascades sites from previous forest-snow ground monitoring efforts by this (Dickerson-Lange et al., 2023). All three sites are in a climate transition zone, just across the eastern slopes of the Cascades Range. The climate is warmer and wetter on the western slopes of the Cascades, and on the eastern slopes of the Cascades, the climate begins to transition to colder, continental conditions (Dickerson-Lange et al., 2023). Furthermore, this region represents a data gap in forest-snow observations (Dickerson-Lange et al., 2021). Dickerson-Lange (2023) provides a description of the ground field campaigns that took place at these sites during the same season as the snow-on lidar acquisition.

The NCALM snow-on lidar dataset was collected on 1 April 2021 near peak snow water equivalent (SWE) for this region, covering 63 km^2 of the Eastern Cascades of Washington, USA. While much of this region is covered with snow-off lidar acquisitions, this dataset is the first snow-on lidar dataset over the Eastern Cascades. It covers sites over a range of elevations, aspects, slopes, and forest structures. The dataset is divided into three zones from north to south: Fish Lake (FL), Sassie Ridge (SR), and Cle Elum Ridge (CER) (Figure 3.4).

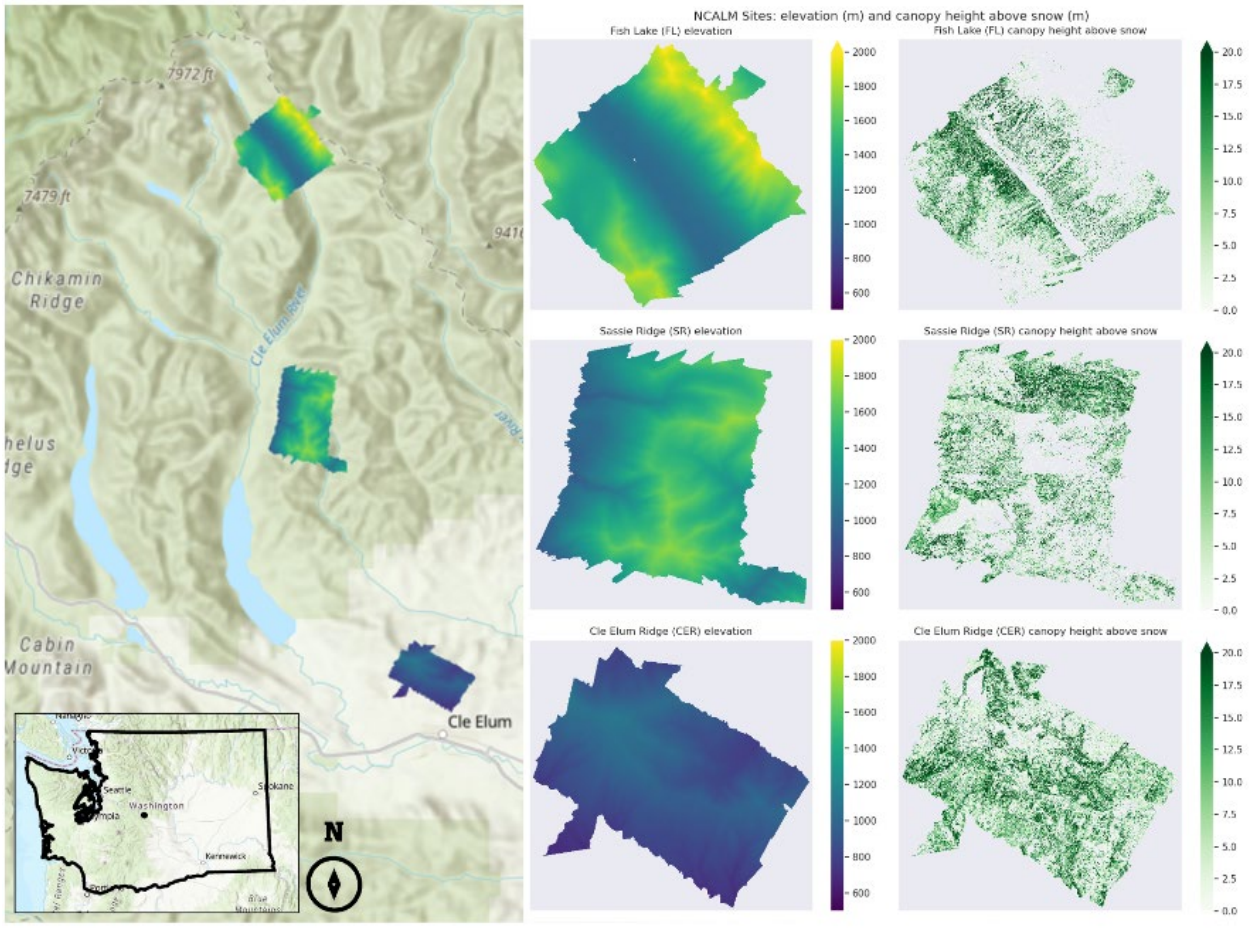

Figure 3.4. *Elevation in meters, and canopy height above the snow in meters for all three NCALM sites. From north to south Fish Lake (FL), Sassie Ridge (SR), and Cle Elum Ridge (CER) in the Eastern Cascades, WA, USA.*

To produce snow depth from the snow-on lidar dataset, snow-off lidar data is needed (Figure 3.2). Depending on the site, we must combine two or more snow-off lidar datasets to cover the entire region of the snow-on lidar dataset (Table 3.1). To resolve this, we combine the different snow-off DTMs or DSMs using the Mosaic to New Raster tool in ArcGIS Pro to create a single snow-off DTM and snow-off DSM for the study domain (Appendix 1).

Table 3.1. *Sites by elevation, meters, and the required snow-off lidar datasets to cover the entire region of the NCALM snow-on lidar dataset.*

Site	Elevation (m)		Lidar Datasets	
	Min	Max	WA DNR snow-off lidar https://lidarportal.dnr.wa.gov/	NCALM snow-on lidar
Cle Elum Ridge (CER)	700	1096	South Area: Yakima_basin_north_2018_dtm_5.tif Yakima_basin_north_2018_dsm_5.tif North Area: Teanaway_2015_dtm_2.tif Teanaway_2015_dsm_2.tif	Entire Area: SOUT_GEF_03F.tif SOUT_GEG_03F.tif
Sassie Ridge (SR)	891	1785	South Area: Yakima_basin_north_2018_dtm_14.tif Yakima_basin_north_2018_dsm_14.tif Middle Area: Yakima_basin_north_2018_dtm_22.tif Yakima_basin_north_2018_dsm_22.tif North Area: East_cascades_south_2020_dsm_654.tif East_cascades_south_2020_dtm_654.tif East_cascades_south_2020_dsm_655.tif East_cascades_south_2020_dtm_655.tif	Entire Area: CENT_GEF_03T.tif CENT_GEG_03T.tif
Fish Lake (FL)	1014	2037	South Area: East_cascades_south_2020_dtm_710.tif East_cascades_south_2020_dsm_710.tif East_cascades_south_2020_dtm_711.tif East_cascades_south_2020_dsm_711.tif North Area: East_cascades_north_2020_dtm_84.tif East_cascades_north_2020_dsm_84.tif East_cascades_north_2020_dtm_85.tif East_cascades_north_2020_dsm_85.tif	Entire Area: NORT_GEF_03T.tif NORT_GEG_03T.tif

3.2.4.1. Cle Elum Ridge (CER)

Cle Elum Ridge (CER) is the furthest south of the NCALM sites, with the lowest elevations, ranging from 700 to 1096 meters, located in the Douglas fir and Ponderosa Pine forest zone (Table 3.1). The ridge that makes CER runs almost exactly east to west, dividing the snowmelt from CER into two watershed scale USGS Hydrologic Unit Codes (HUC-10; https://nas.er.usgs.gov/hucs.aspx). The north side of the ridge HUC-10 is Middle Fork Teanaway River—Teanaway River and the south side is Kachess River –Yakima River (Dickerson-Lange et al., 2023). CER is the only site of the three that is not co-located with a SNOTEL station.

This lidar acquisition took place pre-forest-treatment on CER (see Section 3.1.2 Project background). Thus, the steep north slope of the ridge is primarily full of overly dense, third growth forests. There are some logging corridors in the region, with recently harvested clear cut areas. The less steep south slope has only patches of third growth forest and otherwise, has thin forested areas and open, grass-dominated meadows (Dickerson-Lange et al., 2023).

CER is the southern polygon of the NCALM snow-on lidar dataset (SOUT; Table 3.1). Two different snow-off lidar datasets are required to cover the entire area of the snow-on dataset for CER. The southern region of CER is covered by the Yakima Basin North 2018 lidar dataset (#5), and the northern region is covered by the Teanaway 2015 lidar dataset (#2).

3.2.4.2. Sassie Ridge (SR)

Sassie Ridge (SR) is the center site of the three NCALM sites, with an elevation range from 891 to 1785 meters, located in the Douglas fir and western hemlock forest zone (Table 3.1). The Jolly Mountain Fire came through SR in 2017; as a result, the forest cover is patchy with burned regions. SR is in the Cle Elum River HUC-10 unit. There is a SNOTEL station in the lidar domain, SNOTEL station number 734.

SR is the center polygon of the NCALM snow-on lidar dataset (CENT; Table 3.1). Two separate snow-off lidar datasets are required to cover the entire region of the snow-on dataset for SR. The Yakima Basin North 2018 datasets #14 and #22 cover the southern and center regions, respectively. The Eastern Cascades South dataset covers the northern region where dataset #654 covers the northwest and #655 covers the northeast side of the snow-on SR region.

3.2.4.3. Fish Lake (FL)

Fish Lake (FL) is the furthest north of the NCALM sites, covering the highest elevation and largest range in elevation, from 1014 to 2037 meters, located in the Pacific silver fir and mountain hemlock forest zone (Table 3.1). The FL site covers a range of complex topography and varying forest structure. There are large old growth stands of forest near the bottom of the valley, that decrease in density with elevation. Steeps slopes rise from the valley floor, that give way to deep fishers in the landscape. The overall forest structure becomes mature stand with mixed clumps and gap (Dickerson-Lange et al., 2023). FL is also in the Cle Elum River HUC-10 unit. There is a SNOTEL station in the lidar domain, SNOTEL station number 478.

FL is the northern-most polygon of the NCALM snow-on lidar dataset (NORT; Table 3.1). Two lidar datasets are required to cover the entire snow-on dataset for FL. The Eastern Cascades South 2020 datasets #711and #710 cover most of the domain. The Eastern Cascades North 2020 datasets #84 and #85 fill in the north-east corner, completing the snow-on lidar dataset domain.

3.3. Section 3. Results.

3.3.1. Introduction.

We summarize the results of this work in three main sections. First, we provide a description of the processed lidar datasets into snow depth, elevation, topography index (TPI), canopy height, distance to canopy edge (DCE), aspect, slope, and heat index (DAH) for each site (Sections 3.2).

Next, we visualize the results from the Random Forest model ensemble for each elevation zone with predictive feature importance plots and probability density functions of those input features (Section 3.3). Finally, we visualize the decision tree with the highest accuracy score from the entire Random Forest model ensemble for each elevation zone to understand how each predictive input feature influences snow depth.

We found that both topography and canopy cover matter for snow depth in the Eastern Cascades, where the most snow at all elevations is found in topographically shaded gaps. Distance to canopy edge is the strongest predictor of snow depth in warmer, low elevation terrain (< 1000 m) with large gaps that are greater than half the average tree height on shaded slopes having significantly deeper snow. Lastly, we found that topographic shading, determined by slope angle and slope aspect, becomes more important with increasing elevation. In middle to high elevations (> 1000 m), forest gaps in topographically shaded locations also accumulate the most snow, however, the size of the gap does not matter like it does at lower elevations. We provide our final thoughts for how our results are applicable to forest management in Section 3.4.

3.3.2. Description of Processed Lidar Data.

We use the methods described in Section 3.2.2. to produce snow depth and other landscape scale metrics for the three study sites (Figure 3.5). These are detailed for each site in the subsections below.

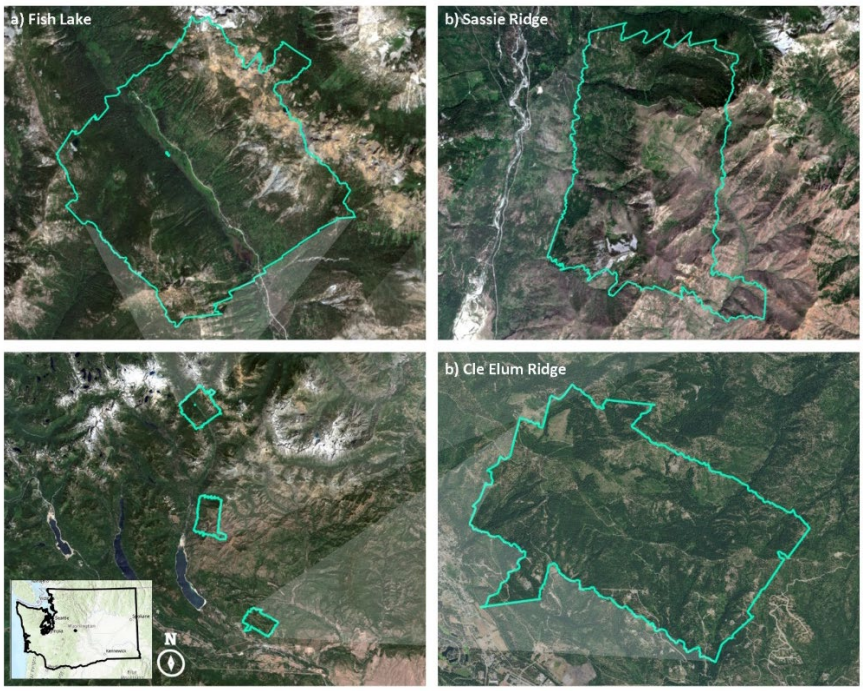

Figure 3.5. *Sentinel-2 10m multispectral satellite imagery over the three study sites a) Fish Lake, b) Sassie Ridge, and c) Cle Elum Ridge.*

3.3.2.1. Cle Elum Ridge (CER)

Cle Elum Ridge is the furthest south of the NCALM sites, with the lowest elevation range and likewise, the lowest snow depth values (Figure 3.6).

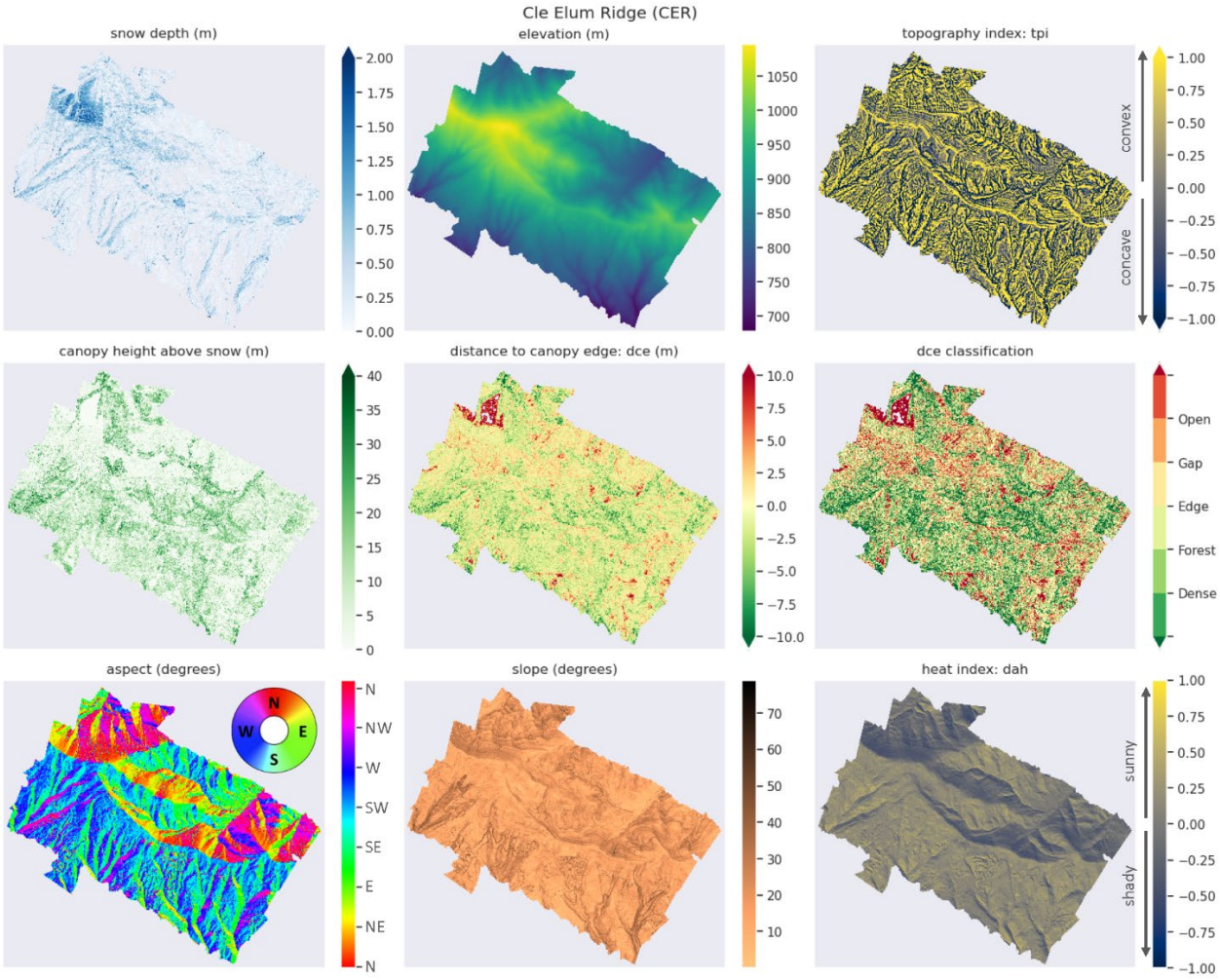

Figure 3.6. *Cle Elum Ridge (CER) processed lidar data, from top left to bottom right: snow depth in meters, elevation in meters, topographic position index (TPI), canopy height above the snow in meters, distance to canopy edge (DCE) in meters, distance to canopy edge in classification groups, slope aspect in degrees, slope angle in degrees, and the diastrophic heat index (DAH).*

The ridge of Cle Elum Ridge dominates the landscape of this domain. The ridge can be seen highlighted in yellow by a high TPI, running east to west. This ridge creates a strong contrast in solar exposure between the north and south sides of the ridge. The north side of the ridge is particularly steep, and the combination of the slope aspect and slope angle creates a large difference in heat index on the north and south side of the ridge. Generally, the deepest snow depths are in gaps or open regions (Figure 3.6), but the strength of this correlation varies by slope aspect and slope angle.

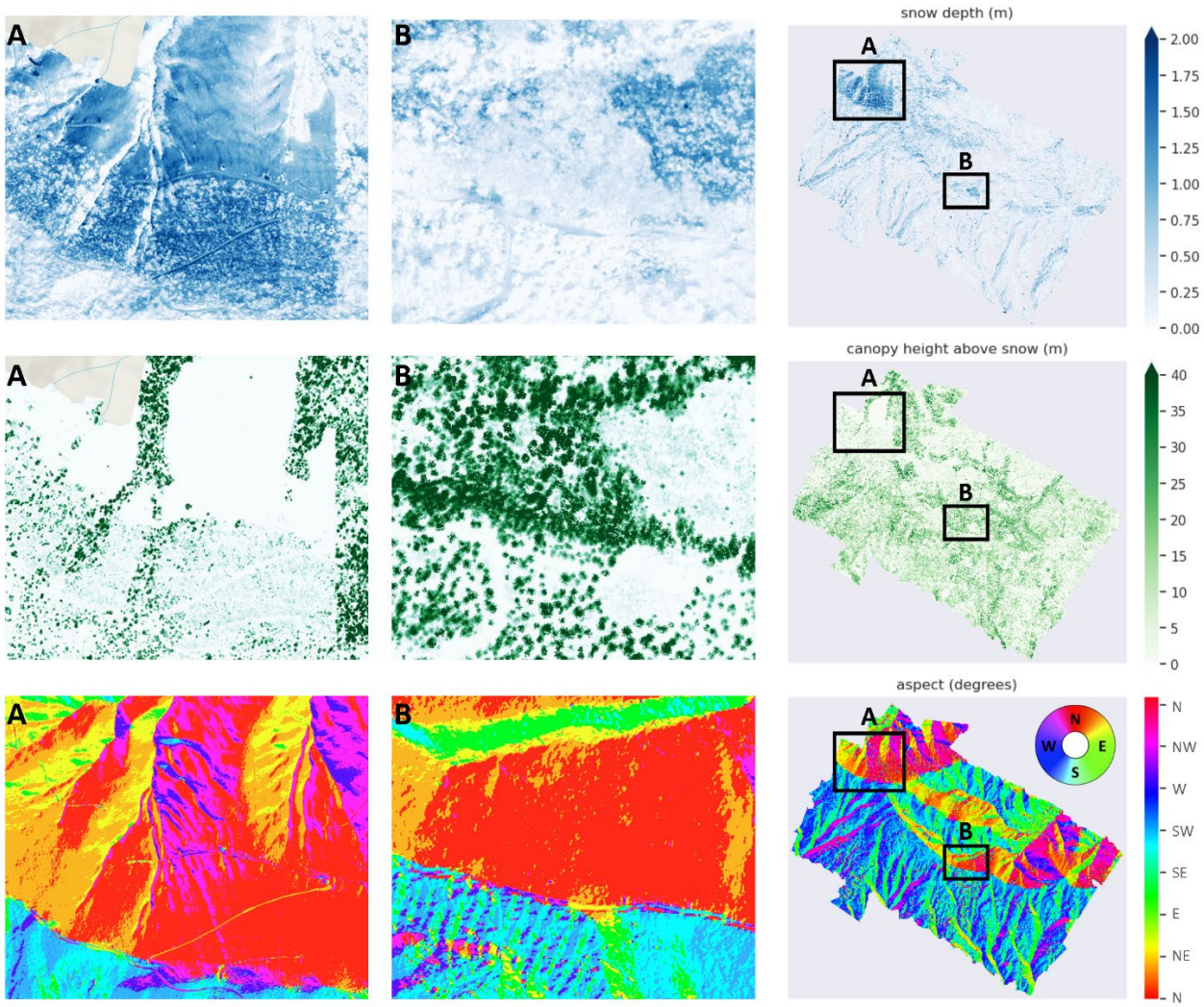

Figure 3.7. *The deepest snow on Cle Elum Ridge is in open regions on the north slopes, as exemplified by A) a clear cut and B) other deep snow in a large north-facing gap near our field sites. There are some deep snow piles along the ridge road (B), but these are not as pronounced as the snow accumulation in the large topographically shaded open regions.*

3.3.2.2. Sassie Ridge (SR)

Sassie Ridge is the central NCALM site, with a greater range of elevation, canopy structure, and snow depths than at CER (Figure 3.8).

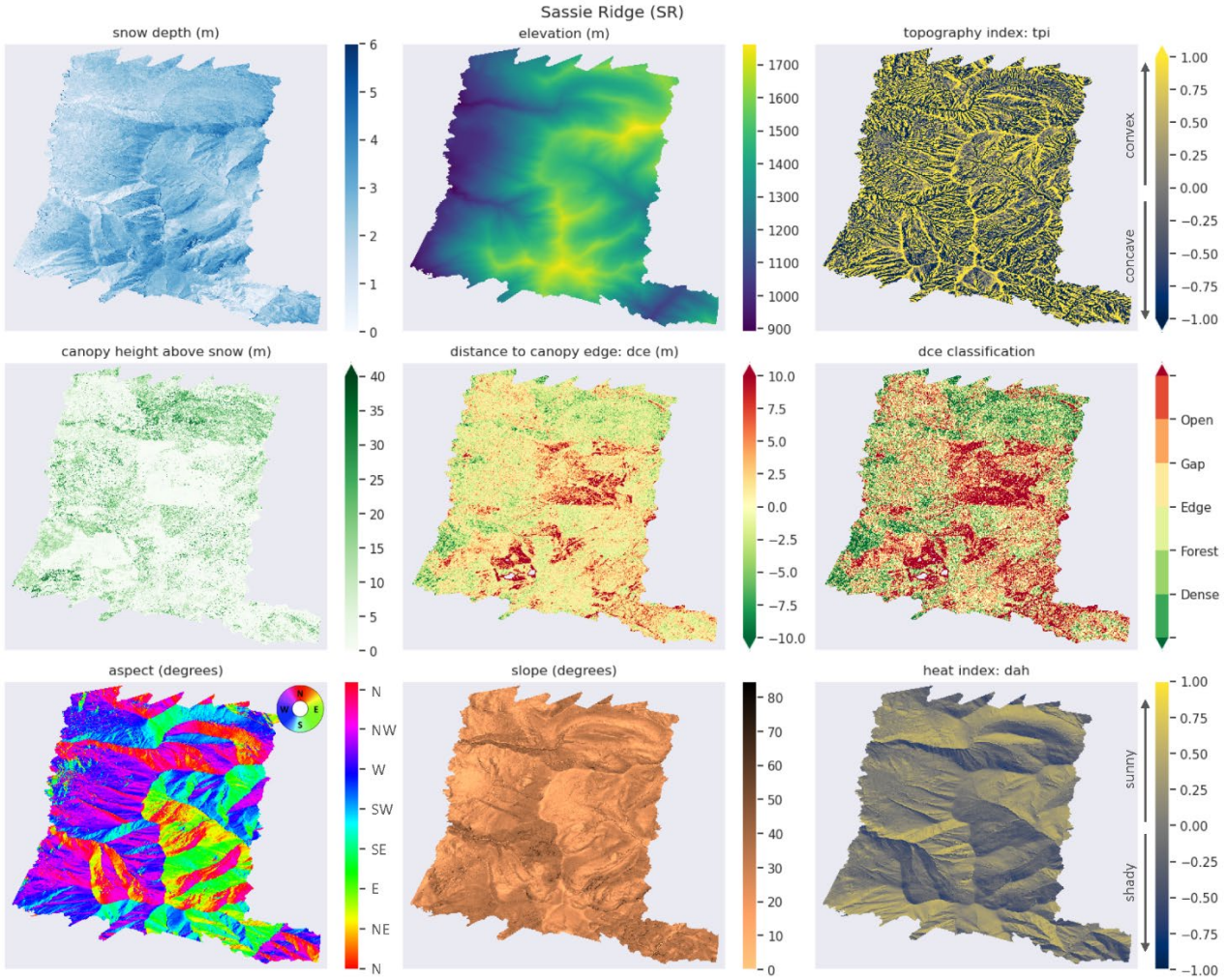

Figure 3.8. *Sassie Ridge (SR) processed lidar data, from top left to bottom right: snow depth in meters, elevation in meters, topography index (TPI), canopy height above the snow in meters, distance to canopy edge (DCE) in meters, distance to canopy edge in classification groups, slope aspect in degrees, slope angle in degrees, and the diastrophic heat index (DAH).*

There is also a ridge that runs through the Sassie Ridge site. This ridge runs primarily north to south and can be seen by the yellow high TPI values and the strong contrast in aspect between south-east and north-west regions. There are large gaps in the forest at this site, where the forest was either logged or disturbed by wildfire (Figures 3.5, 3.8). Snow depth is the deepest in the large, north-facing gaps. Snow depths in the gaps on the south side of the ridge cover a wide range, depending on the exact aspect and heat exposure.

3.3.2.3. Fish Lake (FL)

Fish Lake is the furthest north of the NCALM sites, covering the highest elevation and more complex topography (Figure 3.9).

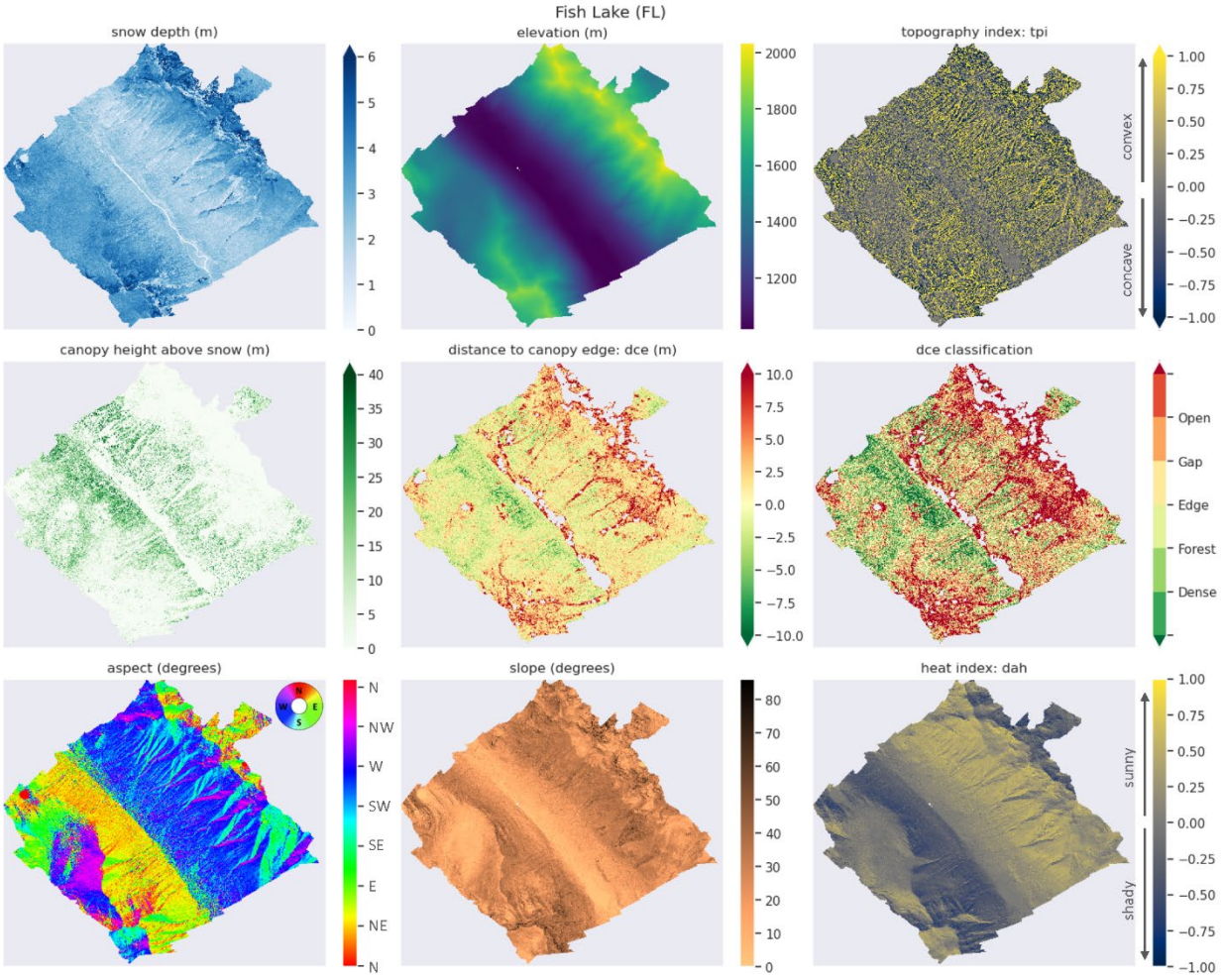

Figure 3.9. *Fish Lake (FL) processed lidar data, from top left to bottom right: snow depth in meters, elevation in meters, topography index (TPI), canopy height above the snow in meters, distance to canopy edge (DCE) in meters, distance to canopy edge in classification groups, slope aspect in degrees, slope angle in degrees, and the diastrophic heat index (DAH).*

Fish Lake covers the largest area, largest range of elevations, and most diverse forest structure of all the sites. The lowest elevation of this site is in the Cle Elum River valley, which has a thin forest structure inside the river flood plain. As elevation increases, the steep valley walls have complex topography and deep fissures in the landscape. This mid-elevation region is densely forested, with the densest forest on the north-east valley wall. Distance to canopy edge is a strong predictor of snow depth in this mid-elevation range. As elevation increases, the forest thins and decreases with height as this region covers the highest elevation terrain in the entire lidar dataset. Snow depth at the highest elevations is determined by mountainous topography.

The large range in elevation at Fish Lake shows us that snow depth varies significantly by elevation. When we visualize elevation and snow depth for all three sites, we see that snow depth increases with elevation and has a higher variability in specific elevation zones (Figure 3.10).

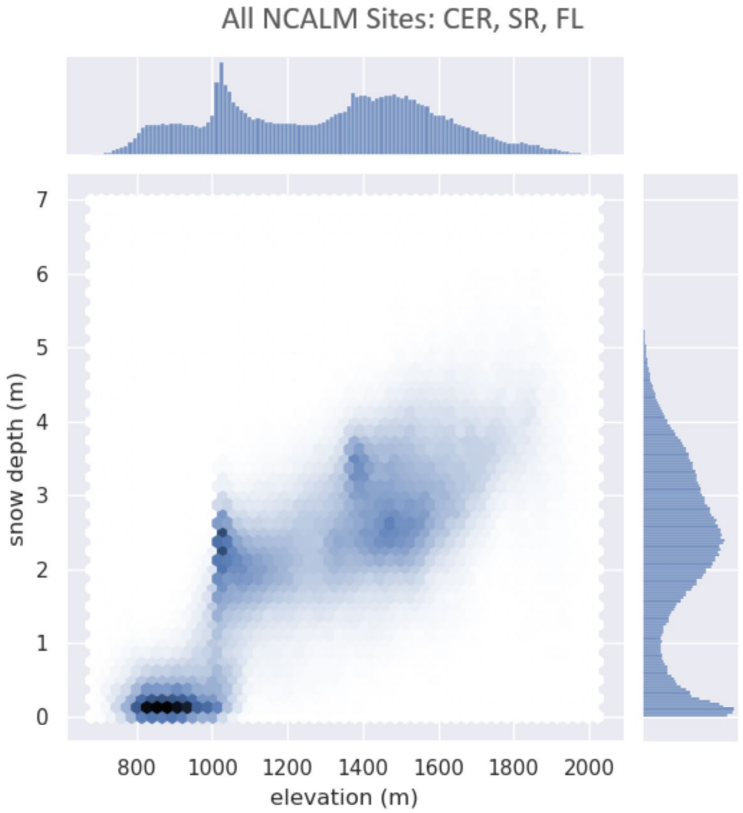

Figure 3.10. *Heat map of elevation (m) and snow depth (m) colored by density of values.*

Between 800 and 1000 m in elevation, snow depth varies between 0 and 1 m. As the elevation approaches 1000 m, snow depth increases in variability where it ranges from 0 to 3.5 m. This elevation corresponds to the average altitude where rain changes to snow in the Cascades. Based on these results, we use Random Forest analysis to closely consider the relationship between snow depth and elevation before considering the other variables as predictors of snow depth.

3.3.3. Statistical Results.

3.3.3.1. Random Forest Model Set Up.

To determine which landscape metrics, elevation (DEM), topographic position (TPI), distance to canopy (DCE), and heat exposure (DAH), are the strongest predictors of snow depth for the Eastern Cascades region, we combine data from all three sites into a single dataset, with snow depth as the target variable, and DEM, DAH, TPI, and DCE as the input features.

Since previous results (Figure 3.10) align with the literature (e.g., Kirchner et al., 2014; Lundquist et al., 2015) in demonstrating that elevation is a strong predictor of snow depth, we first view the partial dependence plot (PDP) of elevation from a Random Forest model (Figure

3.11). Partial dependence plots, known as PDPs, show the dependence between the target variable (i.e., snow depth) and an input feature (i.e., elevation). We can interpret partial dependence plots as the expected snow depth as a function of elevation (Figure 3.11; Pedregosa et al., 2011). We use the partial dependence plot of snow depth on elevation to determine what elevation zones to split the data into to further investigate the impact of other input features in each elevation zone. It is important to remember that the elevation cut offs found in this anaylsis are specific to the year of our dataset collection, water year 2021. Since a strong driver of these cut offs is the rain-snow transition zone, the elevation cut offs may vary from year to year. Thus, a further study would be needed to assess whether these cutoffs should be adjusted for climate change for long-term planning (Dickerson-Lange et al., 2023).

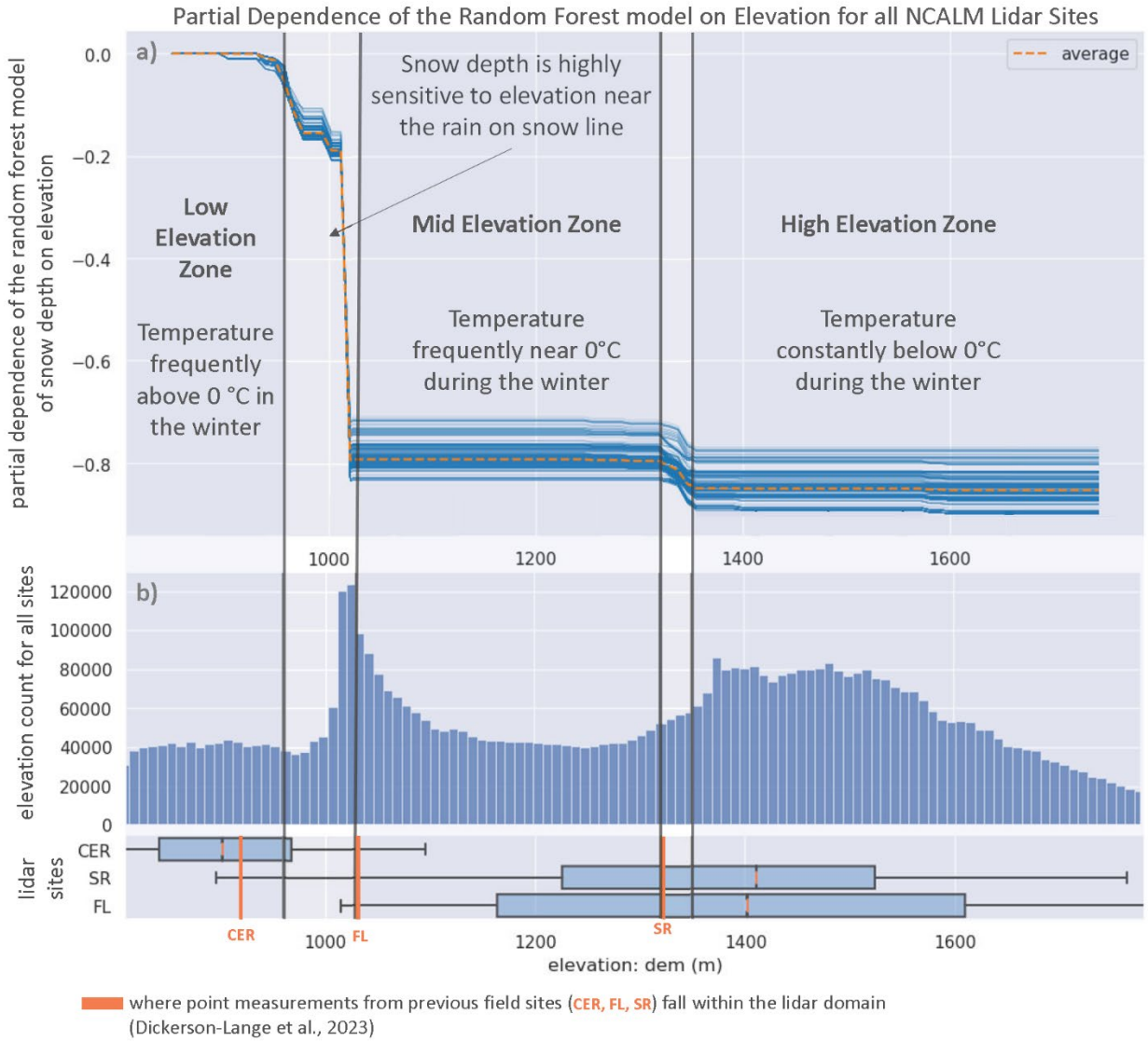

Figure 3.11. a) *Partial dependence plot (PDP) of elevation from all three sites separated into three elevation zones: the low elevation zone (700-960m), where the winter temperature is frequently above 0 ℃, the mid elevation zone (1030-1320m) where the winter temperature is frequently near 0 ℃, and the high elevation zone (1350-2020m) where the winter temperature is*

generally below 0℃ and, a) the distribution of elevation from all three sites. The orange lines indicate where point measurements from previous field sites detailed in Dickerson-Lange et al. (2023) fall within the lidar domain.

We can interpret the partial dependence plot (Figure 3.11a) as the expected snow depth from the Random Forest model as a function of elevation. Flat regions of the partial dependence plot indicate that snow depth is consistent within that elevation zone, while steep regions indicate that snow depth is highly sensitive to elevation changes in that zone (i.e., snow depth varies a lot from a small change in elevation Figure 3.10).

The result of this partial dependence plot provides three clear elevation zones: the low elevation zone of elevations less than 960 meters, the mid elevation zone from 1030 to 1320 meters, and the high elevation zone of elevations greater than 1350 meters (Figure 3.11). We exclude data from elevations in the steep regions of the partial dependence plot from further analysis because these regions have a strong variability in snow depth with small changes in elevation and would not yield clear results for the other predictor feature variables (TPI, DAH, and DCE).

A low elevation zone represents the low elevation snowpack, where the winter temperatures are frequently above 0°C. In a typical season for this region, the rain-on-snow line will fluctuate between 1100 and 1300 meters in elevation (based on historical analysis of the freezing level as measured by Quillayute radiosonde observations). The mid-elevation zone is where winter temperatures are frequently near 0°C. Finally, the high elevation zone is where winter temperatures are consistently above 0° C, and a deeper, consistent snowpack is formed for the entire winter season (Figure 3.11).

Focusing on the three clear elevation zones, within which snow depth does not vary much by elevation, we can visualize the other feature variables, TPI, DAH, and DCE, inside each zone (Figure 3.11). Visually, the deepest snow (darkest color blue in Figure 3.11) tends towards concave topography (negative TPI) and shady slope-aspects (negative DAH), corresponding with open areas (positive DCE).

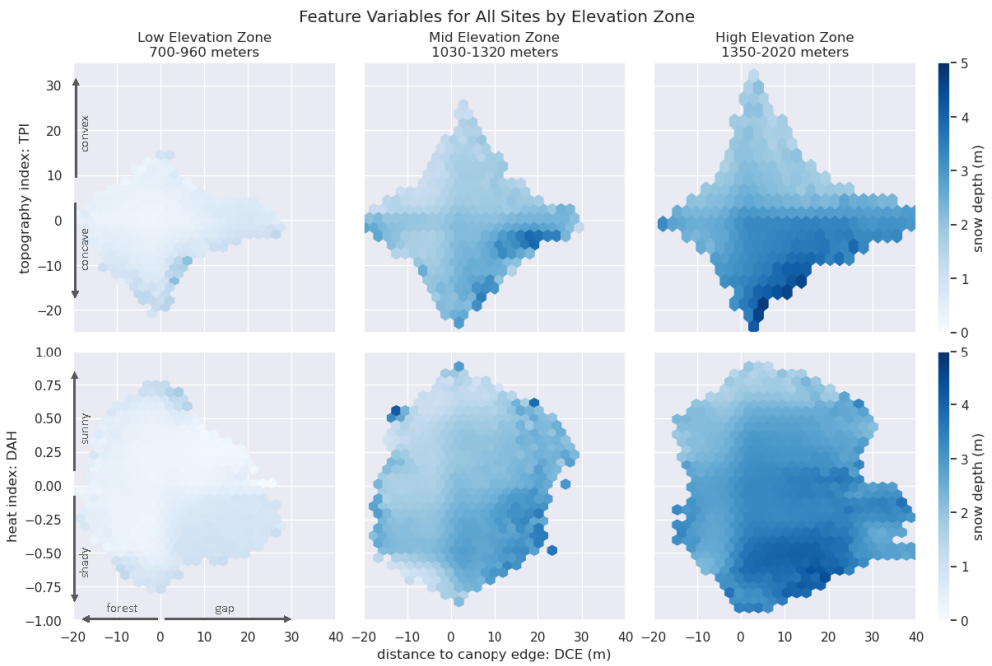

Figure 3.12. *Heat maps of topographic position index (TPI) and heat index (DAH) by distance to canopy edge (DCE) inside each elevation zone, colored by snow depth.*

3.3.3.2. Random Forest Model Results.

We use an ensemble of decision trees, called a Random Forest model (Section 3.2.3.2) to address Activity 1.2 for this work and develop a predictive model from the non-linear relationships between our geographic input features and snow depth. Thus, we ran a Random Forest model within each elevation zone (Section 3.3.3.1) to determine how the input features aside from elevation (TPI, DAH, and DCE) predict snow depth for each elevation zone.

Figure 3.13 illustrates the distribution of each of these metrics within each of the three elevation zones. DAH is bimodal in the low and mid elevation and near uniform in distribution in the highest elevation zone. All three zones have a greater fraction of sunny exposure compared to shaded exposure. TPI has a near-gaussian distribution within each zone. The lowest elevation zone has more area falling beneath forest cover, while the higher elevations zones have more open areas.

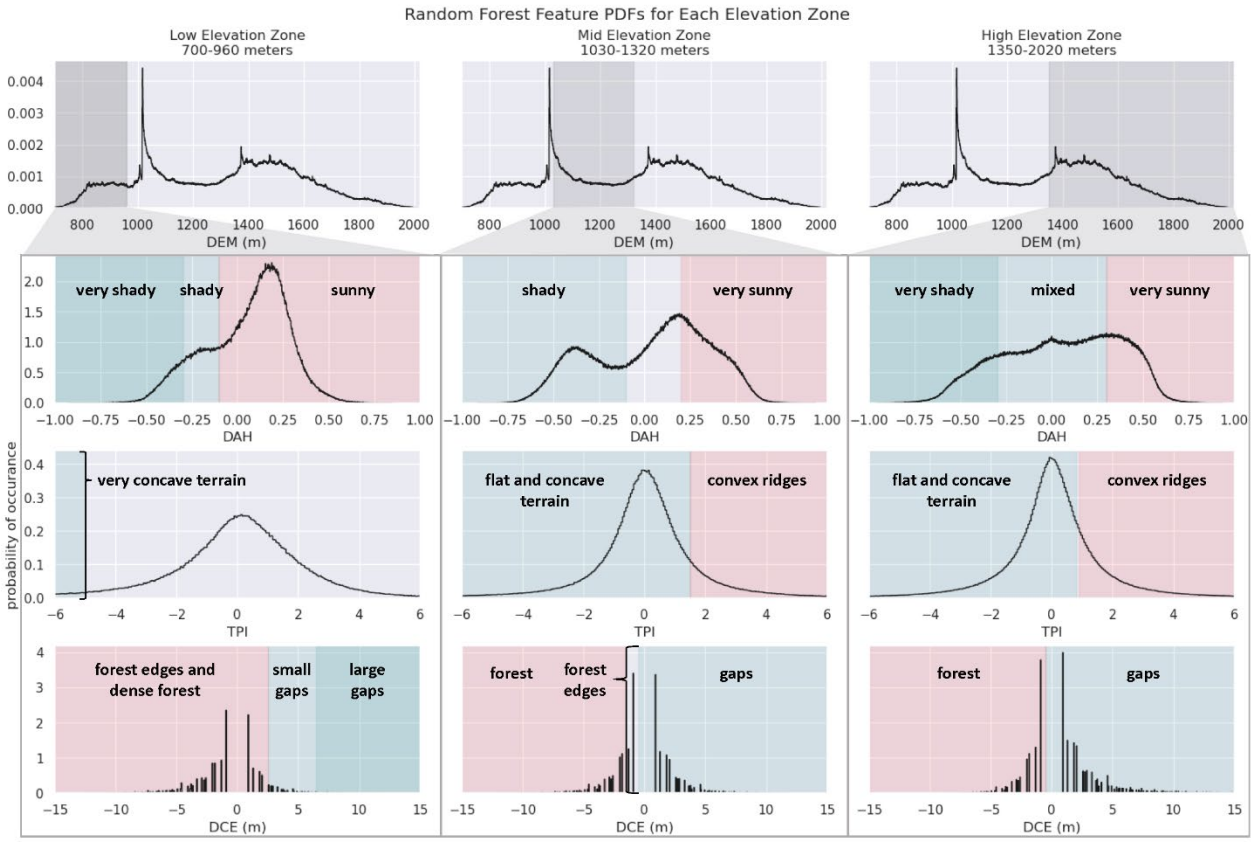

Figure 3.13. *Probability Density Functions (PDF)s for the Random Forest input features in each elevation zone. Colors indicate regions where random forest models identified significant splits in the feature's influence on snow depth, discussed further below.*

The importance of a feature (TPI, DAH, and DCE) in predicting snow depth across the entire Random Forest model ensemble can be understood by the feature's relative importance in informing any given decision tree in the ensemble (Figure 3.14). Distance to canopy edge (DCE) is the dominant feature in the low elevation zone, while heat exposure (DAH) is the dominant feature in the mid and high elevation zones (Figure 3.14).

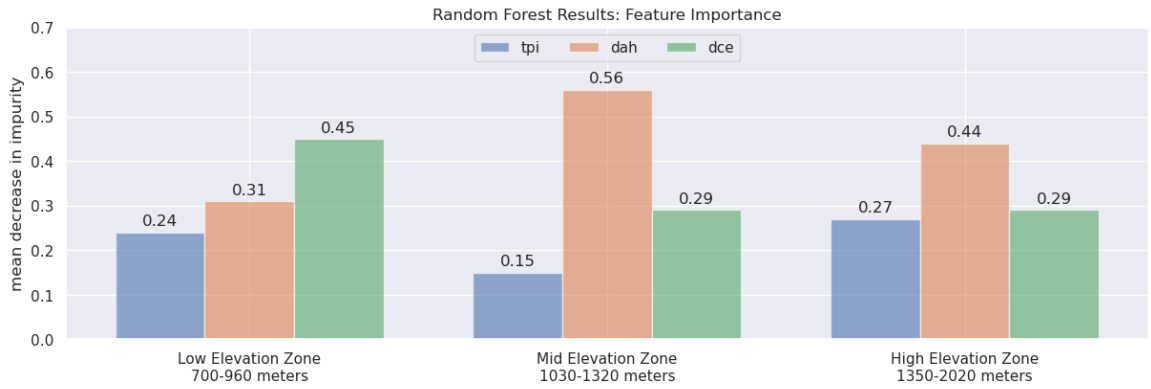

Figure 3.14. *Random Forest Feature Importance of TPI in blue, DAH in orange, and DCE green inside each elevation zone, based on the number of times each variable was a predictor in all 1000 decision trees.*

Visualizing a decision tree from the Random Forest model ensemble provides an intuitive method for visualizing the machine learning model results. A decision tree illustrates how the Random Forest model subsets the target dataset based on each input feature. As discussed in Section 3.2.3.2, the Random Forest model sorts the data into subgroups that maximize the difference between groups while minimizing the difference within groups. It does this by determining cut-off values in one or more of the input features that best divide groups in greater vs. lesser snow depth. We provide an example decision tree (Figure 3.15) to explain the decision tree anatomy before diving into the Random Forest model results.

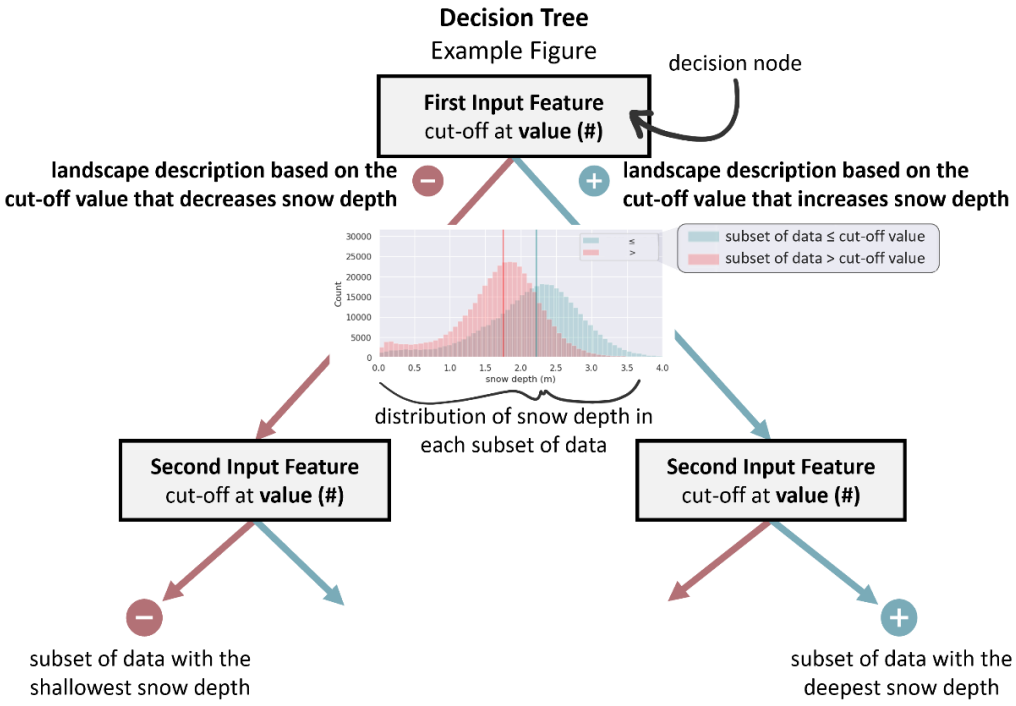

Figure 3.15. *An example decision tree to explain the terminology used to discuss Figures 3.16, 3.17, and 3.18. Note that the + and – signs and directions in each split refer to the data subset*

leading to more or less snow depth, respectively. The legends within each distribution graph indicate which color is associated with input feature values greater than or less than the cut-off value.

The decision node on a decision tree (Figure 3.15) determines the split of one input feature at a time. The first decision node marks the most significant split in the data, and the lower decision nodes create further subsets of the data (Molnar, 2023; Figure 3.15). We can track the decision nodes through the tree where the first decision represents the largest split in the data, while remembering that the data in each node is a subset of data from the previous node (each split in the data is connected to the previous split by "AND"; Molnar, 2023). Recall that we ran a Random Forest ensemble of 1000 decision trees (Section 3.2.3.2) in each elevation zone and visualize a single decision tree from each zone with the highest accuracy score (i.e., we visualize the decision tree out of 1000 which provides the best prediction of snow depth for the entire dataset).

To visualize how each decision node impacts snow depth, we show the distribution of snow depth in each subset of data (Figure 3.15). We arrange the decision trees so that subsets of the data to the left result in less snow (indicated by the red – symbol) and subsets of the data to the right result in more snow (indicated by the blue + symbol). The subset of data furthest left has the shallowest snow depth, and the subset of the data furthest right has the deepest snow depth (Figure 3.15). The legends of each snow distribution graph indicate if the subset of data that results in more snow is less than or greater than the cut-off value indicated in the decision node box (Figure 3.15).

We provide landscape descriptions of the subset of data at each decision node (Figure 3.15). The description of the landscape is also indicated with coloring for the cut-off value in the decision tree in the PDFs shown in Figure 3.13. Given that each elevation band has unique cut-off values, the labels refer to ranges of the input feature that are significant for that elevation band (Figure 3.13, 15). The colored shading on the PDFs of each feature in Figure 3.13 correspond with the cut-offs for each feature as shown in the decision trees for each elevation band.

We visualize the decision tree with the highest accuracy score from the entire Random Forest model ensemble for each elevation zone to understand how each predictive feature influences snow depth (Pedregosa et al., 2011; Figures 3.16, 3.17, 3.18). Since Random Forest models are trained on a subset of the data, they are designed to not overfit decisions a specific site. Thus, our results should be representative for much of the Eastern Cascades of Washington State within a similar elevation range.

The decision tree with the highest accuracy score from the entire Random Forest model ensemble for the low-elevation zone is shown in Figure 3.16.

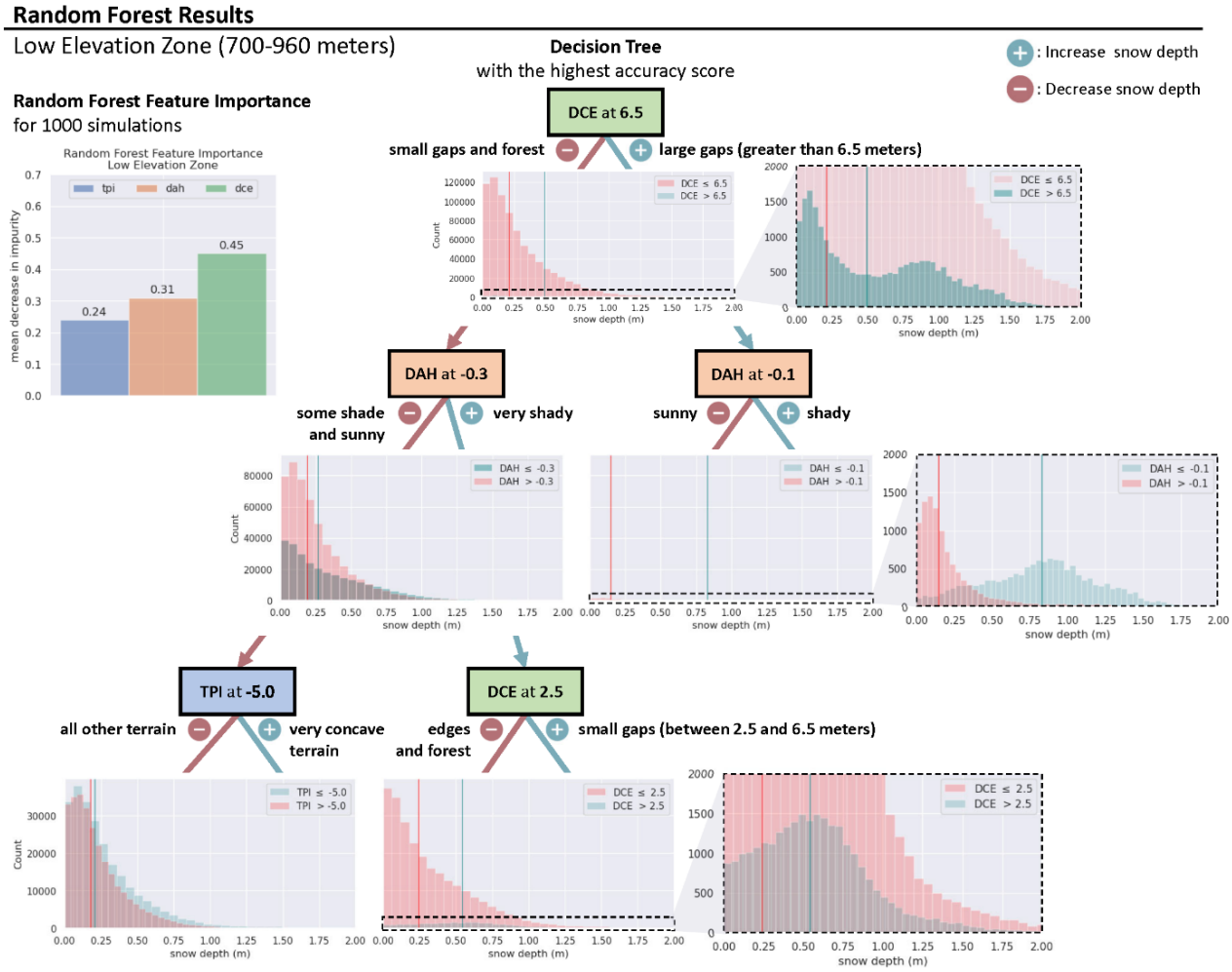

Figure 3.16. *Random Forest Results for the low elevation zone (700-960 meters). Decision nodes that split in DCE are in green, orange for DAH, and blue for TPI. The value inside the box indicates the cut-off value where the decision node split (i.e., DCE at 6.5, means distance to canopy edge split at 6.5 meters). The blue color indicates an increase in snow depth, and the pink color indicates a decrease in snow depth from the decision node split. These colors correspond to changes in background shading in the center column PDFs in Figure 3.13. The values all the way to the right indicate the features with the deepest snow depth, and the values all the way to the left indicate the features with the shallowest snowpack. Counts are held constant across all histograms to illustrate which categories have the largest numbers of data points.*

The first decision node on the low elevation zone decision tree is distance to canopy edge (DCE) at 6.5 (Figure 3.16). This means that the distance to canopy edge splits the dataset into two subsets: one subset, to the left, is where the distance to canopy edge is less than or equal to 6.5 meters and the other subset, to the right, is where the distance to canopy edge is greater than 6.5

meters. Since distance to canopy edge is the first decision node, we know that it represents the most significant split in this elevation range in determining snow depth. Also note that while pixels in large openings (DCE > 6.5 m) have the deepest snow (see Figures 3.6, 3.7 for illustration of these regions on the landscape), this subset of data makes up a relatively small total fraction of the study area. While we set the maximum decision node depth at three, if the minimum sample size required for a node to split is not met, then that side of the tree ends (Section 3.2.3.2). This can be seen on the right side of Figure 3.16, where the data is not subset a third time and ends after only two decision nodes for large gaps.

Distance to canopy edge (DCE) is the most important feature in the low elevation zone for determining snow depth (Figures 3.14 & 3.16). Not only does it matter for snow depth if a location is in the forest or a gap, but the size of the gap matters for snow depth in this elevation zone. Gaps greater than 6.5 m (about half the average tree height) have the most snow. Shaded terrain significantly increases snow depth in large gaps (right side of Figure 3.16). Small gaps have a lot of snow in very shaded areas (DAH < -0.3). This means that terrain must be very shaded for the impacts of solar exposure to be mitigated at low elevations (left side of Figure 3.16).

Key points for management in the low elevation zone.

- Large, shaded gaps that are greater than half the average tree height have the most snow.
- Smaller gaps need more shade (compared to large gaps) to retain significantly more snow (DAH < -0.3 for small compared to DAH < .1 for large gaps).
- Forest management should target opening gaps in topographically shaded terrain to maximize snow accumulation and retention.
- Exposed (sunny) terrain in this low elevation zone is not likely to accumulate much snow regardless of forest management.

The decision tree with the highest accuracy score from the entire Random Forest model ensemble for the mid-elevation zone is shown in Figure 3.17.

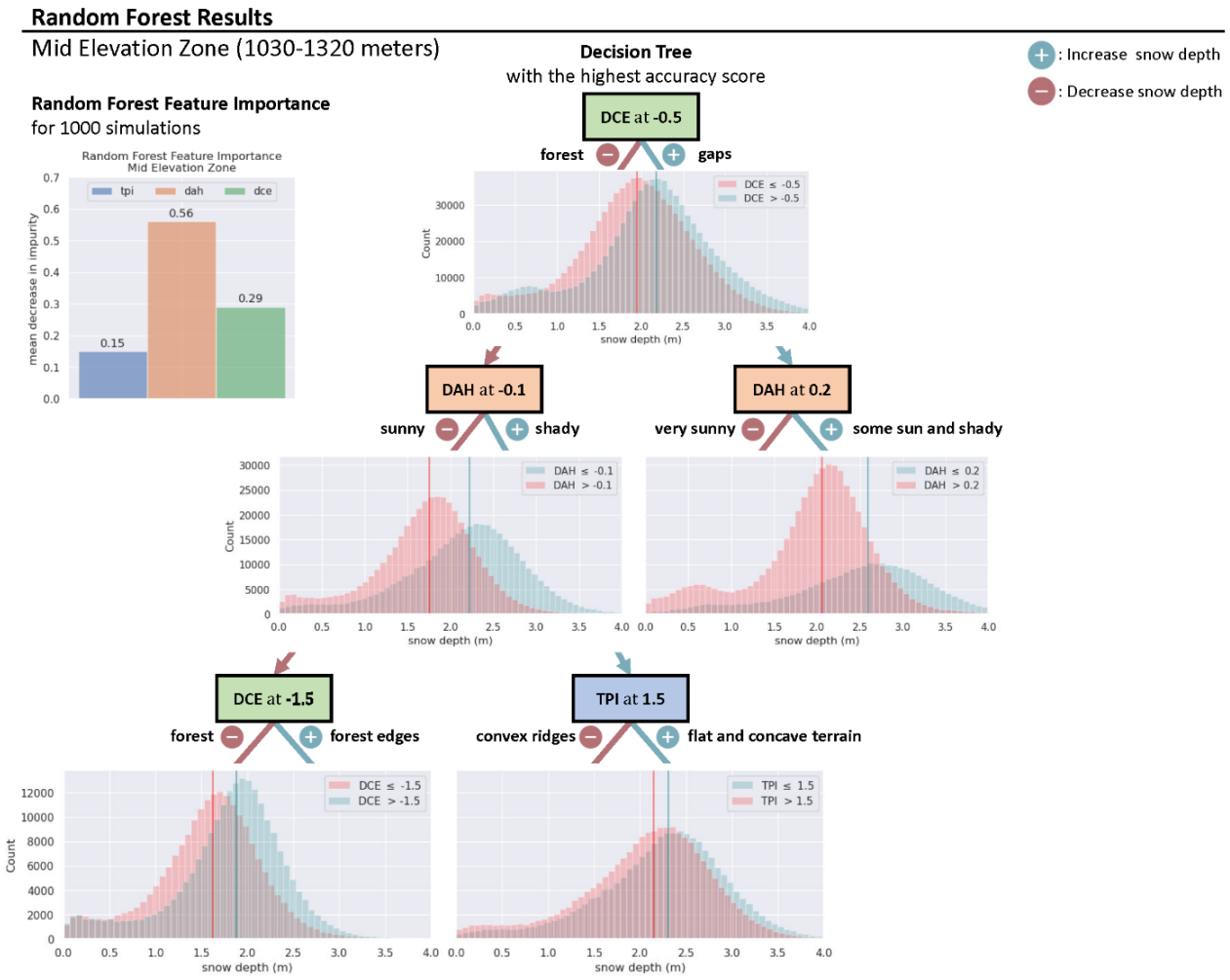

Figure 3.17. *Random Forest Results for the mid elevation zone (1030-1320 meters). Decision nodes that split in DCE are in green, orange for DAH, and blue for TPI. The value inside the box indicates the cut-off value where the decision node split (i.e., DCE at -0.5, means distance to canopy edge split at -0.5 meters). The blue color indicates an increase in snow depth, and the pink color indicates a decrease in snow depth from the decision node split. These colors correspond to changes in background shading in the center column PDFs in Figure 3.13. The values all the way to the right indicate the features with the deepest snow depth, and the values all the way to the left indicate the features with the shallowest snowpack. Counts are held constant across all histograms to illustrate which categories have the largest numbers of data points.*

DAH is the most important feature in the mid-elevation zone (Figure 3.14, 3.17). The size of the gap does not matter as much as in the low elevation zone; instead, the largest split in the data is simply between all forested regions and gaps of all sizes. We can see from the right side of the decision tree that DAH is the only feature which matters in gaps in this elevation zone (right side

of Figure 3.17). A heat index above 0.2 in gaps of any size will significantly decrease snow depth within these elevations (right side of Figure 3.17). Like in the low elevation zone, shaded gaps have the most snow. The left side of the decision tree shows that shaded forests have more snow than sun-exposed forests. For areas that have a high heat index in the forest, forest edges (-1.5 to -0.5 meters into the forest) have more snow than areas near the middle of a dense forest. Shady forest locations on convex ridges have slightly less snow than those on concave locations, but solar exposure (DAH) matters more than topographic position (TPI) in this elevation zone.

Key points for management in the mid elevation zone.

- In general, more snow accumulates in forest openings regardless of their size.
- However, heat exposure from topographic shading has an overall greater impact on snow depth than forest gaps, where topographic positions that receive more afternoon sun accumulate less snow.
- The cut-off value for how much sun exposure (DAH) makes a difference in snow accumulation is higher in the mid elevation zone than in the low elevation zone (Figure 3.13). In other words, flat and semi-shaded terrain still has more snow than sunny terrain, but very sunny terrain is needed to significantly reduce snow depth in gaps.
- Like in the low elevation zone, forest management should preferentially create gaps in topographically shaded or semi-shaded locations.

The decision tree with the highest accuracy score from the entire Random Forest model ensemble for the high-elevation zone is shown in Figure 3.18.

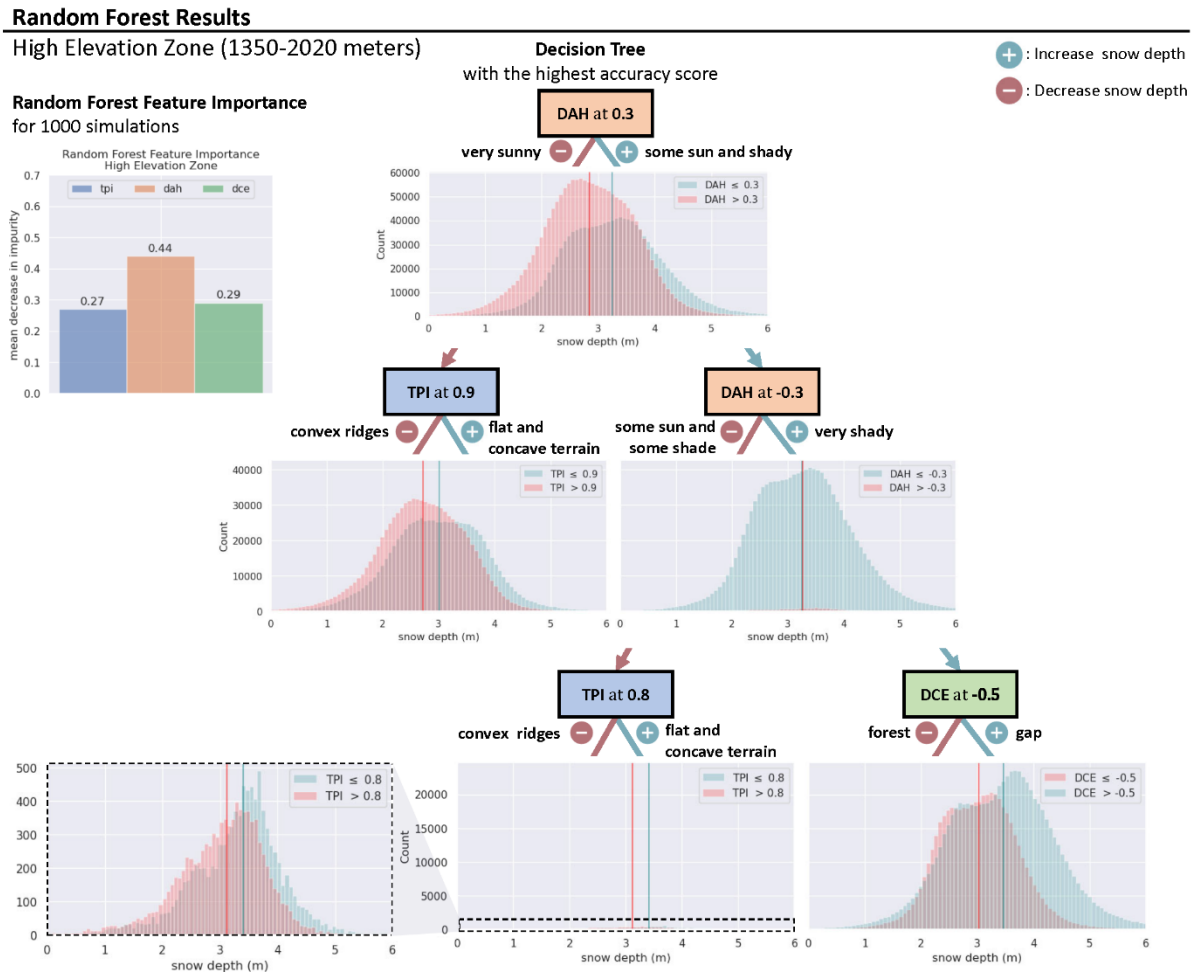

Figure 3.18. *Random Forest Results for the high elevation zone (1350-2020 meters). Decision nodes that split in DCE are in green, orange for DAH, and blue for TPI. The value inside the box indicates the cut-off value where the decision node split (i.e., DAH at 0.3, means the heat index split at a value of 0.3). The blue color indicates an increase in snow depth, and the pink color indicates a decrease in snow depth from the decision node split. These colors correspond to changes in background shading in the center column PDFs in Figure 3.13. The values all the way to the right indicate the features with the deepest snow depth, and the values all the way to the left indicate the features with the shallowest snowpack. Counts are held constant across all histograms to illustrate which categories have the largest numbers of data points.*

While heat index (DAH) is the most important feature in the high elevation zone, as it was in the mid-elevation zone, the role of topographic position (TPI) in determining snow depth increases with elevation (Figure 3.14, 3.18). Distance to canopy edge (DCE) is only important in determining snow depth at high elevations in very shaded terrain (DAH < -0.3). The right side of the decision tree shows that the deepest snow in this elevation range is in very shaded gaps

(Figure 3.18). Like the mid elevation zone, the high elevation zone is less sensitive to lower heat index values and thus, very sunny terrain is required to significantly decrease snow depth.

Key points for management in the high elevation zone.

- Like in the mid-elevation zone, topographic heat exposure (DAH) is the dominant control on snow depth.
- In very shaded terrain, the distance to canopy edge can matter. A shaded gap at this elevation will have a lot of snow. Otherwise, topography and heat index dominate snow depth patterns.

3.3.4. Summary: Key Points from the Results for Forest Management.

Prior work (Dickerson-Lange et al., 2021 and 2023) identified the eastern Washington Cascades as a transitional zone in the effects of forest cover on snow accumulation and retention. This work suggested that within this zone, secondary factors, such as topographic position would have increasingly important roles in snow depth patterns. Dickerson-Lange et al. (2023) identified one topographically shaded field site in the region that had substantially more snow accumulation in a gap compared to under the forest, whereas the snow metrics in other paired forest and gap study sites in the region were very similar.

Elevation has the greatest control on snow depth in the region (Figure 3.11), with substantially less snow accumulating at elevations below 1000 m. This low elevation zone is subject to frequent rain on snow and mid-winter melt. Thus, the only locations on the landscape with more than 1 meter of snow are very large gaps on topographically shaded terrain (Figure 3.12, 3.16). These locations have minimum possible snow losses; the location characteristics minimize snow interception, solar radiative heating, and longwave heating from nearby trees. Statistical analysis shows that within this zone, deeper snow is found in gaps greater than 6.5 m (about half the tree height) and in topographic locations with a diurnal anisotropic heat index (DAH) less than -0.01 (Figure 3.16), which occurs on slopes with a north or northwest aspect (Figure 3.6, 3.7). Smaller gaps (between 2.5 and 6.5 m) also accumulate more snow on shaded aspects than under forest cover, but the difference in mean snow depth observed between these groups is smaller (0.5 m compared to 0.25 m).

Middle and higher elevations (> 1000 m) accumulate substantially more snow (Figure 3.10, 3.12), and the amount of mid-winter melt is less. Within these zones, heat exposure associated with topographic orientation (DAH) is the greatest predictor of snow depth, with forest canopy characteristics playing a secondary role. Gaps still accumulate more snow than locations under the forest canopy (Figure 3.17, 3.18), but this effect matters most on topographically shadier locations. Convex vs. concave topography (TPI) has the greatest effect in the highest elevation zone (Figure 3.18). Opening gaps in topographically shaded locations in the middle elevation zone would likely have the largest impact on basin-average snow depth, with an average difference of about 30 cm (Figure 3.17) over a substantial portion of the landscape. The impact of large gaps in very shaded locations at lower elevations is larger (with a mean snow depth difference of about 75 cm; Figure 3.16), but the area on the landscape is so much less that the influence on streamflow will likely be small. However, we will explore the impacts of thinning

within this low elevation zone, as described in the fieldwork section (Section 3.4), to determine if greater areas within this low elevation zone can accumulate more snow with active management.

Plain Language Summary of the Key Results.

- Both topography and canopy cover matter for snow depth in the Eastern Cascades, where the deepest snow at all elevations can be found in topographically shaded gaps in the forest.
- Distance to canopy edge is the strongest predictor of snow depth in warmer, low elevation terrain (<1000 m) where large gaps (greater than half the average tree height) on shaded slopes significantly increase snow depth.
- Topographic shading, determined by slope angle and slope aspect, becomes more important with increasing elevation. In middle and high elevations (>1000 m), forest gaps in topographically shaded locations also accumulate the most snow, however, the size of the gap does not matter like it does at lower elevations.

3.4. Section 4. Post-treatment Fieldwork.

3.4.1. Introduction.

We completed all proposed fieldwork since the start of this funding in Fall 2023. The proposed fieldwork is part of a follow-up project funded by TNC, which begins immediately after the WA DNR funding ends, to evaluate forest prescriptions taking place on Cle Elum Ridge (Figure 3.19). The proposal stated that we engage in "fieldwork at the treatment sites to understand the forest prescriptions and how they fit into the geospatial analysis." To fulfill this, one field campaign involved deploying snow monitoring field sites in the recent forest treatments on Cle Elum Ridge, with the goal of measuring the impact of the forest treatments on the snowpack. Another field campaign set out stream sensors in drainages off Cle Elum Ridge to capture the stream temperature response from the forest treatments. Those two field campaigns are discussed in Sections 3.4.2 and 3.4.3, respectively.

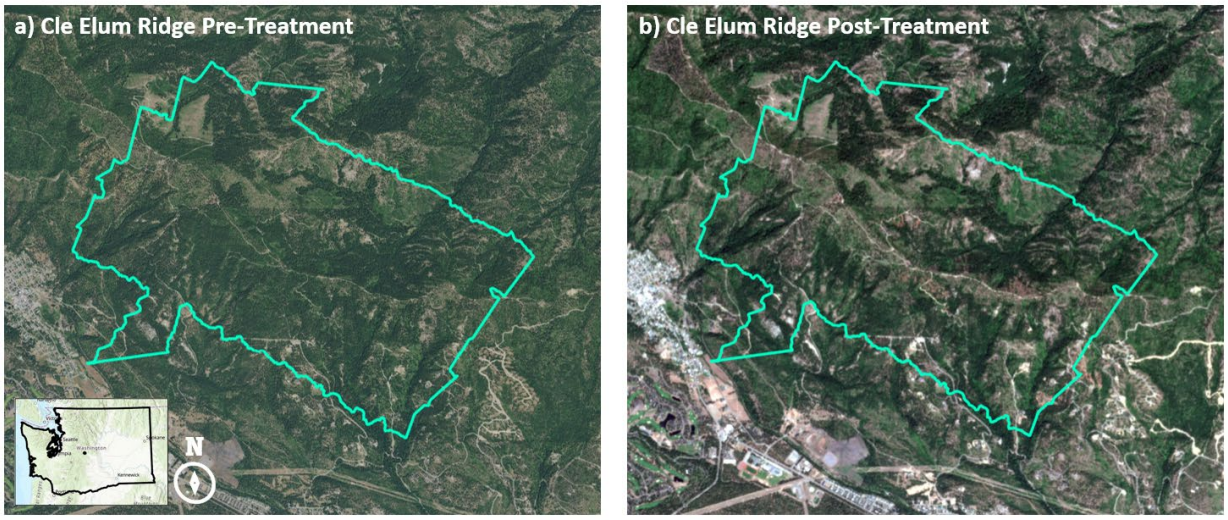

Figure 3.19. *Sentinel-2 10m multispectral satellite imagery over Cle Elum Ridge a) pre- and c) post-treatment.*

3.4.2. Snowpack Monitoring at Cle Elum Ridge.

In Fall 2022, Emily Howe and Cassie Lumbrazo led a successful field campaign to deploy the post-treatment snow monitoring stations on Cle Elum Ridge for WY 2023 (Figure 3.20).

Figure 3.20. *Photos taken of a) Emily Howe and b) and c) Cassie Lumbrazo in the field during the fall 2022 Cle Elum Ridge field campaign. Photo credit: Mark Stone (UW).*

Over 3 days (27 October, 10 and 17 November 2022) we deployed 12 total snow monitoring stations, with 6 sites on the north side and 6 sites on the south side of Cle Elum Ridge (Figure 3.21). Each site contains 9 temperature sensors spaced out on a 10m x 10 m grid, 3 snow depth poles, and 2 timelapse cameras for redundancy. We took a hemispherical image at every corner of the grid and at every snow pole to calculate the fraction forest cover area for each point in space. The methods for this field campaign replicate those described in Dickerson-Lange et al. (2023) in the same location.

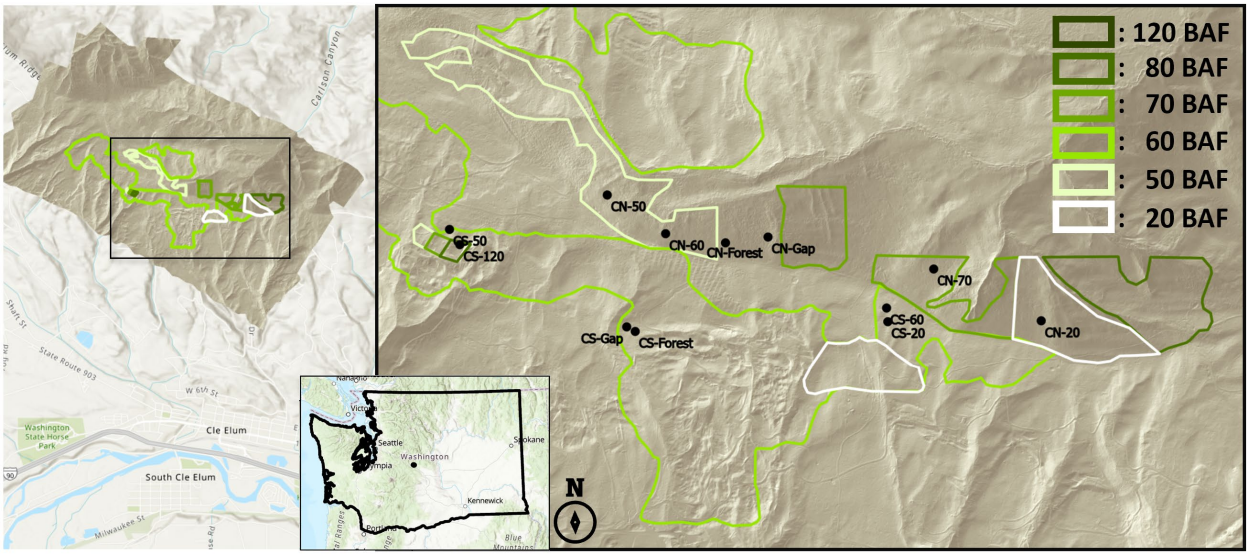

Figure 3.21 *A hillshade map of Cle Elum Ridge, produced with the NCALM lidar data, mapped with the WY2023 snow monitoring field sites in black and forest treatment polygons colored by basal area factor (BAF). The sites' naming convention: C for Cle Elum Ridge, S/N for the south*

and north side of the ridge, and the number representing the BAF for the site. The forest and gap sites are repeat sites from previous field campaigns on Cle Elum Ridge.

We strategically selected the location for field sites to cover all the forest treatment polygons provided by the logger and TNC foresters (Figure 3.21). The forest treatment polygons simply estimate the BAF for each site; thus, while in the field, TNC Forester, Herman Flamenco, evaluated the BAF at the center of each site using a basal area factor- scope, called a dendrometer.

In June 2023, we collected the snow monitoring stations from Cle Elum Ridge. Cassie Lumbrazo and an undergraduate research assistant, John Cramblitt, are currently working to process the dataset (Figure 3.22) and will complete the processing during summer 2023. This work is part of the follow up project funded by TNC (beginning immediately), with the goal of evaluating the snowpack for the post-treatment forest for WY 2023.

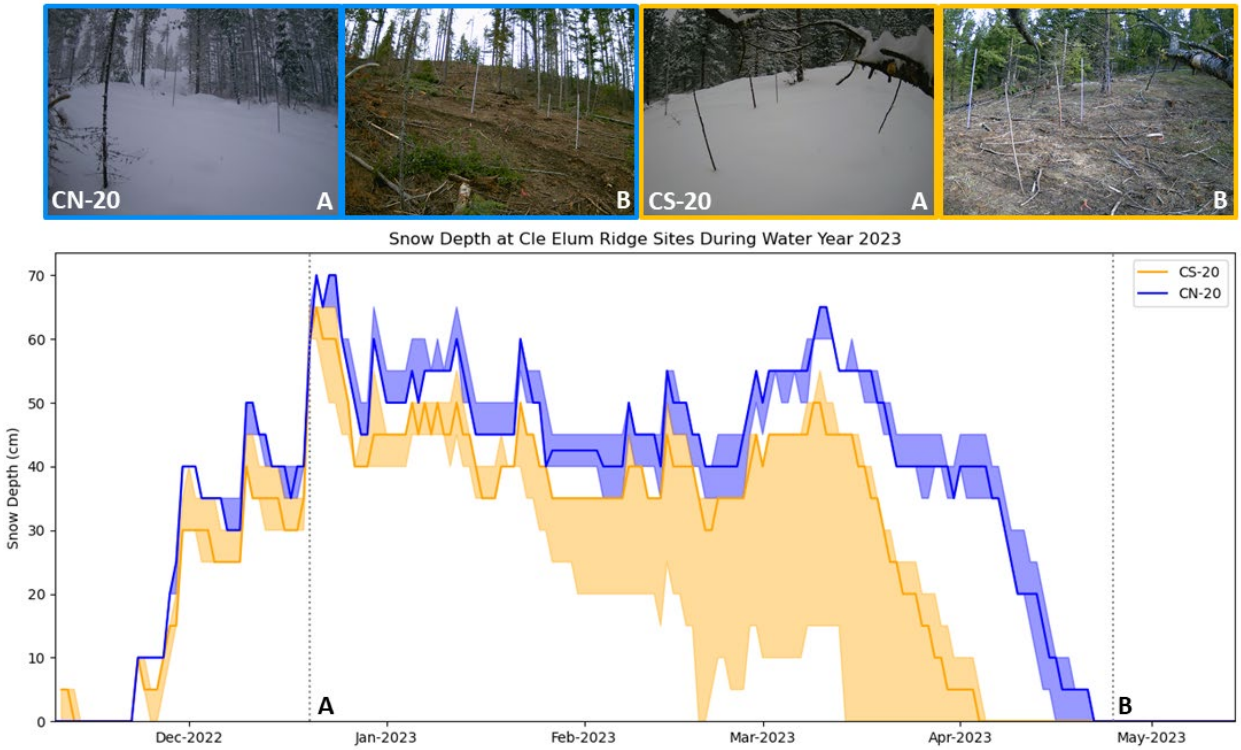

Figure 3.22. *Preliminary results of snow depth at Cle Elum Ridge for WY2023 for two sites: CS-20 in orange and CN-20 in blue. Snow depth variability across each site is represented by the filled region with the median in bold. We strategically placed three snow depth poles across each site to cover the intra site forest cover variability. The two sites have an 18-day difference in snow disappearance date (22 April for CN-20, 4 April for CS-20). Figure created by John Cramblitt.*

3.4.3. Stream Sensors at Cle Elum Ridge.

We installed three stream temperature sensors on the north side of Cle Elum Ridge in May 2023 (Figure 3.23).

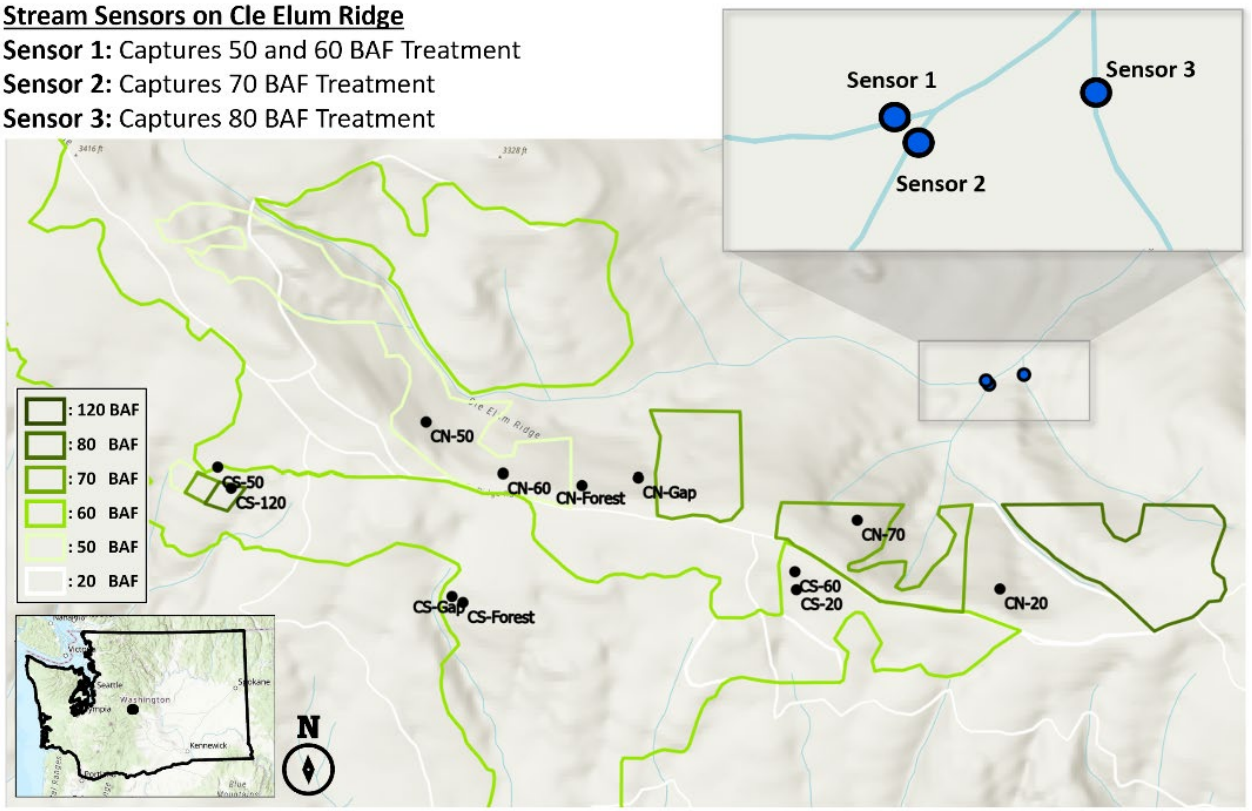

Figure 3.23. *Stream sensors we installed on Cle Elum Ridge to capture different forest treatments. Sensor 1 captures 50 and 60 BAF treatment, sensor 2 captures 70 BAF treatment, and sensor 3 captures 80 BAF treatment.*

We strategically placed the stream sensors to capture the stream temperature response from three different drainages off Cle Elum Ridge. Sensor 1 captures the tributary from the furthest west treatments, 50 and 60 BAF. Sensor 2 captures the 70 BAF treatment and sensor 3 captures the 80 BAF treatment furthest east. We placed the stream sensors as close to the forest treatments as complex terrain access would allow. All three tributaries flow into Carlson Canyon, which leads to the Teanaway River.

3.5. Section 5. Additional Information.

3.5.1. Acknowledgements.

Thank you to the Mountain Hydrology Research Group for their continuous emotional support and motivation. A special thanks to Steven Pestana for your genuine interest in this science and continuous feedback throughout the analysis. Thank you to Hannah Besso for sharing valuable friendship, motivation, and knowledge on dealing with verticle datums. Thank you to Eli Schwat and Danny Hogan for the introduction to VS code, and for all the assistance while setting up computing resources that made this analysis possible. Thank you to Friedrich Knuth for sharing your personal scripts to perform memory-efficient raster computation methods that made working with this data possible. Thank you to Michelle Hu for help with lidar data analysis, and for sharing random forest machine learning wisdom that helped us understand the results of this study. Thank you to Steven Pestana, Mackenzie Stuart, John Cramblitt, Mark Stone, and Mari Cleven for spending your valuable time in the field with us throughout this project—we truly enjoyed your company on Cle Elum Ridge and thank you for your efforts. A very special thank you to the TNC Forester, Herman Flamenco, and his lovely dog, Remus, for spending many days in the field with us on Cle Elum Ridge and sharing your invaluable knowledge of the forest.

3.5.2. Open Data Access

We processed the raw raster datasets in ArcGIS Pro. The exact steps are detailed in the Appendix. We moved the processed raster datasets into python for the remainder of the analysis. All of the python scripts used to perform this lidar data analysis and random forest analysis can be found in the GitHub repository cassielumbrazo/NCALM_raster_analysis (*https://github.com/cassielumbrazo/NCALM_raster_analysis*). The raw lidar data used in this analysis can be found in the WADNR lidar portal (*https://lidarportal.dnr.wa.gov/*) for the snow-off lidar data and in the NCALM lidar portal (*https://doi.org/10.5069/G989142F*) for the snow-on lidar data. We are temporarily storing the cleaned netCDFs for all the sites in this Google Drive (*https://drive.google.com/drive/folders/1CIYYDUK1RBsmb3s3OXvnr6ptFkhHbZ5r?usp=drive_link*). This drive is linked to a student google account and a more permanent storage solution is required to provide all the datasets. For now, all the processed TIFs for Cle Elum Ridge are in the drive. We are happy to provide the processed TIFs for all the sites to WA DNR and support them being shared publicly for others to use.

3.5.3. Appendix.

We provide three separate resources that can be used independently or together that provide instructions to reproduce the anaylsis outlined in this work. First, Appendix 1 provides written step-by-step instructions to reproduce the lidar data analysis manually in ArcGIS Pro. Second, an automated model, named **NCALMLidarModel.py**, provides an automated ArcGIS Pro model to reproduce all the steps outlined in Appendix 1. Lastly, we created a **YouTube video** which provides live instructions for how to download lidar data from the WA DNR lidar portal and reproduce the analysis in Appendix 1. The YouTube video can be found at this external link: https://youtu.be/UZrwIEDxuWs

Please contact us with any questions (lumbraca@uw.edu).

Chapter 4. Forest treatments for fire resilience result in more snow storage on north-facing aspects in the Eastern Cascades, Washington, USA

Cassie Lumbrazo[1], Steven Pestana[1], John Cramblitt[1], Emily Howe[3], Susan Dickerson-Lange[2], Jessica D. Lundquist[1]

[1]Civil and Environmental Engineering, University of Washington, Seattle, Washington, USA

[2]Natural Systems Design, Seattle, Washington, USA

[3]The Nature Conservancy of Washington, Seattle, Washington, USA

Note: This chapter will be submitted for peer-review.

Key Points.

- Forest treatments on north-facing aspects increase snow storage in the climate transition zone.
- Forest treatments in locations with greater solar exposure do not significantly affect snow depth.
- Forest managers should open canopy-gaps on north-facing slopes to increase snow retention.

Abstract.

Forests impact snow accumulation totals and ablation rates to influence total snow storage amounts and duration. Forests treatments, such as prescribed burns and forest thinning, are being implemented to increase wildfire resilience across the western U.S. in areas that also rely on seasonal snow for water resources. Watersheds just east of the Cascade crest in Washington are already climate-vulnerable due to their heavy dependence on low elevation seasonal snow. It is important that forest management practices do not push snow storage in the same direction as climate change, and rather act as a buffer against it. Multiple studies have hypothesized forest thinning and canopy gap-creation on north-facing slopes could maximize snow storage. To test this hypothesis, experimental forest treatments, covering a gradient of forest thinning, were implemented on Cle Elum Ridge at headwaters of the Yakima River Basin. Ground observations from time-lapse cameras, and snow-on lidar data before and after forest treatments, demonstrate that thinning can increase total snow storage. The forest treatments resulted in 92.3 acre-ft of SWE over the domain, compared to 34.4 acre-ft if the forest treatments were not there. A majority of this water derived from the north-facing forest treatment areas, which had 140 mm of SWE per unit area, compared to 84.5 mm of SWE per unit area in the north-facing control areas. Forest treatments on the south-facing slopes had negligible effects on snow accumulation. Thus, forest thinning and especially canopy-gap creation, on north-facing slopes provides a viable path for managing forests for both fire and hydrologic resiliency in this climate zone.

4.1. Introduction.

4.1.1. Forest-snow interactions and management.

In the western United States, foresters are using thinning to reduce forest density and prescribed burns to reduce understory fuels in an effort to prevent high severity wildfires (Churchill et al., 2013; Everett et al., 2000; Prichard et al., 2021). Forest managers are aware that changing the forest structure to create healthy, resilient forests can impact wildlife habitat, water resources availability, and susceptibility to other disturbances, such as insect outbreaks and drought. The goal of forest management is to create resilient forests but to curate management practices which act as a buffer against climate change and other stressors (Dickerson-Lange et al., 2023).

Forests provide shade and shelter to the snowpack, which slows melting from shortwave radiation and wind; however solar radiation also heats canopy elements, which emit longwave radiation that melt the snowpack (Dickerson-Lange et al., 2021; Goeking & Tarboton, 2020; Lundquist et al., 2013). In addition, forests intercept snowfall, which can unload or melt onto the snowpack below or return to the atmosphere through sublimation (Lumbrazo et al., 2022).

Previous studies have shown that the net effect of forest density on snow storage, whether forests retain snow longer or lose snow earlier than an adjacent opening, varies with climate (Lundquist et al., 2013). In warm maritime climates, forest cover reduces snow storage and duration because longwave radiation dominates, and the trees melt the snowpack. However, in cold continental climates, forest cover increases snow storage because incoming shortwave radiation dominates, and trees provide shade to the snowpack. A meta-anaylsis of previous global forest-snow field observations suggested that in regions with a mean winter temperature above -1°C, decreasing forest density likely increases snow storage (Lundquist et al., 2013). However, observations from this study either had mean winter temperatures well above or well below 1°C since there are few field observations of forest-snow interactions in climate transition zone.

Dickerson-Lange et al., (2023) extended this work by focusing on the zone with winter temperatures close to the freezing point. Within this zone, they observed that snow disappears at about the same time under forests and in the open, but more total snow accumulates in the open (Dickerson-Lange et al., 2023). They observed the greatest difference in snow accumulation and disappearance on north-facing slopes and thus argue that to extend snow storage duration in this zone, forest management should focus on thinning and canopy gap-creation on north-facing aspects. However, more observations over a larger spatial area on multiple aspects in this climate zone are needed to test this hypothesis.

4.1.2. Project Background.

The upper Yakima watershed is a critical area for endangered salmonids which depend on streamflow timing and magnitude to regulate their in-stream growth, juvenile outmigration timing, adult return migration ability, and spawning success (Vano et al., 2010). Located just east of the Cascade crest, this region is climate-vulnerable due to its heavy dependence on snowpack and its relatively low elevation headwaters (Donley et al., 2012). State and federal management agencies aim to restore forest health and increase wildfire resilience across 1.25 million acres of

the Eastern Cascades in the next 20 years through forest treatments such as thinning and prescribed burns (Washington State Department of Natural Resources, 2018). Much of these forests overlap with critical season snowpacks, which provide 75% of water supply downstream for endangered fish and a multi-billion dollar agricultural industry (Li et al., 2017). The Eastern Cascades is in the climate transitional zone focused on by Dickerson-Lange et al. (2023).

In this study, we directly test the forest-management hypotheses in Dickerson-Lange et al. (2023) through evaluating the snow storage duration before and after forest experimental forest treatments were performed in this climate zone. Through a collaborative process, the Tapash executive team and The Nature Conservancy (TNC) foresters implemented 6-levels of forest thinning treatments on Cle Elum Ridge during water year 2022 (WY; 1 October 2021 to 30 September 2022) through an experimental design to test these hypotheses. The forest treatments range from 6-levels of thinning prescriptions, representing a gradient of heavy thinning to light thinning on the north and south aspects of Cle Elum Ridge (Basal Area Factor (BAF) 20, 50, 60, 70, 80, 120; Figure 4.1D). During the forest treatments, the larger, more fire resilient tree species such as Ponderosa Pine were kept, while smaller Douglas and Grand Fir species with more fuels were selectively thinned. The forest treatments reflect practicable forestry prescriptions for fire-resilient, dry forests in the Eastern Cascades. In this work, we use ground observations and snow-on lidar data before and after the forest treatments to determine how these forest treatments, hypothesized to increase total snow storage on north-facing slopes, actually impacted total snow storage on Cle Elum Ridge.

4.2. Methods.

4.2.1. Field site and forest treatments.

Cle Elum Ridge is located just north of the city of Cle Elum on the arid eastern side of the Cascades in Washington State (Figure 4.1D). The forested terrain ranges from 840 to 1000 meters in elevation in the Douglas Fir and Ponderosa Pine forest zone with an average tree height near 20 m, and the tallest trees just above 40 m in height (Figure 4.1A). The ridge that creates Cle Elum Ridge runs almost exactly east to west, dividing the snowmelt from the ridge into two watershed scale USGS Hydrologic Unit Codes (HUC-10) (Figure 4.1BD). The north side of the ridge drains to the Middle Fork Teanaway River, and the south side drains to the Kachess River which both eventually drain into the Yakima River (Figure 4.1BD) (Dickerson-Lange et al., 2023).

For this study, we focus on a reduced domain from the pre-treatment anaylsis in Dissertation Chapter 3, which is defined by the post-treatment lidar domain centered on the forest treatment areas and snow monitoring field sites (Figure 4.1D). Our field site on Cle Elum Ridge was the site of previous field campaigns before the forest treatments occurred (Dickerson-Lange et al., 2023).

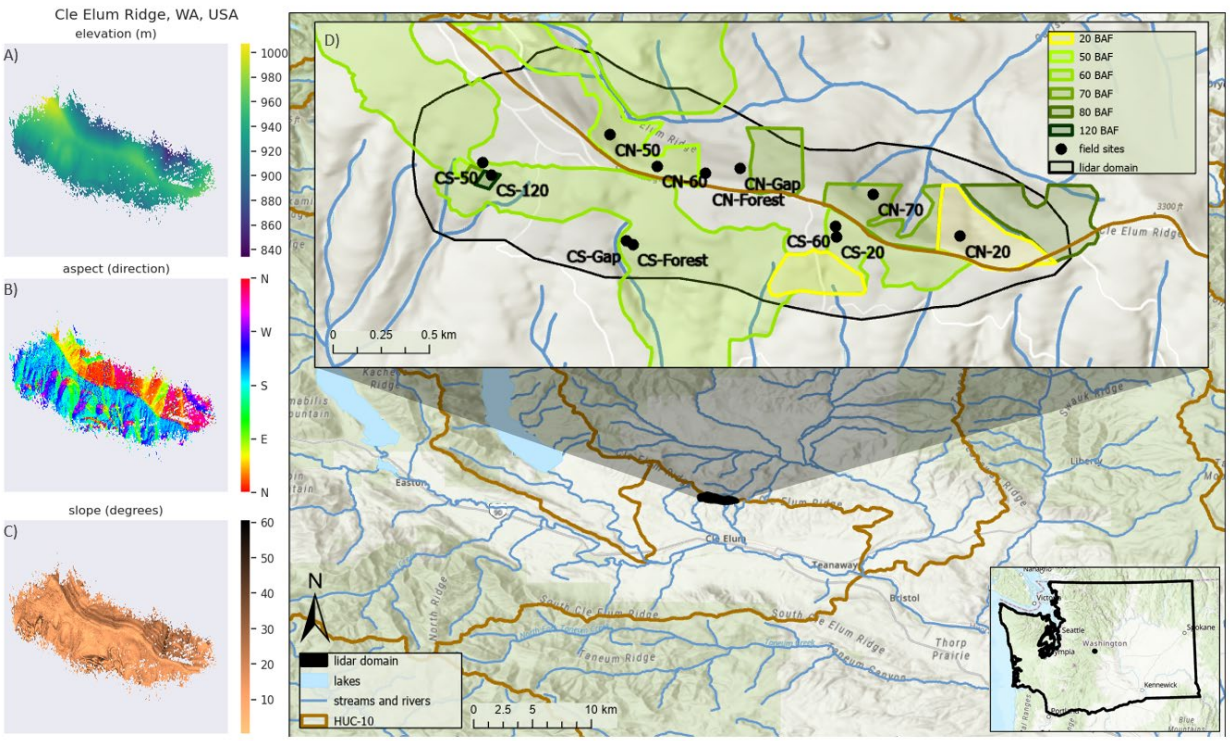

Figure 4.1. *The A) elevation (m), B) slope aspect (direction N/S/E/W), and C) slope angle (degrees) for D) the forest treatment sites on Cle Elum Ridge in the Eastern Cascades of Washington State, USA. The basal area factor (BAF) forest treatment polygons are in increasing shades of green for increasing BAF, the post-treatment snow monitoring field sites and lidar domain are in black.*

4.2.2. Snow monitoring field sites methods.

We built off of a longer time series from Dickerson-Lange et al. (2023), which established four snow monitoring field sites on Cle Elum Ridge in WY2020 and WY2021. These sites serve as control sites, established before the forest treatments with a "forest" and "gap" site on the north and south aspects of Cle Elum Ridge (named CER-N/S Forest and Gap; Dickerson-Lange et al., 2023). The forest structure at the control sites was left unchanged during forest treatments. After the treatments occurred, we established 8 more snow monitoring field sites on Cle Elum Ridge in WY2023 which span a gradient of forest thinning treatments. On the north aspect are (CN) 20/50/60/70, and on the south aspect are (CS) 20/50/60/120 in addition to the forest and gap control sites. The numbers correspond to the basal area factor (BAF) associated with that site, as estimated by TNC forester, Herman Flamenco (Figure 4.1).

At each site, we deployed remote instrumentation to observe a time series of snow depth, snow presence, and air temperature following the methods of the already established control sites detailed in Dickerson-Lange et al. (2023). We deployed three poles at each site within the view of time-lapse cameras. The three poles were strategically placed across the plots to cover the largest variability in forest cover. One pole was often placed against the base of a tree in the plot,

a second below the edge of the tree canopy, and a third in the center of the most open area of the plot. We created a daily time series of snow depth from each pole, rounded up to the nearest 5cm, through visual inspection of the time-lapse images. Hemispherical photography was taken at each snow depth pole which we used to calculate the sky view fraction, %, directly above each pole. Due to the remoteness of the field sites, the hemispherical images were taken opportunistically under patchy cloud-cover conditions, thus five images covering a variety of exposures were taken at each pole to minimize the impact of over exposure.

4.2.3. Lidar data methods.

4.2.3.1. Lidar data collection and ground validation methods.

We used snow-off lidar data over Cle Elum Ridge from the WADNR lidar portal (https://lidarportal.dnr.wa.gov/) which required two separate lidar flights to cover the full domain (Yakima Basin North 2018 and Teanaway 2015; details in Dissertation Chapter 3). NCALM snow-on lidar was collected on 1 April 2021 over the domain quantifying the pre-treatment forest structure and snow depth (dataset named SOUT_GEG/F; https://doi.org/10.5069/G989142F). Finally, we collaborated with the NHERI Natural Hazards Reconnaissance (RAPID) facility at the University of Washington to collect post-treatment snow-on lidar data over the domain on 6 March 2023. This field campaign included 5 lidar flights, using the Freefly Alta X with the Phoenix MiniRanger, which covered all the snow monitoring field sites and nearly all the forest treatment areas defined by the polygons (Figure 4.1D). The field campaign was completed with ground validation snow depths throughout the lidar flights, and snow pits including snow density and stratigraphy on the north and south aspects of the ridge covering a range of forest structures.

To determine the average snow density at Cle Elum Ridge, we dug snow pits in a variety of locations during the lidar flight and used a 250-cc cutter weigh the snow every 10 cm to observe a density profile; these data were aggregated to determine average density per pit (Table 4.1). Density is reported as a ratio, the fraction of the vertical snowpack made up of water, such that the snow depth times the average density equals the snow water equivalent (SWE). The average density across all of the snow pits was 0.31. Areas with greater solar exposure (i.e., south-facing aspects with a high heat index) had consistently higher densities, with an average of 0.34, compared to shaded locations (i.e., north-facing aspect with a low heat index), that had an average of 0.29 (Table 4.1).

Table 4.1. *Post-treatment lidar flight ground validation data.*

Pit Location	Pit Depth	Density Range	Average Density	Notes
South Slope CER-S	65 cm	0.19-0.44	0.35	In open, between 2 small ponderosa pine
North Slope CER-N	71 cm	0.14-0.38	0.30	In open, no ice layers
South of Ridge, CER-S	32 cm	0.25-0.39	0.32	In open, had an ice layer
North Slope, CER-N	54 cm	0.18-0.36	0.29	In open, no ice layer

A survey of the area was conducted to verify the representativeness of the snow pits. In general, the snowpack was made up of two layers, with a layer of fresh lower-density snow on top and rounded grains beneath. Layer thicknesses varied dramatically spatially, so bulk densities were used. Snow on the south-facing slope was of higher density and more likely to have an ice layer than snow on the north-facing slope. The highest density sites were generally directly under trees or where the surface was exposed to direct sun, where melt and re-freeze would affect the snow.

4.2.3.2. Post-treatment lidar data processing methods.

We processed the lidar data point clouds into 1-m resolution gridded raster digital terrain and digital surface models. We used the snow-off lidar data to calculate landscape metrics, such as slope, aspect, and elevation. To determine canopy height from the pre- and post-treatment lidar datasets, we difference the snow-off digital terrain model from the snow-on digital surface models. To determine snow depth from the pre- and post-treatment lidar datasets, we difference the snow-off digital terrain model from the snow-on digital terrain models. Since snow depth on Cle Elum Ridge was rarely over 2 meters in depth at the time of both lidar flights, we were careful to threshold canopy calculations over 2 meters in height to be sure we account for changes in snow depth on the ground. Additional details on these gridded raster dataset calculations can be found in Dissertation Chapter 3.

The TNC foresters provided a qualitative map of what areas were treated (Figure 4.2D), and we quantified the forest structure change by differencing the post-treatment canopy height (Figure 4.2B) from the pre-treatment canopy height (Figure 4.2A) to create a difference in canopy height map between the lidar flights as a result of the forest treatments (Figure 4.2C). We made a few assumptions to identify what differences in canopy height between the pre- and post-treatment lidar flights (Figure 4.2C) are from forest treatments. We assumed that positive values in the difference map are from snow depth or growth in vegetation, while negative values greater than 2 meters indicate forest cover change (Figure 4.2C). When differencing the snow-off digital terrain model from the snow-on digital terrain model, we assume that the ground surface did not change between the two lidar flights.

We threshold the difference map at negative 5 meters, meaning any regions where there was a loss in vegetation of 5 meters or more was classified as canopy change while any values from the difference map of greater than or equal to zero, are classified as no canopy change. Lastly, we apply a 2-meter buffer to account for edge effects around the areas where the canopy was changed over 5 meters to create the final lidar-derived binary canopy change map used in the remainder of this anaylsis (Figure 4.2F).

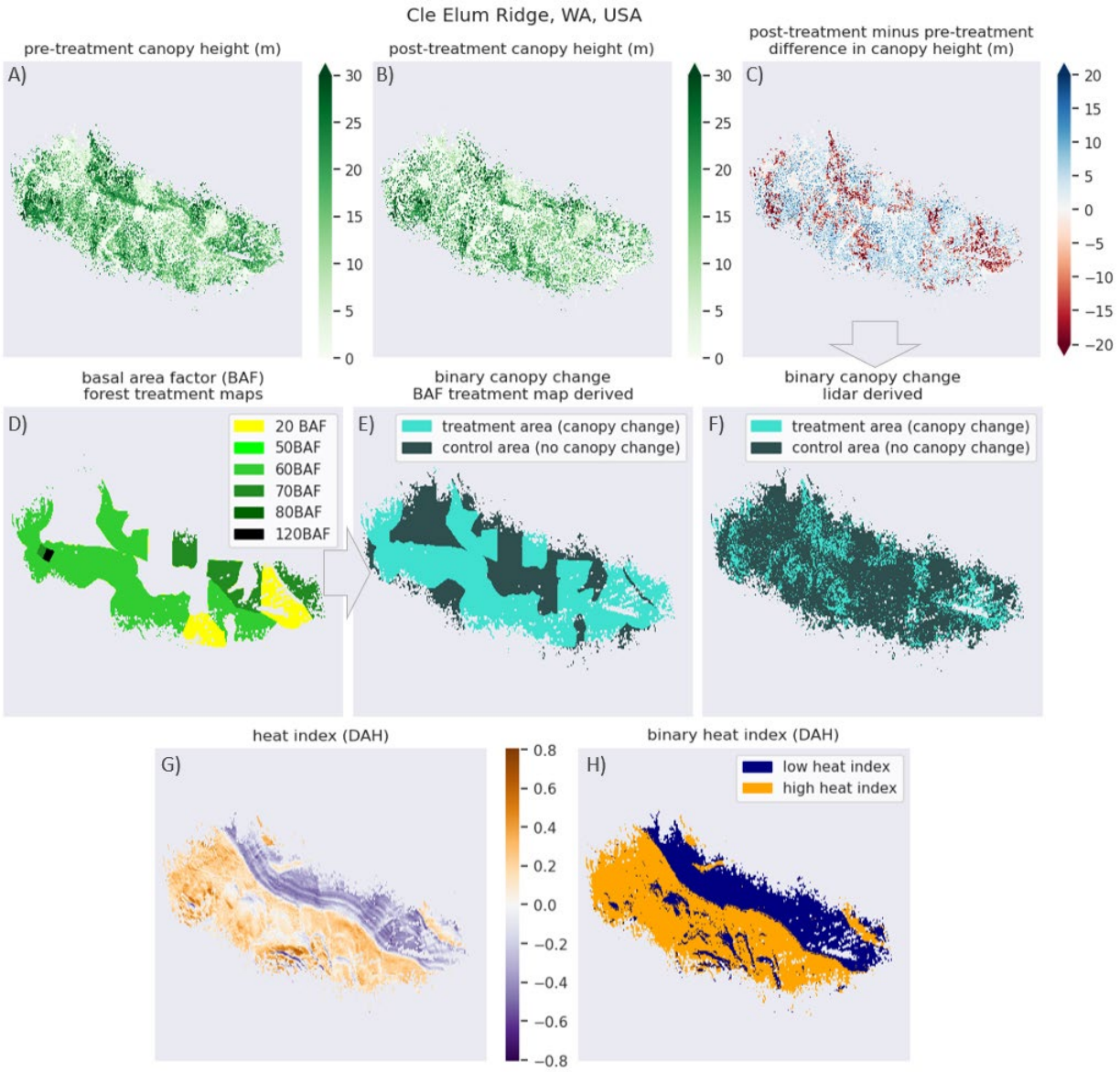

Figure 4.2. *Lidar derived landscape metrics on Cle Elum Ridge, WA of A) pre-treatment canopy height (m) collected in WY2021, B) post-treatment canopy height (m) from lidar data collected in WY2023, C) the difference in canopy height (m) map with post-treatment minus pre-treatment canopy height, D) the basal area factor (BAF) forest treatment polygon map, E) binary canopy change map derived by the BAF treatment maps, and F) binary canopy change map derived by the lidar change map. Lastly, G) the landscape diurnal anisotropic heating index (DAH) is H) binarized to identify regions which receive low and high solar radiative heat on the ridge.*

In previous work studying pre-treatment forest-snow interactions on Cle Elum Ridge, we found forest structure and the radiative heat a point on the landscape receives to be the two dominant landscape metrics that determine snow depth in this low elevation zone (Dissertation Chapter 3). Thus, for this analysis of the post-treatment forest-snow interactions, we calculate the diurnal anisotropic heating index (DAH) to capture the landscape scale ablation effects estimated from slope aspect and slope angle (Cristea et al., 2017). We calculate DAH as,

$$DAH = \cos(\alpha_{max} - \alpha) * \arctan(\beta), \quad where\ DAH < 0, low\ heat\ index \quad \text{Eq}(4.1)$$
$$where\ DAH \geq 0, high\ heat\ index$$

where α_{max} = 202.5° (SSW) is the slope aspect that receives the most heat, and α is the slope angle. DAH ranges from negative one to one and is zero in flat terrain (Figure 4.2F). The highest DAH values are on steep southwest-facing slopes, and lowest are on steep north-facing slopes (Cristea et al., 2017). In the pre-treatment forest-snow analysis, we found that snow is deeper where DAH is negative because it is shaded from the sun and that snow depth is shallower where DAH is positive because of heating from the sun (Dissertation Chapter 3). For the analysis, we classify the heat index, DAH, by areas of high heat index where DAH is greater than or equal to zero, and areas of low heat index where DAH is less than zero (Eq 4.1).

4.2.3.3. Compare pre- and post-treatment lidar datasets.

Before any of the forest treatments were implemented on Cle Elum Ridge, on 1 April 2021 snow-on lidar was flown by NCALM in a few locations of the Eastern Cascades. The background on processing this lidar dataset can be found in Dissertation Chapter 3. Since this pre-treatment lidar dataset from NCALM and the post-treatment lidar dataset from RAPID are both snow-on datasets, we can combine these datasets with snow-off lidar to compare not only the forest structure change between the two years, but the snow depth distribution across the ridge.

Meterological conditions of a certain year, such as changes in air temperature and precipitation, cause natural variations in snow depth from year to year at a single location. These variations make it challenging to compare snow depth year to year directly. However, previous studies have shown that while snow depth totals might change, snow depth patterns often persist (Pflug & Lundquist, 2020; Sturm & Wagner, 2010). Thus, if we are interested in comparing snow depth from one year to another, we can normalize by the snow depth patterns over the study domain to compare. One method of doing this is using the standardized depth value (SDV) from Sturm & Wagner (2010) which defines SDV_i as the standardized snow depth value at any gridcell, i, as,

$$SDV_i = \frac{(di - \mu_d)}{\sigma_d}, \quad \text{Eq}(4.2)$$

where d_i is the observed snow depth at any gridcell, μ_d is the domain mean snow depth, and σ_d is the domain snow depth standard deviation (Pflug & Lundquist, 2020; Sturm & Wagner, 2010).

Typically, the domain is simply defined as the entire lidar domain, assuming that the landscape scale metrics that influence snow depth, such as complex topography, aspect, and canopy cover are unchanged between the lidar flights. In our situation, the dominant control on snow depth is forest structure, and the forest structure changes within our domain from the forest treatments. Thus, we define our domain as the lidar domain which remained unchanged from the forest treatments (indicated as control areas in Figure 4.2E) and proceed with the SDV calculations for the pre- and post-treatment snow depth raster datasets from WY2021 and WY2023, respectively. We subtract the post-treatment SDV from the pre-treatment SDV to evaluate the differences between normalized snow depth values before and after the treatments.

4.3. Results.

4.3.1. Snow depth from pre- and post-treatment field site and lidar comparison.

4.3.1.1. Snow depth from snow monitoring field sites and lidar data pre- and post-treatment.

We compare snow depth time series at the control snow monitoring field sites from before (WY 2021) and after (WY 2023) the forest treatments on Cle Elum Ridge (Figure 4.3). The forest structure at the control field sites was left untouched during the forest treatments, thus we use the control sites to compare the natural variations in snow depth between the two years. We use the time series of snow depth from each year to evaluate where in the snow season the snow-on lidar data was flown (Figure 4.3AB) to better understand the spatial snow pattern on the landscape at the time of the lidar flight (Figure 4.3CD).

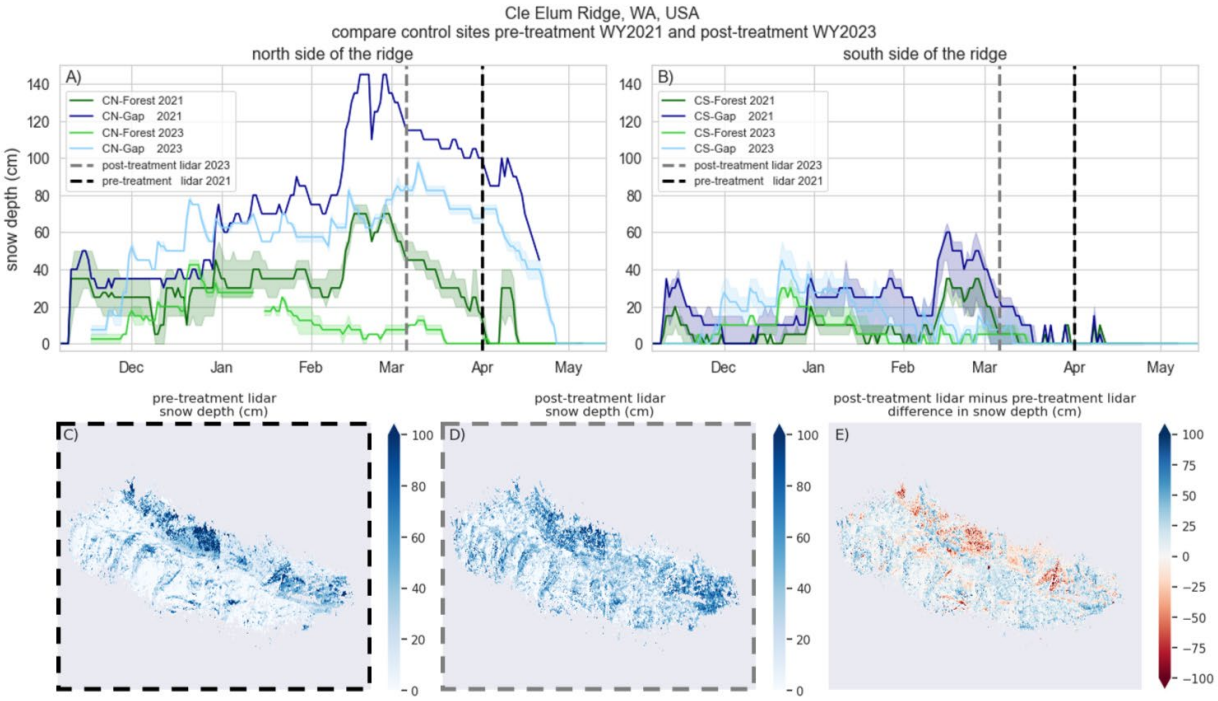

Figure 4.3. *Comparing the pre-treatment (WY2021) and post-treatment (WY2023) snow depth, cm, at Cle Elum Ridge from the control snow monitoring field sites on the A) north, CN, and B) south, CS, sides of Cle Elum Ridge with the pre-treatment, black dashed line, and post-treatment, grey dashed line, lidar flight dates indicated on the time series plots. C) Snow depth, cm, from the pre-treatment lidar flight, D) snow depth, cm, from the post-treatment lidar flight, and D) the difference in snow depth, cm, between the lidar flights.*

Generally, the snow was deeper during WY2021 on Cle Elum Ridge compared to WY2023, however similar patterns in snow depth at the four sites emerge (Figure 4.3). The deepest snow both years is at the CN-Gap site which is a gap in the forest on the north side of the ridge (Figure 4.3A). The snowpack is generally deeper on the north side of the ridge and melts out later both years compared to the south side of the ridge (Figure 4.3A). However, a generally shallow snowpack during WY2023 resulted in frequent mid-winter melt out events on the south side of the ridge which still occurred but were less common during WY2021 (Figure 4.3B).

When comparing these lidar flights in future analysis, it is important to consider the difference in time of the snow year the lidar data was collected (Figure 4.3AB). While the RAPID lidar dataset was flown on 6 March, and captures the peak snow depth right before ablation, the NCALM post-treatment lidar data was flown on 1 April, which misses peak snow depth for that year and instead captures the pattern resulting from snow ablation on the land surface (Figure 4.3AB). WY2021 was a bigger snow year, resulting in a generally deeper snowpack compared to WY2023. From previous work on Cle Elum Ridge (Dickerson-Lange et al., 2023), we know that snow is shallower on the south aspect and melts out faster compared to the north aspect. Since WY2021 was a deeper snow year and the lidar flight captured the pattern of snow ablation, the

snow depth on the north aspect was deeper than WY2023; however, due to snow melt starting on the south aspect, snow depth on the south aspect was shallower than WY2023 (Figure 4.3CDE). There is a large difference in the net energy available between 6 March and 1 April which leads to melting at the low elevation sites, such as Cle Elum Ridge, during that time of year. We proceed to use SDV to compare the lidar flights between the two years, but keep in mind that the snow depth patterns between the two years received different amounts of net radiation. Thus, any differences in the snow depth between the control locations are likely attributed to natural variations in meterological conditions and differences in a nearly 1 month-lag between lidar flight at the end of their respective snow seasons (Figure 4.3E).

4.3.1.2. Pre- and post-treatment lidar data standardized depth values (SDV) difference.

We compute the difference between the pre- and post-treatment standardized depth values (SDV) to compare the difference in snow depth in the treatment areas and the control areas, before and after the areas were treated (Figure 4.4).

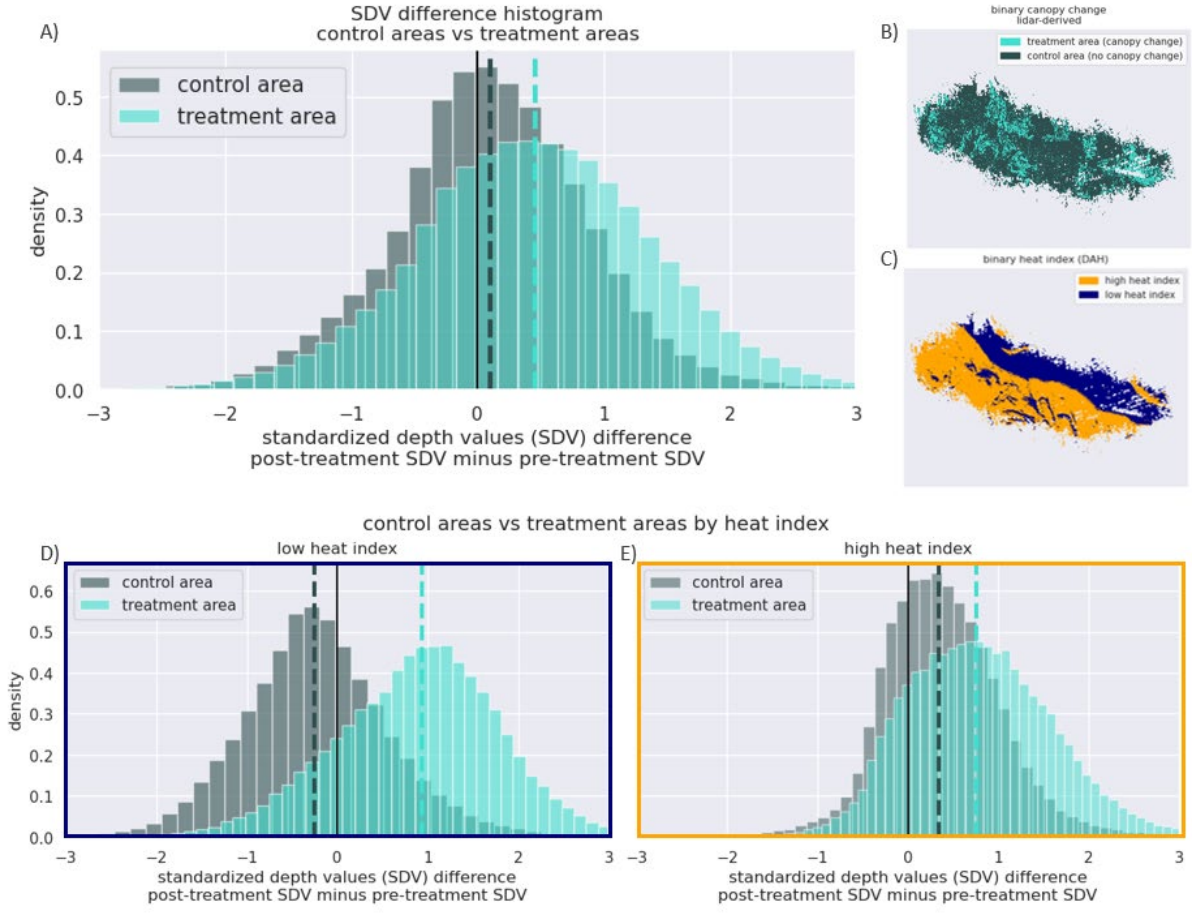

Figure 4.4. *A) The standardized depth values (SDV) difference density histograms for the B) lidar-defined control areas, in slate grey, and the treatment areas, in cyan. C) the binary heat*

index zones with high heat index zones in orange, and low heat index zones in deep blue and the SDV difference density histograms separated by the D) low heat index, and E) high heat index zones. The dashed verticle lines indicate the median of each group, and the SDV difference is post-treatment SDV minus pre-treatment SDV, where the zero line, in black, indicates snow depth from the two years being the same.

The SDV difference for the control areas where the canopy was unchanged both years is 0.1 compared to 0.45 in the treatment areas where the canopy was changed after treatments (Figure 4.4A; Table 4.2). Our results suggest that snow depth was slightly deeper in the control areas post-treatment, but even deeper in the treatment areas post-treatment on all aspects.

We visualize the SDV difference for both the control and treatment areas by areas of low and high index and find that the SDV difference between control and treatment areas is larger in low heat index terrain compared to high heat index terrain (Figure 4.4DE; Table 4.2). In terrain with a low heat index, the SDV difference in control areas is -0.26 compared to 0.94 in treatment areas (Table 4.2). These results suggest that in control areas with a low heat index, the snow depth was only slightly deeper pre-treatment attributed to differences in lidar flight dates (Results 4.3.1.1.); however, in the treatment areas the large SDV difference is attributed to deeper snow in the post-treatment forest after trees were removed.

Table 4.2. *Total area, snow depth, SWE, and SDV differences by control and treatment area classifications in high and low heat index areas.*

Domain Definition	**Control Areas**		**Treatment Areas**	
Heat Index (DAH) Classification *DAH < 0: low, DAH ≥0, high*	*High heat index*	*Low heat index*	*High heat index*	*Low heat index*
post-treatment snow depth				
total area (km^2)	0.41		0.31	
	0.26	0.15	0.21	0.10
total area (acres)	101		76.6	
	64.2	37.1	51.9	24.7
median snow depth (m)	0.19		0.35	
	0.16	0.22	0.21	0.48
standard deviation snow depth (m)	0.21	0.27	0.23	0.29
post-treatment snow water equivalent (SWE)* **calculated with 31% density everywhere (Table 4.1)*				
mm of SWE per unit area	147		173	
SWE per area to compare event areas	62.7	84.5	33.1	140
total SWE (acre-ft)	48.9		43.5	
total SWE over uneven size total area	13.2	10.3	5.64	11.4
post-treatment snow water equivalent (SWE)*				

**calculated with 34% and 29% density on high and low heat index respectively (Table 4.1)*				
mm of SWE per unit area	148		167	
SWE per area to compare event areas	68.8	79.1	36.3	131
total SWE (acre-ft)	49.2		42.1	
total SWE over uneven size total area	14.5	9.62	6.18	10.6
post-treatment SDV minus pre-treatment SDV				
median SDV difference	0.10		0.45	
	0.34	-0.26	0.75	0.94

4.3.2. Snow water equivalent (SWE) post-treatment.

4.3.2.1. Compare control and treatment areas.

We visualize the post-treatment snow depth in four landscape classifications based on canopy change (Figure 4.5A) and heat index (Figure 4.5B). The four landscape classifications are defined as treatment areas with a high heat index (i.e., DAH ≥ 0; Eq 4.1), treatment areas with a low heat index (i.e., DAH < 0; Eq 4.1), control areas with a high heat index, and control areas with a low heat index (Figure 4.5C). We found the total treatment area covers 0.31 km^2 and the total control area covers 0.41 km^2 (Figure 4.5E; Table 4.2). When classified by heat index, the high heat index treatment areas cover 0.21 km^2 and the low heat index treatment areas cover 0.1 km^2 compared to high and low heat index control areas which cover 0.26 km^2 and 0.15 km^2, respectively (Figure 4.5E; Table 4.2).

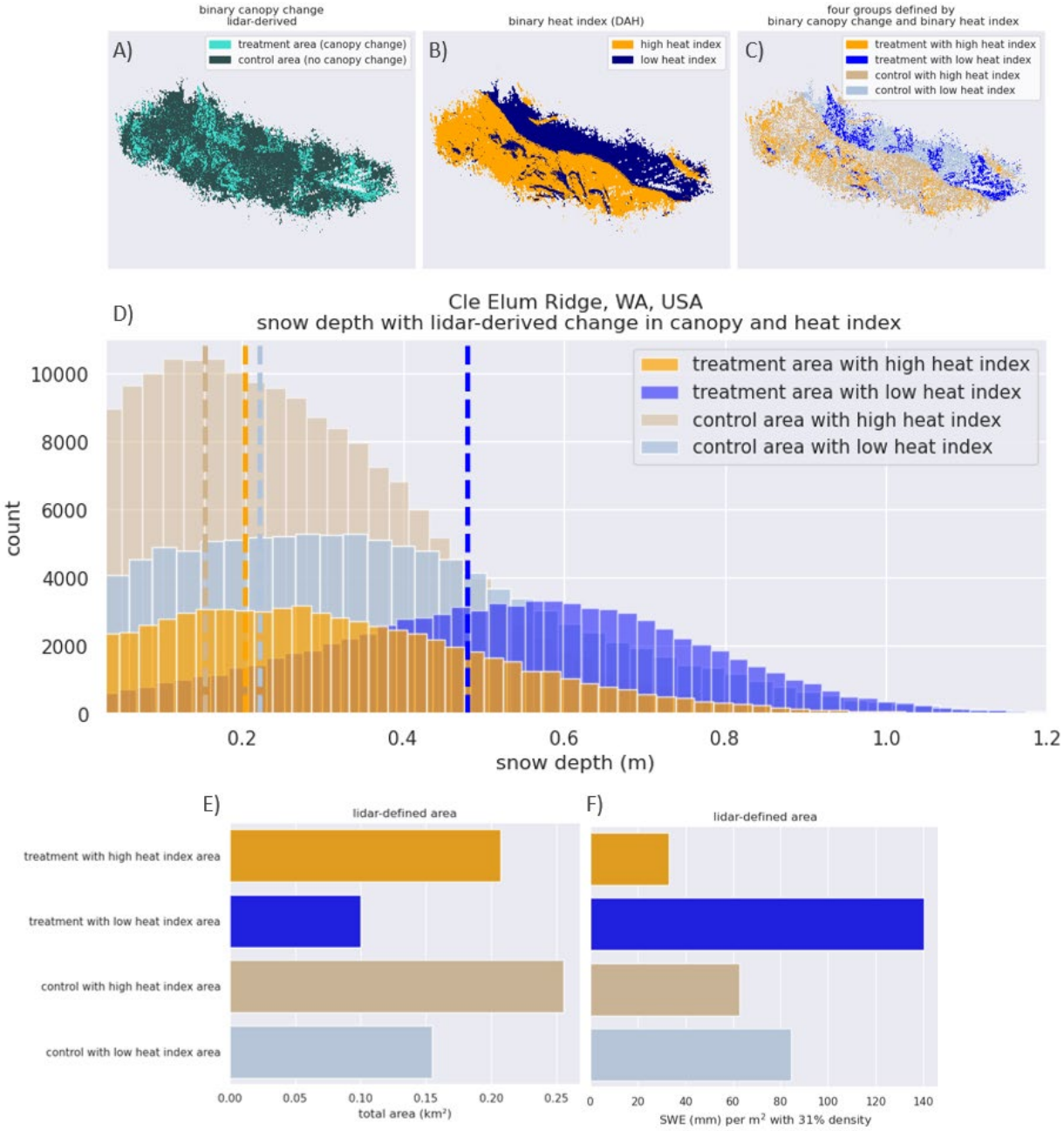

Figure 4.5. *Post-treatment A) lidar-derived binary canopy change map, and B) binary heat index map which are combined to create C) a map of four groups: the treatment areas with high heat index in orange, the treatment areas with low heat index in deep blue, the control areas with high heat index in tan, and the control areas with a low heat index in steel blue. D) Snow depth from the post-treatment lidar data in those four groups with the y-axis indicating the total count for each group and the verticle line indicating the median snow depth, m. E) The total area for each group, km^2, F) the snow water equivalent (SWE), in mm per m^2 calculated using a 31% snow density on all slopes.*

The total area differences between the groups can also be seen by the total count in the histograms of snow depth, where we see the deepest snow depth in the treatment areas with a low heat index, which has a median snow depth value of 0.48 cm (Figure 4.5D; Table 4.2). The other three groups range in median snow depths from 26 cm to 15 cm with the low heat index control area having the second deepest median snow depth and the high heat index control group having the shallowest median snow depth (Figure 4.5D; Table 4.2).

While the low heat index treatment area covers the smallest total area in the domain, it accounts for the most total SWE of the four groups, with 140 mm of SWE per m^2 when calculated using an average 31% density everywhere (Figure 4.5F; Table 4.2). The low heat index control area accounts for the second largest amount of SWE per area, with 84 mm of SWE per m^2 (Figure 4.5F; Table 4.2). We see a higher median snow depth and more total SWE per area in the forest treatment areas compared to the control areas for areas with a low heat index. These results suggest that the forest treatments increased total snow depth and total SWE per area in low heat index terrain.

In contrast, the high heat index treatment area covers the largest total area in the domain, yet it accounts for the least amount of total SWE, with only 33.1 mm of SWE per m^2 when calculated using an average 31% density everywhere (Figure 4.5F; Table 4.2). Thus, we see a higher median snow depth but less total SWE per area in the forest treatment areas compared to control areas for areas with a high heat index. These results suggest that the forest treatments decreased total SWE per area in high heat index terrain. However, during sensitivity tests we saw that the result in total SWE over an area of high heat index is sensitive to how the treatment and control areas are defined. We show results in the above analysis on treatment and control areas defined by differences in the lidar canopy height maps (Methods 4.2.3.2.). However, we provide the results using other methods of calculating treatment and control areas in Supplemental Materials.

4.3.2.2. Total SWE with and without the forest treatments.

To determine if the forest treatments resulted in more water available on Cle Elum Ridge, we calculate the total SWE using two methods. In one method, we presume that the forest treatments were not performed, and use the median snow depth in the control areas over the entire domain to determine total SWE if the treatments did not occur. In the second method, we use the median snow depth for the control areas and median snow depth for the treatment areas to determine total SWE when the treatments do exisit. We compare these two total SWE results to determine if there is more water available on Cle Elum Ridge as a result of the forest treatments (Figure 4.6; Table 4.3).

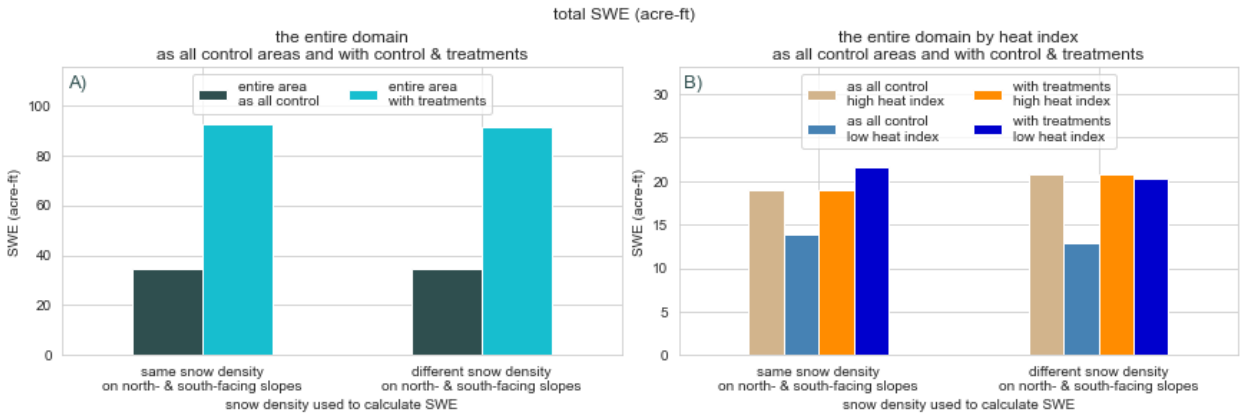

Figure 4.6. *Calculations for total SWE (acre-ft) using median snow depth for A) the entire domain presuming all areas were control areas, in dark slate grey, and for the entire domain with the control and treatment areas, in cyan. B) The same calculations for total SWE (acre-ft) separated by heat index with calculations as if all high and low heat index slopes were control area median snow depth, in tan and steel blue, respectively. And, with control and treatment area snow depths by high and low heat index, in orange and deep blue, respectively. Total SWE is calculated using two different snow density values (Table 4.1). Median snow depth and area values used to calculate total SWE can be found in Table 4.3.*

Presuming the forest treatments were not performed, the total SWE on Cle Elum Ridge on the day of the lidar flight is 34.5 acre-ft, compared to 91.2 acre-ft with the forest treatments (Figure 4.6A; Table 4.3). When we take a sum of SWE over the entire domain, we see very small differences in using different snow density values for the north and south side of the ridge (Figure 4.6A). These results suggest that the forest treatments doubled the amount of water available on Cle Elum Ridge over a 0.72 km^2 area.

When we breakdown the domain by areas of high and low heat index, we see that the forest treatments had the largest impact in the low heat index terrain (Figure 4.6B; Table 4.3). When we presume all the low heat index areas have a median control snow depth, the total SWE is 12.9 acre-ft compared to 20.2 acre-ft with the forest treatments (Figure 4.6B; Table 4.3). However, there is no difference in total SWE when we presume the high heat index terrain has a median control snow depth, compared to with the treatments. These results suggest that the forest treatments did not change total SWE in high heat index terrain but increased total SWE in low heat index terrain.

Table 4.3. *Total SWE calculated presuming there were no forest treatments (i.e., if the entire domain was control areas only) and total SWE calculated with the forest treatments, over the entire domain using median snow depth values in high and low heat index zones.*

Domain Definition	**Entire Area presuming control area snow depth only**		**Entire Area with control and treatment snow depth**	
	i.e., without treatments		***i.e., with treatments***	
heat index (DAH) classification *DAH ≥0 is high and DAH < 0 is low,*	*high heat index*	*low heat index*	*high heat index*	*low heat index*
post-treatment snow depth				
total area (km^2)	0.72		**control and treatment area breakdowns in Table 4.2*	
	0.47	0.25		
total area (acres)	178			
	116	61.8		
median snow depth (m)	0.19		0.27	
	0.16	0.22	0.19	0.35
snow water equivalent (SWE)* **calculated with 31% density everywhere (Table 4.1)*				
total SWE (m^3)	42408		113900	
	23312	17050	23253	26675
total SWE (acre-ft)	34.4		92.3	
	18.9	13.8	18.9	21.6
snow water equivalent (SWE)* **calculated with 34% and 29% density on high and low heat index respectively (Table 4.1)*				
total SWE (m^3)	42552		112502	
	25568	15950	25511	24965
total SWE (acre-ft)	34.5		91.2	
	20.7	12.9	20.7	20.2

4.4. Discussion.

4.4.1. Snow depth variability within the forest treatment areas.

Our results focused on the difference in snow depth and SWE between untreated (i.e., control areas) and treatment areas on Cle Elum Ridge. While we previously grouped all the forest treatment areas together, there is a range of forest thinning treatments within those areas; The forest treatments range from 6-levels of thinning prescriptions, representing a gradient of heavy thinning to light thinning (see Section 4.1.2). In addition to the control snow monitoring field sites (Figure 4.3), we established 8 post-treatment snow monitoring field sites covering a range of forest thinning variability on the north and south aspects of Cle Elum Ridge (Figure 4.7).

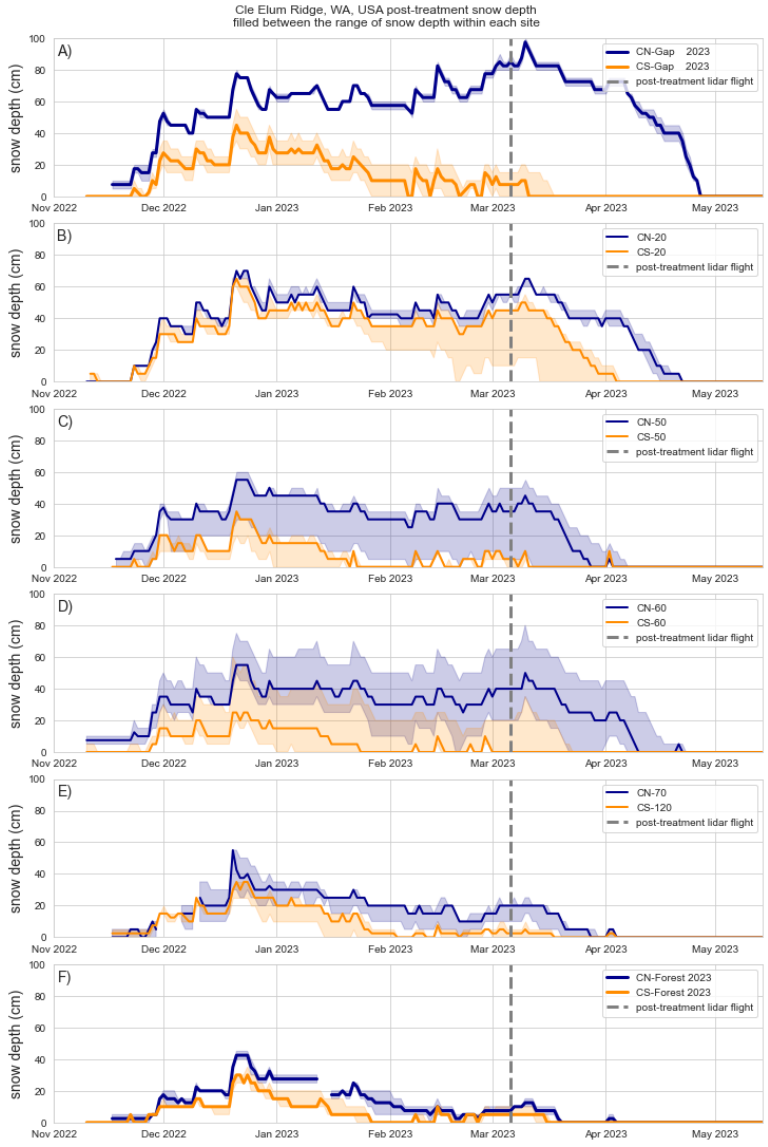

Figure 4.7. *All 12 post-treatment snow monitoring field sites on Cle Elum Ridge covering a range of forest thinning variability on the north (CN), in blue, and south (CS), in orange, aspects of Cle Elum Ridge during WY2023. There are 3 snow poles at each site to capture the intra-site*

variability, the solid line represents the median pole, and the filled area represents the variability from the minimum to the maximum snow depth pole at each site. The figures descend from lowest to highest BAF, between the A) control gap sites and F) control forest sites. The dashed verticle lines indicate the date of the post-treatment lidar flight.

There is a large amount of snow depth variability across the gradient of forest thinning treatments, with the most obvious variability across treatments on the north side of Cle Elum Ridge (Figure 4.7). The three snow depth poles at each site were strategically placed to cover the most canopy cover variability across the site (see Section 4.2.2.1.). The most open sites (i.e., CN/CS-Gap, CN/CS-20 BAF; Figure 4.7AB) and the most densely forested sites (i.e., CN/CS-Forest, CN/CS-70/120; Figure 4.7EF) have the less intra-site variability, compared to CN/CS-50/60 which both have a large range of snow depth variability within the sites (Figure 4.7CD). This suggests that while BAF on the extreme sides of the spectrum might have a stronger relationship with snow depth at this location, moderate BAF values between 50-60 do not. We know from previous studies that the distance to canopy edge (DCE) of a point on the ground is a strong predictor of snow depth (Mazzotti et al., 2019). In an analysis of landscape metrics at Cle Elum Ridge in Dissertation Chapter 3, we found that distance to canopy edge is the strongest predictor of snow depth at this location when compared to slope, aspect, and topography (Dissertation Chapter 3). Thus, we hypothesize that when BAF is on the extreme ends of the spectrum (i.e., very open, BAF-20, or very dense forest, BAF-120) the distance to canopy edge is more consistent across a site compared to more moderate BAF values (i.e., BAF-50/60) which can have a large variability of distance to canopy edge values within a site, and thus, have a large intra-site snow depth variability.

While we see some loose relationships between BAF and snow depth, there is still large variability in snow depth within sites with a single basal area factor on the north and south aspects of the ridge. To better understand the relationship between forest structure and snow depth within the forest treatments, we visualize snow depth from each pole as a function of sky view fraction, % (Figure 4.8).

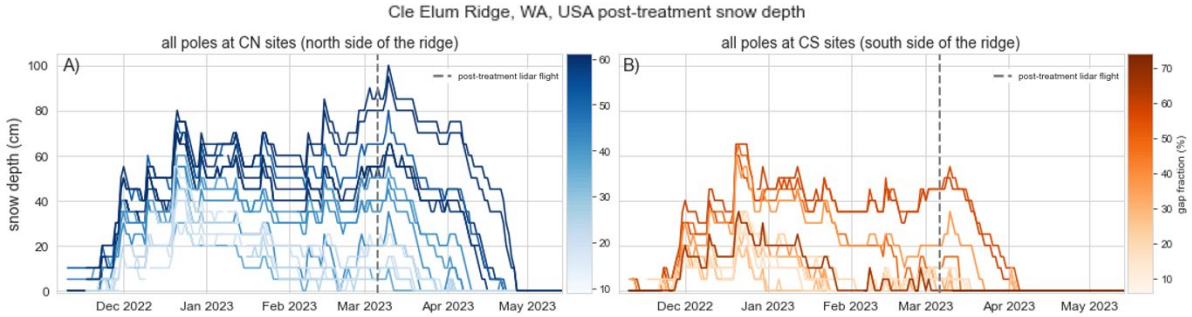

Figure 4.8. *Post-treatment snow depth time series for WY 2023 at Cle Elum Ridge for all the snow depth poles by gap fraction, %, determined by hemispherical photography at the location of each pole on A) the north side of the ridge, CN sites, in blue, and C) the south side of the ridge, CS sites, in orange. The depth of color increases with increases gap fraction.*

We see that gap fraction (i.e., sky view fraction) is a strong predictor of snow depth on the north side of Cle Elum Ridge, where the more open the canopy is overhead, the deeper the snowpack is on the ground, however the relationship is not as linear on the south side of the ridge (Figure 4.8). These results align with previous work in Dissertation Chapter 3, where we found a strong relationship between distance to canopy edge and snow depth on the north side of the ridge before the forest treatments (Dissertation Chapter 3). While distance to canopy edge can only be determined from lidar data, the sky view fraction from simple hemispherical photography taken on the ground provides a similar indicator for how far a point on the ground is from the canopy overhead (Webster et al., 2020). Foresters and forest managers often communicate forest treatments and changes in forest structure in terms of BAF, and future work is needed to make the connect between BAF, distance to canopy edge, and gap fraction in predicting snow depth on the ground to bridge the gap between the two sciences. For now, we provide preliminary analysis on BAF in the Supplemental Materials and highlight the importance of future work on this subject to effectively co-manage forests for wildfire and water resource resilience.

4.4.2. Methods for defining forest treatments.

Since the high-resolution canopy structure information was available to use, we used the lidar-derived binary canopy change map (Figure 4.2F) to determine forest treatment and control areas. However, if the only forest treatment information available to us was the basal area factor (BAF) forest treatment polygon maps (Figure 4.2D) then we would proceed with classifying regions within the polygons as forest treatment areas and areas outside the polygons as control areas (Figure 4.2E). We provide the exact results from this anaylsis reproduced with the BAF-derived treatment areas (Figure 4.2E) instead of the lidar-derived treatment areas (Figure 4.2F) in Supplemental Materials. In short, the results showed the same signal in the data throughout the methods, with a dampened magnitude.

Evaluating the impact of forest treatments on snow storage is contingent on how the treatment area is defined. From the literature, we know that a tree removed in any given location does not only impact that exact location, but the impacts of the removed tree can be felt on the snow surface many meters away (Currier & Lundquist, 2018; Mazzotti et al., 2019). An important area of future work is to compare many different methods for classifying the forest treatment areas. A few methods include applying an increased buffer around areas where the lidar data identified canopy changes, coarsening the resolution of the gridded raster dataset to cover a larger total area, or using a different metric such as difference in distance to canopy edge before and after the forest treatments. We provide diagrams illustrating the differences between these methods in Supplemental Materials, and suggest future work be performed comparing these methods to quantify the bias associated with each.

4.4.3. Management applications.

A relatively small area of forest treatments on the north-facing aspect of Cle Elum Ridge resulted in more water available compared to the larger forest treatment areas across the south-facing aspects. The magnitude of the impact of forest treatments is a function of how much snow there

is in the first place. Due to frequent mid-winter melt events on the already shallow south-facing slope snowpack, the forest treatments had little impact on total water availability. A combination of the slope angle and slope aspect on the north side of Cle Elum Ridge result in more snow accumulation in canopy gaps that is exposed to limited solar radiation. These steep north-facing slopes can be challenging to access, thus there is a tradeoff to consider in the effort required to access the terrain and perform complex forest thinning treatments, and the water resources benefit as a result of that effort. We found that the snow monitoring field sites with the lowest BAF (i.e., BAF-20) resulted in the deepest snowpack on north-facing aspects. Thus, if removing individual trees or performing light thinning is too challenging in steep terrain, our results suggest that opening larger gaps in the canopy and performing heavy thinning in one area will have a positive impact on snow storage on north-facing aspects.

BAF on the extreme sides of the spectrum have a stronger relationship to snow depth and can be used as a proxy for distance to canopy edge, however moderate BAF values are not a strong predictor for snow depth. We suggest quantifying gap fraction at a point on the ground in the field and distance to canopy edge when lidar data is available to predict the relationship between forest structure and snow depth.

As Dickerson-Lange et al. (2023) highlights, these suggestions contradict current forest treatment recommendations for north-facing forests. Restoring north-facing slopes to their healthy, historical state before years of fire suppression does not require the intensive thinning that the south-facing slopes do. The results from this study can simply provide information to forest managers, who are making decisions to manage forests to restore historical forest standards and ensure the future of water availability in a changing climate.

4.5. Conclusions.

Through field-based observations and lidar data before and after forest treatments occurred, we quantified the effect of forest treatments on snow storage duration at Cle Elum Ridge in the Eastern Cascades, WA. We calculated the standardized depth value (SDV) to account for the natural variations in snow depth between the two years and lidar data flights. We found that in terrain with a low heat index, the SDV difference in control areas is -0.26 compared to 0.94 in treatment areas. These results suggest that in control areas with a low heat index, the snow depth was only slightly deeper pre-treatment attributed to differences in lidar flight dates; however, in the treatment areas the large SDV difference is attributed to deeper snow in the post-treatment forest after trees were removed.

Using snow depth from the post-treatment lidar data, we calculated total mm of SWE per unit area in the forest treatment areas compared to the control areas. We found that the low heat index treatment area covers the smallest total area in the domain, yet it accounts for the most total SWE with 140 mm of SWE per unit area when calculated using an average 31% density. The low heat index control area accounts for the second largest amount of SWE per area, with 84 mm of SWE per unit area (Figure 4.5F; Table 4.2). We see a higher median snow depth and more total SWE per area in the forest treatment areas compared to the control areas for areas with a low heat

index. These results suggest that the forest treatments increased total snow depth and total SWE per area in low heat index terrain. The forest treatments resulted in 92.3 acre-ft of SWE over the domain, compared to 34.3 acre-fit if the forest treatments were not there.

In this study, we were able to directly test hypotheses established over many years that forest thinning and gap-creation on north-facing slopes would increase total snow storage in this climate transition zone. Our results show that while forest treatments on the south-facing slopes had negligible effects on snow accumulation, forest treatments on north-facing slopes increased total snow storage. Thus, forest thinning and especially canopy-gap creation, on north-facing slopes provides a viable path forward for managing forests for both fire and hydrologic resilience in this climate zone.

4.6. Additional Information.

4.6.1. Data Availability.

The post-treatment snow monitoring field site data from WY2023 on Cle Elum Ridge will be published in a repository matching the structure of previous datasets at this location, in Dickerson-Lange et al. (2023). A detailed description of the archived snow-off and pre-treatment lidar data can be found in the data availability statement in Dissertation Chapter 3. The post-treatment lidar data point clouds is to be published by the NHERI Natural Hazards Reconnaissance (RAPID) Facility upon manuscript publication.

4.6.2. Funding and Acknowledgements.

The data collected during this research would not have been possible without the NHERI Natural Hazards Reconnaissance (RAPID) Facility. The coauthors would like to thank all of those who participated in the forest treatments on Cle Elum Ridge, namely Rob and Herman. Thank you both for your tremendous effort which made this research possible. This work was funded by the Washington State Department of Natural Resources and the Washington State Nature Conservancy.

And a final note to anyone reading this dissertation—thank you.

References.

Abatzoglou, J., & Williams, A. P. (2016). *Impact of anthropogenic climate change on wildfire across western US forests*. https://www.pnas.org/doi/abs/10.1073/pnas.1607171113

Andreadis, K. M., Storck, P., & Lettenmaier, D. P. (2009). Modeling snow accumulation and ablation processes in forested environments. *Water Resources Research*, *45*(5). https://doi.org/10.1029/2008WR007042

Betts, A. K., & Ball, J. H. (1997). Albedo over the boreal forest. *Journal of Geophysical Research: Atmospheres*, *102*(D24), 28901–28909. https://doi.org/10.1029/96JD03876

Bunnell, F. L., McNay, R. S., & Shank, C. C. (1985). *Trees and snow: The deposition of snow on the ground- A review and quantitative synthesis.* Research, Ministries of Environment and Forests. IWIFR-17. Victoria, Province of British Columbia.

Burns, S. P., Blanken, P. D., Turnipseed, A. A., Hu, J., Monson, R. K. 2015. The Influence Of Warm-Season Precipitation On The Diel Cycle Of The Surface Energy Balance And Carbon Dioxide At A Colorado Subalpine Forest Site, Biogeosciences, 12:23, 7349-7377.

Churchill, D. J., Larson, A. J., Dahlgreen, M. C., Franklin, J. F., Hessburg, P. F., & Lutz, J. A. (2013). Restoring forest resilience: From reference spatial patterns to silvicultural prescriptions and monitoring. *Forest Ecology and Management*, *291*, 442–457. https://doi.org/10.1016/j.foreco.2012.11.007

Cline, T. J., Schindler, D. E., Walsworth, T. E., French, D. W., & Lisi, P. J. (2020). Low snowpack reduces thermal response diversity among streams across a landscape. *Limnology and Oceanography Letters*, *5*(3), 254–263. https://doi.org/10.1002/lol2.10148

Cristea, N. C., Breckheimer, I., Raleigh, M. S., HilleRisLambers, J., & Lundquist, J. D. (2017). An evaluation of terrain-based downscaling of fractional snow covered area data sets based on LiDAR-derived snow data and orthoimagery. *Water Resources Research*, *53*(8), 6802–6820. https://doi.org/10.1002/2017WR020799

Currier, W. R., & Lundquist, J. D. (2018). Snow Depth Variability at the Forest Edge in Multiple Climates in the Western United States. *Water Resources Research*, *54*(11), 8756–8773. https://doi.org/10.1029/2018WR022553

Currier, W. R., Pflug, J., Mazzotti, G., Jonas, T., Deems, J. S., Bormann, K. J., Painter, T. H., Hiemstra, C. A., Gelvin, A., Uhlmann, Z., Spaete, L., Glenn, N. F., & Lundquist, J. D. (2019). Comparing Aerial Lidar Observations With Terrestrial Lidar and Snow-Probe Transects From NASA's 2017 SnowEx Campaign. *Water Resources Research*, *55*(7), 6285–6294. https://doi.org/10.1029/2018WR024533

Currier, W. R., Sun, N., Wigmosta, M., Cristea, N., & Lundquist, J. D. (2022). The impact of forest-controlled snow variability on late-season streamflow varies by climatic region and forest structure. *Hydrological Processes*, *36*(6), e14614. https://doi.org/10.1002/hyp.14614

Dickerson-Lange, S. E., Howe, E. R., Patrick, K., Gersonde, R., & Lundquist, J. D. (2023). Forest gap effects on snow storage in the transitional climate of the Eastern Cascade Range, Washington, United States. *Frontiers in Water*, *5*. https://www.frontiersin.org/articles/10.3389/frwa.2023.1115264

Dickerson-Lange, S. E., Vano, J. A., Gersonde, R., & Lundquist, J. D. (2021). Ranking Forest Effects on Snow Storage: A Decision Tool for Forest Management. *Water Resources Research*, *57*(10), e2020WR027926. https://doi.org/10.1029/2020WR027926

Donley, E. E., Naiman, R. J., & Marineau, M. D. (2012). Strategic planning for instream flow restoration: A case study of potential climate change impacts in the central Columbia River basin. *Global Change Biology*, *18*(10), 3071–3086. https://doi.org/10.1111/j.1365-2486.2012.02773.x

Duan, K., Sun, G., McNulty, S. G., Caldwell, P. V., Cohen, E. C., Sun, S., Aldridge, H. D., Zhou, D., Zhang, L., & Zhang, Y. (2017). Future shift of the relative roles of precipitation and temperature in controlling annual runoff in the conterminous United States. *Hydrology and Earth System Sciences*, *21*(11), 5517–5529. https://doi.org/10.5194/hess-21-5517-2017

Essery, R. (1998). Boreal forests and snow in climate models. *Hydrological Processes*, *12*(10–11), 1561–1567. https://doi.org/10.1002/(SICI)1099-1085(199808/09)12:10/11<1561::AID-HYP681>3.0.CO;2-B

Essery, R., Kontu, A., Lemmetyinen, J., Dumont, M., & Ménard, C. B. (2016). A 7-year dataset for driving and evaluating snow models at an Arctic site (Sodankylä, Finland). *Geoscientific Instrumentation, Methods and Data Systems*, *5*(1), 219–227. https://doi.org/10.5194/gi-5-219-2016

Everett, R. L., Schellhaas, R., Keenum, D., Spurbeck, D., & Ohlson, P. (2000). Fire history in the ponderosa pine/Douglas-fir forests on the east slope of the Washington Cascades. *Forest Ecology and Management*, *129*(1), 207–225. https://doi.org/10.1016/S0378-1127(99)00168-1

Filhol, S., & Sturm, M. (2019). The smoothing of landscapes during snowfall with no wind. *Journal of Glaciology*, *65*, 1–15. https://doi.org/10.1017/jog.2018.104

FAO, 2010. Global forest resources assessment 2010: Main report.

Gleason, K. E., Nolin, A. W., & Roth, T. R. (2013). Charred forests increase snowmelt: Effects of burned woody debris and incoming solar radiation on snow ablation. *Geophysical Research Letters*, *40*(17), 4654–4661. https://doi.org/10.1002/grl.50896

Goeking, S. A., & Tarboton, D. G. (2020). Forests and Water Yield: A Synthesis of Disturbance Effects on Streamflow and Snowpack in Western Coniferous Forests. *Journal of Forestry*, *118*(2), 172–192. https://doi.org/10.1093/jofore/fvz069

Halofsky, J. E., Peterson, D. L., & Harvey, B. J. (2020). Changing wildfire, changing forests: The effects of climate change on fire regimes and vegetation in the Pacific Northwest, USA. *Fire Ecology*, *16*(1), 4. https://doi.org/10.1186/s42408-019-0062-8

Harpold, A. A., Krogh, S. A., Kohler, M., Eckberg, D., Greenberg, J., Sterle, G., & Broxton, P. D. (2020). Increasing the efficacy of forest thinning for snow using high-resolution modeling: A proof of concept in the Lake Tahoe Basin, California, USA. *Ecohydrology*, *13*(4), e2203. https://doi.org/10.1002/eco.2203

Hedstrom, N. R., & Pomeroy, J. W. (1998). Measurements and modelling of snow interception in the boreal forest. *Hydrological Processes*, *12*(10–11), 1611–1625. https://doi.org/10.1002/(SICI)1099-1085(199808/09)12:10/11<1611::AID-HYP684>3.0.CO;2-4

Hu, J. M., & Shean, D. (2022). Improving Mountain Snow and Land Cover Mapping Using Very-High-Resolution (VHR) Optical Satellite Images and Random Forest Machine Learning Models. *Remote Sensing*, *14*(17), Article 17. https://doi.org/10.3390/rs14174227

Immerzeel, W. W., Lutz, A. F., Andrade, M., Bahl, A., Biemans, H., Bolch, T., Hyde, S., Brumby, S., Davies, B. J., Elmore, A. C., Emmer, A., Feng, M., Fernández, A., Haritashya, U., Kargel, J. S., Koppes, M., Kraaijenbrink, P. D. A., Kulkarni, A. V., Mayewski, P. A., … Baillie, J. E. M. (2020). Importance and vulnerability of the world's water towers. *Nature*, *577*(7790), Article 7790. https://doi.org/10.1038/s41586-019-1822-y

Isaak, D. J., Wollrab, S., Horan, D., & Chandler, G. (2012). Climate change effects on stream and river temperatures across the northwest U.S. from 1980–2009 and implications for salmonid fishes. *Climatic Change*, *113*(2), 499–524. https://doi.org/10.1007/s10584-011-0326-z

Kim, E., Gatebe, C., Hall, D., Newlin, J., Misakonis, A., Elder, K., Marshall, H. P., Hiemstra, C., Brucker, L., De Marco, E., Crawford, C., Kang, D. H., & Entin, J. (2017). NASA's snowex campaign: Observing seasonal snow in a forested environment. *2017 IEEE International Geoscience and Remote Sensing Symposium (IGARSS)*, 1388–1390. https://doi.org/10.1109/IGARSS.2017.8127222

Kirchner, P. B., Bales, R. C., Molotch, N. P., Flanagan, J., & Guo, Q. (2014). LiDAR measurement of seasonal snow accumulation along an elevation gradient in the southern Sierra Nevada, California. *Hydrology and Earth System Sciences*, *18*(10), 4261–4275. https://doi.org/10.5194/hess-18-4261-2014

Kobayashi, D. (1987). Snow accumulation on a narrow board. *Cold Regions Science and Technology*, *13*(3), 239–245. https://doi.org/10.1016/0165-232X(87)90005-X

Kock, T. J., Perry, R. W., & Hansen, A. C. (2016). Survival of juvenile chinook salmon and coho salmon in the Roza Dam fish bypass and in downstream reaches of the Yakima River, Washington, 2016. In *Survival of juvenile chinook salmon and coho salmon in the Roza Dam fish bypass and in downstream reaches of the Yakima River, Washington, 2016* (USGS Numbered Series 2016–1210; Open-File Report, Vols. 2016–1210, p. 42). U.S. Geological Survey. https://doi.org/10.3133/ofr20161210

Lemmetyinen, J., Kontu, A., Pulliainen, J., Vehviläinen, J., Rautiainen, K., Wiesmann, A., Mätzler, C., Werner, C., Rott, H., Nagler, T., Schneebeli, M., Proksch, M., Schüttemeyer, D., Kern, M., & Davidson, M. W. J. (2016). Nordic Snow Radar Experiment. *Geoscientific*

Instrumentation, Methods and Data Systems, *5*(2), 403–415. https://doi.org/10.5194/gi-5-403-2016

Leppänen, L., Kontu, A., Hannula, H.-R., Sjöblom, H., & Pulliainen, J. (2016). Sodankylä manual snow survey program. *Geoscientific Instrumentation, Methods and Data Systems*, *5*(1), 163–179. https://doi.org/10.5194/gi-5-163-2016

Li, D., Wrzesien, M. L., Durand, M., Adam, J., & Lettenmaier, D. P. (2017). How much runoff originates as snow in the western United States, and how will that change in the future? *Geophysical Research Letters*, *44*(12), 6163–6172. https://doi.org/10.1002/2017GL073551

Lumbrazo, C., Bennett, A., Currier, W. R., Nijssen, B., & Lundquist, J. (2022). Evaluating Multiple Canopy-Snow Unloading Parameterizations in SUMMA With Time-Lapse Photography Characterized by Citizen Scientists. *Water Resources Research*, *58*(6), e2021WR030852. https://doi.org/10.1029/2021WR030852

Lundquist, J. D., Dickerson-Lange, S. E., Lutz, J. A., & Cristea, N. C. (2013). Lower forest density enhances snow retention in regions with warmer winters: A global framework developed from plot-scale observations and modeling. *Water Resources Research*, *49*(10), 6356–6370. https://doi.org/10.1002/wrcr.20504

Lundquist, J. D., Dickerson-Lange, S., Gutmann, E., Jonas, T., Lumbrazo, C., & Reynolds, D. (2021). Snow interception modelling: Isolated observations have led to many land surface models lacking appropriate temperature sensitivities. *Hydrological Processes*, *35*(7), e14274. https://doi.org/10.1002/hyp.14274

Lundquist, J. D., Hughes, M., Henn, B., Gutmann, E. D., Livneh, B., Dozier, J., & Neiman, P. (2015). High-Elevation Precipitation Patterns: Using Snow Measurements to Assess Daily Gridded Datasets across the Sierra Nevada, California. *Journal of Hydrometeorology*, *16*(4), 1773–1792. https://doi.org/10.1175/JHM-D-15-0019.1

Malle, J., Rutter, N., Mazzotti, G., & Jonas, T. (2019). Shading by Trees and Fractional Snow Cover Control the Subcanopy Radiation Budget. *Journal of Geophysical Research: Atmospheres*, *124*(6), 3195–3207. https://doi.org/10.1029/2018JD029908

Martin, K. A., Van Stan II, J. T., Dickerson-Lange, S. E., Lutz, J. A., Berman, J. W., Gersonde, R., & Lundquist, J. D. (2013). Development and testing of a snow interceptometer to quantify canopy water storage and interception processes in the rain/snow transition zone of the North Cascades, Washington, USA. *Water Resources Research*, *49*(6), 3243–3256. https://doi.org/10.1002/wrcr.20271

Mazzotti, G., Currier, W. R., Deems, J. S., Pflug, J. M., Lundquist, J. D., & Jonas, T. (2019). Revisiting Snow Cover Variability and Canopy Structure Within Forest Stands: Insights From Airborne Lidar Data. *Water Resources Research*, *55*(7), 6198–6216. https://doi.org/10.1029/2019WR024898

Mazzotti, G., Essery, R., Webster, C., Malle, J., & Jonas, T. (2020). Process-Level Evaluation of a Hyper-Resolution Forest Snow Model Using Distributed Multisensor Observations. *Water Resources Research*, *56*(9), e2020WR027572. https://doi.org/10.1029/2020WR027572

Mazzotti, G., Webster, C., Essery, R., & Jonas, T. (2021). Increasing the Physical Representation of Forest-Snow Processes in Coarse-Resolution Models: Lessons Learned From Upscaling Hyper-Resolution Simulations. *Water Resources Research*, *57*(5), e2020WR029064. https://doi.org/10.1029/2020WR029064

McCune, B., & Keon, D. (2022). Equations for potential annual direct incident radiation and heat load. *Journal of Vegetation Science*. https://doi.org/10.1111/j.1654-1103.2002.tb02087.x

Miller, D. H. (1962). Snow in trees: Where does it go? *Proceedings of the Western Snow Conference, 30,* 21-27.

Milliman, T. K. et al. (2018). *PhenoCam Dataset v1.0: Digital Camera Imagery from the PhenoCam Network, 2000-2015.* ORNL DAAC, Oak Ridge, Tennessee, USA.

Moeser, D., Roubinek, J., Schleppi, P., Morsdorf, F., & Jonas, T. (2014). Canopy closure, LAI and radiation transfer from airborne LiDAR synthetic images. *Agricultural and Forest Meteorology*, *197*, 158–168. https://doi.org/10.1016/j.agrformet.2014.06.008

Molnar, C. (2023). *Interpretable Machine Learning. A Guide for Making Black Box Models Explainable.* (2nd ed.). The Leanpub. https://christophm.github.io/interpretable-ml-book/

Mote, P. W., Hamlet, A. F., Clark, M. P., & Lettenmaier, D. P. (2005). Declining Mountain Snowpack in Western North America. *Bulletin of the American Meteorological Society*, *86*(1), 39–50. https://doi.org/10.1175/BAMS-86-1-39

Mote, P. W., Li, S., Lettenmaier, D. P., Xiao, M., & Engel, R. (2018). Dramatic declines in snowpack in the western US. *Npj Climate and Atmospheric Science*, *1*(1), Article 1. https://doi.org/10.1038/s41612-018-0012-1

Musselman, K. N., Clark, M. P., Liu, C., Ikeda, K., & Rasmussen, R. (2017). Slower snowmelt in a warmer world. *Nature Climate Change*, *7*(3), Article 3. https://doi.org/10.1038/nclimate3225

Musselman, K. N., Lehner, F., Ikeda, K., Clark, M. P., Prein, A. F., Liu, C., Barlage, M., & Rasmussen, R. (2018). Projected increases and shifts in rain-on-snow flood risk over western North America. *Nature Climate Change*, *8*(9), Article 9. https://doi.org/10.1038/s41558-018-0236-4

Nakai, Y., Sakamoto, T., Terajima, T., Kitahara, H., & Saito, T. (1994). *Snow interception by forest canopies: Weighing a conifer tree, meteorological observation and analysis by the Penman-Monteith formula*. https://www.semanticscholar.org/paper/Snow-interception-by-forest-canopies%3A-weighing-a-by-Nakai-Sakamoto/9166bf5413b0639deef43b6efb130c1791beece8

Niu, G.-Y., & Yang, Z.-L. (2004). Effects of vegetation canopy processes on snow surface energy and mass balances. *Journal of Geophysical Research: Atmospheres*, *109*(D23). https://doi.org/10.1029/2004JD004884

Pedregosa, F., Varoquaux, G., Gramfort, A., Michel, V., Thirion, B., Grisel, O., Blondel, M., Prettenhofer, P., Weiss, R., Dubourg, V., Vanderplas, J., Passos, A., Cournapeau, D., Brucher, M., Perrot, M., & Duchesnay, É. (2011). Scikit-learn: Machine Learning in Python. *Journal of Machine Learning Research*, *12*(85), 2825–2830.

Pflug, J. M., & Lundquist, J. D. (2020). Inferring Distributed Snow Depth by Leveraging Snow Pattern Repeatability: Investigation Using 47 Lidar Observations in the Tuolumne Watershed, Sierra Nevada, California. *Water Resources Research*, *56*(9), e2020WR027243. https://doi.org/10.1029/2020WR027243

Prichard, S. J., Hessburg, P. F., Hagmann, R. K., Povak, N. A., Dobrowski, S. Z., Hurteau, M. D., Kane, V. R., Keane, R. E., Kobziar, L. N., Kolden, C. A., North, M., Parks, S. A., Safford, H. D., Stevens, J. T., Yocom, L. L., Churchill, D. J., Gray, R. W., Huffman, D. W., Lake, F. K., & Khatri-Chhetri, P. (2021). Adapting western North American forests to climate change and wildfires: 10 common questions. *Ecological Applications*, *31*(8), e02433. https://doi.org/10.1002/eap.2433

Raleigh, M. S., Gutmann, E. D., Van Stan II, J. T., Burns, S. P., Blanken, P. D., & Small, E. E. (2022). Challenges and Capabilities in Estimating Snow Mass Intercepted in Conifer Canopies With Tree Sway Monitoring. *Water Resources Research*, *58*(3), e2021WR030972. https://doi.org/10.1029/2021WR030972

Revuelto, J., López-Moreno, J. I., Azorin-Molina, C., & Vicente-Serrano, S. M. (2014). Topographic control of snowpack distribution in a small catchment in the central Spanish Pyrenees: Intra- and inter-annual persistence. *The Cryosphere*, *8*(5), 1989–2006. https://doi.org/10.5194/tc-8-1989-2014

Roesch, A., Wild, M., Gilgen, H., & Ohmura, A. (2001). A new snow cover fraction parametrization for the ECHAM4 GCM. *Climate Dynamics*, *17*(12), 933–946. https://doi.org/10.1007/s003820100153

Sanmiguel-Vallelado, A., McPhee, J., Esmeralda Ojeda Carreño, P., Morán-Tejeda, E., Julio Camarero, J., & López-Moreno, J. I. (2022). Sensitivity of forest–snow interactions to climate forcing: Local variability in a Pyrenean valley. *Journal of Hydrology*, *605*, 127311. https://doi.org/10.1016/j.jhydrol.2021.127311

Shean, D. E., Alexandrov, O., Moratto, Z. M., Smith, B. E., Joughin, I. R., Porter, C., & Morin, P. (2016). An automated, open-source pipeline for mass production of digital elevation models (DEMs) from very-high-resolution commercial stereo satellite imagery. *ISPRS Journal of Photogrammetry and Remote Sensing*, *116*, 101–117. https://doi.org/10.1016/j.isprsjprs.2016.03.012

Storck, P., Lettenmaier, D. P., & Bolton, S. M. (2002). Measurement of snow interception and canopy effects on snow accumulation and melt in a mountainous maritime climate, Oregon, United States. *Water Resources Research*, *38*(11), 5-1-5–16. https://doi.org/10.1029/2002WR001281

Sturm, M., & Wagner, A. M. (2010). Using repeated patterns in snow distribution modeling: An Arctic example. *Water Resources Research*, *46*(12). https://doi.org/10.1029/2010WR009434

Sun, N., Wigmosta, M., Zhou, T., Lundquist, J., Dickerson-Lange, S., & Cristea, N. (2018). Evaluating the functionality and streamflow impacts of explicitly modeling forest-snow interactions and canopy gaps in a distributed hydrologic model. *Hydrological Processes*, *32*. https://doi.org/10.1002/hyp.13150

Tennant, C. J., Harpold, A. A., Lohse, K. A., Godsey, S. E., Crosby, B. T., Larsen, L. G., Brooks, P. D., Van Kirk, R. W., & Glenn, N. F. (2017). Regional sensitivities of seasonal snowpack to elevation, aspect, and vegetation cover in western North America. *Water Resources Research*, *53*(8), 6908–6926. https://doi.org/10.1002/2016WR019374

Thackeray, C. W., Fletcher, C. G., & Derksen, C. (2014). The influence of canopy snow parameterizations on snow albedo feedback in boreal forest regions. *Journal of Geophysical Research: Atmospheres*, *119*(16), 9810–9821. https://doi.org/10.1002/2014JD021858

Vano, J. A., Scott, M. J., Voisin, N., Stöckle, C. O., Hamlet, A. F., Mickelson, K. E. B., Elsner, M. M., & Lettenmaier, D. P. (2010). Climate change impacts on water management and irrigated agriculture in the Yakima River Basin, Washington, USA. *Climatic Change*, *102*(1), 287–317. https://doi.org/10.1007/s10584-010-9856-z

Washington State Department of Natural Resources. (2018). *20-Year Forest Health Strategic Plan*. Washington, DC: Olympia, WA.

Webster, C., & Jonas, T. (2018). Influence of canopy shading and snow coverage on effective albedo in a snow-dominated evergreen needleleaf forest. *Remote Sensing of Environment*, *214*, 48–58. https://doi.org/10.1016/j.rse.2018.05.023

Webster, C., Mazzotti, G., Essery, R., & Jonas, T. (2020). Enhancing airborne LiDAR data for improved forest structure representation in shortwave transmission models. *Remote Sensing of Environment*, *249*, 112017. https://doi.org/10.1016/j.rse.2020.112017

Webster, C., Rutter, N., Zahner, F., & Jonas, T. (2016). Modeling subcanopy incoming longwave radiation to seasonal snow using air and tree trunk temperatures. *Journal of Geophysical Research: Atmospheres*, *121*(3), 1220–1235. https://doi.org/10.1002/2015JD024099